Downloaded from orbit.dtu.dk on: May 05, 2023

DTU Library

Leveling and Drag Force Studies for Antifouling Coatings

Wang, Xueting

Publication date:
2018

Document Version
Publisher's PDF, also known as Version of record

Link back to DTU Orbit

Citation (APA):
Wang, X. (2018). *Leveling and Drag Force Studies for Antifouling Coatings*. Technical University of Denmark.

General rights
Copyright and moral rights for the publications made accessible in the public portal are retained by the authors and/or other copyright owners and it is a condition of accessing publications that users recognise and abide by the legal requirements associated with these rights.

- Users may download and print one copy of any publication from the public portal for the purpose of private study or research.
- You may not further distribute the material or use it for any profit-making activity or commercial gain
- You may freely distribute the URL identifying the publication in the public portal

If you believe that this document breaches copyright please contact us providing details, and we will remove access to the work immediately and investigate your claim.

Leveling and Drag Force Studies for Antifouling Coatings

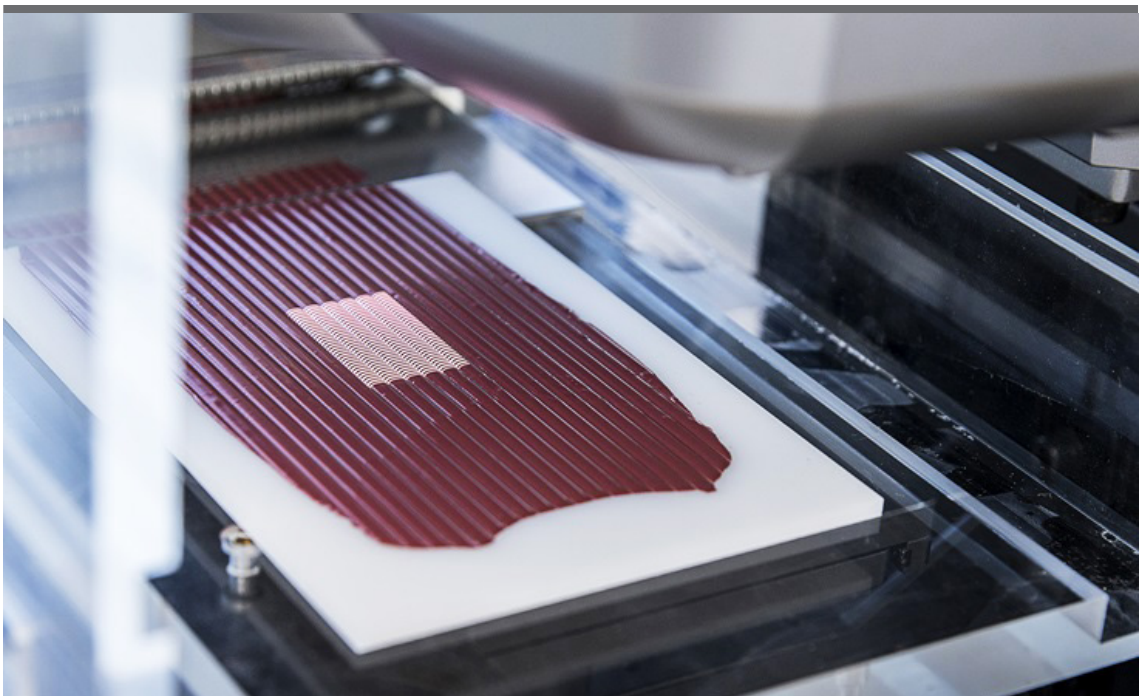

Xueting Wang

PhD Thesis

2018

DTU Chemical Engineering
Department of Chemical and Biochemical Engineering

Technical University of Denmark

Leveling and Drag Force Studies for Antifouling Coatings

by Xueting Wang

PhD thesis

July 31, 2018

Supervisor	Søren Kiil (DTU Chemical Engineering)
Co-supervisors	Claus Erik Weinell (DTU Chemical Engineering)
	Stefan Møller Olsen (Hempel A/S)

DTU Chemical Engineering
Department of Chemical and Biochemical Engineering

HEMPEL

Preface and Acknowledgements

This dissertation is the summary of three years of research, from August 2015 to July 2018, conducted in collaboration among the Technical University of Denmark (DTU), the coating supplier Hempel A/S and the shipping company Maersk Line. Most of the work was conducted in the Hempel Foundation Coatings Science and Technology (CoaST) research center, at DTU Chemical and Biochemical Engineering. The rest of the work was performed in Hempel A/S. This project was conducted under the partnership of Blue INNOship. Financial support from the Hempel Foundation to CoaST and from Innovation Fund Denmark, the Danish Maritime Fund, Hempel A/S, and Maersk Line to the project is gratefully acknowledged.

This PhD work would not have been possible without the support from many people. First of all, I am sincerely grateful to Søren Kiil as my main supervisor for giving me the opportunity to conduct this project, his invaluable input and guidance throughout the whole project, and support under any situations happened along the way. Claus Erik Weinell has been a very helpful and encouraging co-supervisor to me, especially in the laboratory work and practical issues. It has been very pleasant and enjoyable to work and discuss with him. Whenever I was demotivated, he could always motivate me again. I would also like to thank my co-supervisor from Hempel, Stefan Møller Olsen, for his support and encouragement during this project and for playing the project manager role as well. I would like to give my special thanks to Eduardo Andres for being partly involved in my PhD project. Thank you for your enthusiasm and encouragement, especially the sharp insights and guidance to the project. I am also very thankful to Kenneth Nørager Olsen from Maersk Line for his practical input to the project. Thank you all for believing in me.

I would like to express my gratitude to my two former MSc students, Nail Tamaev and Yixin Huang. Without their outstanding contributions, the project would not have been completed. They both have done great job and made a lot of efforts in conducting experiments. I enjoyed being your supervisor and I hope you enjoyed working with me as well.

I would also like to thank all the technicians, Anders, Nikolaj, and Johan, who have helped me with setup or laboratory work. I am especially grateful to the technicians from the workshop, Michael, Benjamin, Søren, Jens, Ivan and Lars for construction, commissioning, and troubleshooting. Everyone has helped me with a thing or another during my PhD. I appreciate that, especially when I needed something urgently. You all gave your full understanding of the situation and your best to help.

I am very grateful to Ciaran Dunbar from Hempel Denmark for his constant help in performing experiments and providing ideas. I would also like to thank Lena Søjbjerg Nielsen from Hempel Denmark for her help with sample preparations and technical guidance in coating production, as well as her constant support and encouragement to my work. In addition, I would like to express my sincere gratitude to Vicenç Tobar from Hempel Spain for sharing his knowledge and experience with me and for his help in coating formulations and support during the PhD. I would like to thank Antoni Sanchez, Kim Flugt Sørensen, Marcus Tullberg and Anders Blom from Hempel for their interesting discussions with me. Besides, I am very thankful to Marta, Nelida, and Markus from Hempel Spain for their kind help and support, especially during my visit in Hempel Spain. I had a good time there with you.

I was very lucky to be in a very pleasant and cheerful working environment, surrounded by many international PhD students, especially Yash, Bozo, Burak, Guoliang, Hadi, Gerard, Victor, Andrea, Guofeng, Sonia, Ting and Ying, who not only provided support and encouragement to my work but also made my days very colorful. I was fortunate to meet them in my life and share a wonderful life journey with them. I enjoyed every joyful conversation with them both in work and outside of work. I learned a lot from everyone. I cherish the moments we have spent together and all good memories we had. I am also very thankful to my friends, Clara Perez and Albert Camós Noguer, who have been giving me support whenever I need.

Last but not least, I would like to thank my parents, my younger brother, my grandparents and my other family members in China for their understanding and support to my PhD studies. Their understanding and support have been essential for me to complete this journey without concerns. Thank you all for your unconditional love and I love you all!

Xueting Wang

July 2018

Lyngby

Summary

Biofouling, defined as the accumulation of marine species on ship hulls, causes a series of consequences, such as extra drag resistance, fuel consumption, and thereby emission of harmful gases (CO_2, SO_2 and NO_x). To combat biofouling, fouling control coatings (FCCs) are widely applied on ship hulls. Two main types of FCCs are commercially available. The conventional antifouling (AF) coatings release biocides to control biofouling. Fouling release (FR) coatings limit biofouling mainly through the smooth surfaces which make it difficult for marine species to adhere with the help of the hydrodynamic force of seawater against the hull of a travelling vessel. Due to the high pigment amount, the conventional AF coatings have rougher surfaces than FR coatings.

Besides biofouling, the ship hull surface conditions, such as rough top FCC surfaces and surface irregularities (e.g., welding seams), also increase the drag resistance. Moreover, rough coating surface affects the esthetics and constitutes sites of weakness, i.e., potential starting points for corrosion, cracking, blistering and biofouling. Consequently, the FCC surface condition is of significant importance in the performance of marine vehicles. Therefore, the final goal of the PhD project is to decrease FCC surface unevenness and thereby the drag resistance. For most coatings, this can be achieved by improving the leveling properties of FCCs.

As the first step, the drag performance of newly applied AF and FR coatings were compared using a pilot-scale rotary setup. Results revealed that FR coatings caused less skin friction than AF coatings. The effects of water absorption on coating surface and frictional resistance were investigated through immersion experiments and standard water absorption tests. Although water absorption amounts for both AF and FR coatings were found to be prominent, the effects of water absorption on drag performance were insignificant for FR coating and water absorption reduced the skin friction of AF coatings. In addition, the effects of welding seams (including welding seam height and density) on drag resistance were thoroughly studied using both experiments with a designed flexible rotor and computational fluid dynamics (CFD) simulations. Significant effects were revealed for both welding seam height and density, especially at high speeds. Therefore, the welding seam height is suggested to be controlled below 5 mm during ship construction to minimize drag resistance and achieve considerable economic benefits. Practically, welding seams can be ground to below 5 mm for the existing ships. Furthermore, experimental results indicated that FCC surfaces led to higher drag resistance than welding seams with seam height below 5 mm at full-scale welding seam density condition. Moreover, CFD results showed that frictional resistance mainly resulting from ship hull

surfaces was the dominating one to the total drag resistance. Thus, FCC surface conditions were confirmed to be crucial and should be improved to minimize the friction and fuel consumption.

Therefore, the following work was to study leveling of liquid coating film to explore methods to improve leveling properties of conventional AF coatings. In all studies, model and commercial AF coatings have been used in experiments with solvent evaporation process involved. As the first step, the rheological effects of coating formulation ingredients on leveling were studied using an advanced rheometer. The shear changing process from application to the subsequent leveling was simulated using flow peak hold and flow sweep tests. It was found that rosins had insignificant rheological effects on the binder systems. In addition, it was inferred that, besides thixotropic agents, some other ingredients in the formulation may have thixotropic effects, such as reaction products between pigments and rosins or additives (e.g., wetting agents). The obtained results from rheological studies were found to be valuable input to coating formulation development work yet very qualitative and inadequate in quantifying leveling performance. Besides, coating samples were found to be very sensitive to the shear history and the expected differences in leveling effects among different coating samples were small. Therefore, a quantitative approach for measuring leveling was needed.

A roughness measurement instrument MarSurf PS10 was found to be insufficient to measure surface texture with wavelength longer than 2.5 mm (waviness characteristics) on the coating surface generated from spiral applicators. Therefore, a novel approach for quantitatively measuring leveling performance including both roughness and waviness characteristics was developed. The approach combined an optical Three-Dimensional (3D) profilometer and a retrofitted automatic film application system. Using this approach, the effects of additives (leveling additives and wetting agents) and solvents on leveling of model AF coatings were investigated. Results revealed that a better leveling performance could be easily compromised by sagging problem and inappropriate spraying application. Therefore, it was concluded that optimizing spraying application may be more vital than improving formulation for better leveling.

As an essential part of leveling study, the underlying leveling mechanisms and kinetics were explored. Leveling rate was found to be strongly coupled to the solvent evaporation rate and the associated development in coating viscosity. In addition, the effects of physical parameters including initial film thickness, wavelength, and viscosity on leveling performance were studied. Experimental results confirmed that higher film thickness, shorter wavelength, and lower viscosity led to better final leveling performance. Besides, the relationships between the final leveling performance and the coating parameters (initial film thickness and wavelength) were correlated successfully. Furthermore, the reason why lower viscosity resulted in better leveling performance was explained by the findings from evaporation rate experiments that coatings with lower viscosity had longer fast-leveling period. Overall, results demonstrated that viscosity is the dominant parameter affecting leveling. On the other hand,

based on the obtained dynamic data of film thickness, wavelength, waviness, and viscosity during leveling process after application, semi-empirical models were developed for describing leveling kinetics of a model AF coating and a commercial AF coating. However, it was not entirely possible to develop a universal model for leveling process because viscosity related rheological behavior varies with formulations containing different additives.

In summary, the drag resistance studies of FCC surfaces and welding seams confirmed the importance of improving hull surface conditions. Improving leveling properties was proved to be a possible way to reduce surface unevenness of AF coatings. However, the inherent sagging problem should always be controlled during leveling improvements in terms of formulation optimizations. Viscosity was concluded to be the most important controlling parameter for both leveling and sagging. Therefore, rheological studies are necessary and special attention should be paid to the solvent evaporation process. Moreover, the effects of the spraying application process on leveling should be considered in the future work.

Dansk resumé (Summary in Danish)

Biofouling, defineret som ophobning af marine organismer på f.eks. skibskrog, medfører en række konsekvenser, såsom ekstra friktionsmodstand af skibet gennem vandet, øget brændstofforbrug og dermed øget udledning af skadelige gasser (CO_2, SO_2 og NO_x). Til at bekæmpe biofouling anvendes i vid udstrækning fouling control coatings (FCCs). Der skelnes typisk mellem to typer af FCC coatings, som er kommercielt tilgængelige. Den ene type er de konventionelle antifouling (AF) coatings, som frigiver biocider til bekæmpelse af biofouling. Den anden type tilhører de såkaldte fouling-release (FR) coatings, som med en glat overflade og lav overfladespænding gør det vanskeligt for marine organismer at hæfte sig til overfladen. På grund af det høje pigmentindhold har de konventionelle AF-coatings typisk en grovere overflade end FR-coatings, hvilket også vil have en indflydelse på friktionsmodstanden.

Ud over biofouling og malingens naturlige ruhed vil andre uregelmæssigheder på overfladen (fx svejsesøm og rust) også øge friktionsmodstanden. Desuden påvirker den ru overflade skibets æstetik og udgør svage punkter for begyndende korrosion, revner, blærer og biofouling. Derfor er FCC-overfladebetingelsen af stor betydning for et marint fartøjs driftsbetingelser. Formålet med dette Ph.d.-projekt er at reducere FCC overfladens ruhed og dermed friktionsmodstanden, hvilket kan opnås ved at forbedre udglatningsegenskaberne af de anvendte FCCs.

Som det første trin blev friktionsmodstanden af nyligt påførte AF- og FR-belægninger sammenlignet ved anvendelse af en roteropstilling i pilotskala størrelse. Denne rotoropstilling simulerer en skibssides fremdrift gennem vandet. Resultaterne viste, at FR-belægninger gav mindre friktion end AF-belægninger. Virkningen af vandabsorption af belægningsoverfladerne på friktionsmodstanden blev også undersøgt gennem nedsænkningseksperimenter efterfulgt af friktionsforsøg på rotoropstillingen. Selv om vandabsorptionsmængder for både AF- og FR-belægninger viste sig at være betragtelige, var virkningen af vandabsorption på friktionsmodstanden ubetydelig for FR-belægning, mens vandabsorption faktisk reducerede friktionen af AF-belægning. Effekten af svejsesømme (herunder svejsesøms højde og densitet) på friktionsmodstanden blev undersøgt ved anvendelse af både eksperimenter med simulerede svejsesøm på rotor opstillingen og ved fluiddynamiske (CFD) beregninger. Der blev fundet signifikante virkninger af både svejsesømmenes højde og deres tæthed på det simulerede skibsskrog især ved høje hastigheder. Derfor blev det foreslået at reducere svejsesøms højde til under 5 mm under skibsbygning for at reducere friktionsmodstanden og dermed opnå betydelige økonomiske fordele. I praksis kan svejsesøm slibes ned til under 5 mm højde for allerede eksisterende skibe. CFD-beregningerne viste, at friktionsmodstand fra selve skibsoverfladen, er den

dominerende faktor i den samlede modstand. Således blev vigtigheden af FCC overfladebetingelser fundet til at være afgørende og bør forbedres for at minimere friktion og brændstofforbrug.

Det efterfølgende arbejde fokuserede på udglatningsegenskaberne for konventionelle AF-coatings. I alle undersøgelser blev model coatings og kommercielle AF-overflader indeholdende organiske opløsningsmidler anvendt. Som et væsentligt skridt blev de reologiske effekter af forskellige coatings ingredienser på udglatning undersøgt ved anvendelse af et avanceret reometer. Processen fra påføring til den efterfølgende udglatning blev simuleret ved anvendelse af flowstop hold og flow sweep tests. Det viste sig, at coatingens binder (rosin) havde ubetydelig reologisk effekt på malingssystemet. Derudover blev det fundet, at foruden de thixotropiske komponenter, kunne andre bestanddele i formuleringen have reologiske virkninger, såsom reaktionsprodukter mellem pigmenter og bindemidler eller additiver (f.eks. befugtningsmidler). De opnåede resultater fra reologiundersøgelsen viste sig at være værdifulde for det videre coating formuleringsarbejde på et kvalitativt plan men utilstrækkelige til at evaluere udglatningsevnen ved de forskellige forskydnings spændninger der opstår fra påføring til fuldstændig tørring. Derfor var en kvantitativ tilgang til måling af udglatning nødvendig.

Et ruhedsmåle instrument MarSurf PS10 viste sig at være utilstrækkeligt til at måle bølgelængdeelementer længere end 2.5 mm (bølgekarakteristika) på belægningsfladen og apparatet kan desuden kun måle på en tør overflade. Derfor blev der udviklet en ny fremgangsmåde til kvantitativ måling af udglatning, der omfatter både fin ruhed og bølge egenskaber. Tilgangen til dette var en kombination af et optisk berøringsfrit 3D profilometer (Keyence VHX 6000) og et retrofitted automatisk malingspåføringssystem. Effekten af diverse additiver (dispergerings- og befugtningsmidler) og opløsningsmidler på udglatning blev undersøgt med dette set-up. Resultaterne viste, at en bedre udglatning kunne kompromitteres af at coating løber nedad på lodrette flader (sagging). Derfor kan optimering af sprøjtepåføring være vigtigere end at forbedre formuleringen for bedre udglatning.

Som en væsentlig del af denne undersøgelse blev de underliggende udglatningsmekanismer og kinetik undersøgt. Udglatning viste sig at være koblet til fordampningshastigheden af organiske opløsningsmidler og den tilhørende ændring i viskositet. Derudover blev virkningerne af andre fysiske parametre, herunder gennemsnitlig filmtykkelse, bølgelængde og viskositet på udglatningsevne undersøgt. For det første bekræftede de eksperimentelle resultater, at højere filmtykkelse, kortere bølgelængde og lavere viskositet førte til bedre udglatning. Derudover kunne forholdet mellem den endelige udglatning og påføringsparametrene (filmtykkelse og bølgelængde) korreleres. Desuden kunne årsagen til at lavere viskositet giver bedre udglatning forklares med, at coatings med lavere viskositet har længere udglatningsperiode (hovedsageligt bestemt af fordampningshastighedsheden). Resultaterne viste, at viskositeten er den dominerende parameter, der påvirker udglatning. Der blev udviklet semi-empiriske modeller baseret på de opnåede dynamiske data af filmtykkelse, bølgelængde, og viskositet

under udglatning efter påføring for at beskrive udglatningsprocessen for en model AF-belægning og en kommerciel AF-belægning. Det var imidlertid ikke helt muligt at udvikle en universel model til udglatning, fordi viskositetsrelateret reologisk adfærd varierer med de forskellige tilsætningsstoffer i formulationen.

Sammenfattende bekræfter disse modstandsstudier af FCC overflader og svejsesøm vigtigheden af at forbedre skibsskrogets overfladebetingelser. En forbedring af udglatningsegenskaberne af AF belægninger er en mulighed for at reducere overfladeujævnheder, men der skal tages hensyn til det indbyggede sagging problem, når der ændres på malingsformulationen. I den forbindelse viste viskositeten sig at være den vigtigste parameter for både udglatning og sagging. Derfor er reologiske studier nødvendige, og særlig opmærksomhed bør gives til fordampningsprocessen af de organiske opløsningsmidler. Det anbefales yderligere i fremtidigt arbejde at undersøge indflydelsen af sprøjtepåføring på udglatningsprocessen.

Contents

List of Figures

List of Tables

Abbreviations and Symbols

Abbreviations

AF	Antifouling
AHR	Average hull roughness
CFD	Computational fluid dynamics
CoaST	Hempel Foundation Coatings Science and Technology
3D	Three-Dimensional
DHR	Discovery Hybrid Rheometer
DNS	Direct Numerical Solution
DPC	Danish Polymer Centre
DTU	Technical University of Denmark
FCC(s)	Fouling control coating(s)
FR	Fouling release
HR	Resistance on hull surfaces
ISO	International Organization for Standardization
LES	Large Eddy Simulation
LVER	Linear viscoelastic region
PDMS	Poly(dimethyl)siloxane
PVC	Polyvinyl chloride
RANS	Reynolds Averaged Navier-Stokes
RPM	Revolutions per minute
SPC	Self-polishing copolymer
SST	Shear-stress transport
WR	Resistance on welding seams
W/T%	Force ratio between welding seams and total in percentage

Symbols

Latin

A	Peak-to-valley height	m
a	Exponent for average film thickness	-

a_0	Amplitude at time 0	m
a_t	Amplitude at time t	m
b	Exponent for wavelength	-
c	Exponent for viscosity	-
C_A	Air resistance coefficient	-
C_F	Skin friction coefficient	-
C_R	Residuary resistance coefficient	-
C_T	Total resistance coefficient	-
d	Constant	$m^{b-a-c}kg^{c}s^{-c-1}$
dx	Each layer thickness for sagging	m
e	Exponent for viscosity	-
E	Constant	$m^{-\beta}$
E'	Constant	$m^{-\gamma}$
f	Constant	$kg^{e}m^{-e}s^{-e-1}$
F_A	Air resistance force	N
F_F	Skin friction force	N
F_R	Residuary drag force	N
F_T	Total drag resistance	N
g	Acceleration of gravity	m/s^2
h	Average film thickness	m
k	Turbulence kinetic energy	-
l	Cylinder height	m
M_b	Torque from bearings	Nm
M_c	Torque from the cylinder periphery surface	Nm
M_{cor}	A correction torque	Nm
M_d	Torque from the top and bottom surfaces of the cylinder	Nm
M_s	Torque from the outer shaft surface area	Nm
M_t	Measured total torque	Nm
n	Number of experimental data sets	-
PC	Propulsive coefficient	-
P_E	Towing power	W
r	Radius of cylinder	m
Ra	Average height for roughness profile	m
Rt	Maximum peak-to-valley height for roughness profile	m
$Rt(50)$	Maximum peak-to-valley height in any given 50 mm of ship hull	m

Rz	Average maximum peak-to-valley height for roughness profile	m
S	Wetted hull surface area	m^2
Sa	Average height in the scanned sampling area	m
S_{air}	Cross-sectional area of the ship above water	m^2
S_{min}	Sum of squared residuals	-
SP	Shaft power	W
t	Time	s
U	Mean velocity of the ship or cylinder	m/s
U_∞	Free-stream-velocity	m/s
U^+	Non-dimensional mean velocity	-
V_s	Total volume of coating that sags over a unit cross section of the film	m^3
Wa	Average height for waviness profile	m
Wa_0	Average height for waviness profile at time 0	m
Wa_t	Average height for waviness profile at time t	m
Wz	Average maximum peak-to-valley height for waviness profile	m
x	Total film thickness that sags	m
X	Total thickness of the applied coating film	m
y^+	Non-dimensional normal distance from the boundary	-

Greek

β	Exponent for average film thickness	-
γ	Exponent for wavelength	-
ε	Rate of dissipation of turbulence energy	-
η	Viscosity	Pa·s
λ	Wavelength	m
λ_c	Cut-off wavelength	m
λ_f	Cut-off wavelength	m
λ_s	Cut-off wavelength	m
v_0	Velocity of coating sagging on a surface	m/s
π	Mathematical constant	-
ρ	Density	kg/m^3
σ	Surface tension	N/m
τ_w	Wall shear stress	Pa
ω	Specific rate of dissipation of turbulence kinetic energy	-

1 Introduction

Biofouling, defined as the accumulation of micro- and macro-organisms on ship hulls, is undesired because it causes serious consequences. One consequence is the increased drag resistance which can lead to reduced sailing speed, increased fuel consumption and associated higher emissions of the harmful gases (CO_2, SO_2 and NO_x). The frequency of dry dockings and translocation of invasive species also go up.[1,2] In addition, the risk of accidents will be higher when a ship is fouled because of the reduced maneuverability. For heavily fouled ships, an increase of up to 86% in shaft power may result, to compensate for the speed loss due to the increased drag.[3]

Fouling control coatings (FCCs) are widely applied on ship hulls to combat biofouling, typically with a lifetime of 3-5 years (some up to 7.5 years).[2] Commercially, there are two main types of FCCs, the conventional biocide-based antifouling (AF) coatings and the fouling release (FR) coatings. The conventional AF coatings release biocides to combat biofouling and the outermost layer erodes to ensure a stable biocide release rate. The FR coatings have a relatively smooth surface, which makes it difficult for marine species to adhere under the assistance of the hydrodynamic force of seawater against the hull of a travelling vessel. Normally, AF coatings have rougher surfaces than FR coatings due to the high pigment amount.

The increased drag resistance is attributed not only to biofouling, but also to rough hull surface conditions including a non-smooth coating surface and surface irregularities (e.g., welding seams) when the ship hull is still free of biofouling. On some hull types, the frictional resistance can account for as much as 90% of the total drag resistance even without biofouling.[4] Furthermore, a rough coating surface constitutes sites of weakness, i.e., potential starting points for corrosion, cracking, blistering and biofouling.[5, 6]

Consequently, the coating surface condition is of significant importance in the performance of marine vessels from both economic and environmental points of view. Decreasing the coating surface unevenness and thereby the frictional resistance is an essential step to achieve high fuel efficiency. For most coatings, a smoother surface can be achieved by improving the leveling properties of the coating film.

1.1 Project objectives

This project has been a collaboration among the Technical University of Denmark, the coating supplier Hempel A/S, and the shipping company Maersk Line. The overall focus of the project was drag resistance related ship hull surface condition studies in the absence of biofouling. Hence, biofouling and its effects on drag resistance were not part of this project. The final goal was to explore methods of optimizing leveling to obtain smoother FCC surfaces and to reduce the frictional resistance and thereby the fuel consumption and harmful gas emissions. To realize that, the following objectives were formulated:

- Compare the drag resistance of two FCC technologies with different surface conditions and investigate the effects of water absorption on the coating surface and thereby on the drag resistance during seawater immersion
- Investigate the effects on drag resistance of welding seams on ship hulls (including welding seam height and density) and compare the effects with those of coating surface conditions
- Study the effects of relevant formulation ingredients and various physical parameters on leveling properties and kinetics of AF coatings and explore methods to improve their leveling properties

1.2 Structure of this thesis

The thesis has been divided into eight chapters. Among all, chapters 4, 6, and 7 have been written in manuscript format. The contents of each chapter are summarized as follows:

Chapter 2: Literature survey on drag resistance and coating leveling

This chapter introduces the concepts of biofouling, FCCs, drag resistance of ship hulls, surface roughness and waviness, and leveling. Experimental setups for drag measurements are briefly discussed. In addition, parameters affecting drag resistance are summarized and the effects of FCC surface condition and surface irregularities on ship hulls are highlighted. Moreover, differentiation and measurements of roughness and waviness profiles are introduced in this chapter. Furthermore, previous studies of leveling and challenges considering sagging problem and leveling measurements are presented. In the end of the chapter, possible ways to optimize leveling are concluded.

Chapter 3: Scientific hypotheses

This brief chapter presents all hypotheses behind the thesis and the corresponding original motivations.

Chapter 4: Drag resistance of ship hulls with FCCs and welding seams

This chapter presents the effects of surface conditions of newly applied FCCs, coating water absorption, and welding seams on drag resistance. Skin frictions of different newly applied FCCs are compared using a pilot-scale rotary setup. The effects of coating water absorption on drag resistance are studied through immersion experiments and standard water absorption tests. A flexible rotor is designed to investigate the effects of welding seam height and density on drag resistance and the effects are subsequently compared with those of FCCs. Further studies on the effects of welding seams on drag resistance using computational fluid dynamics (CFD) simulations are also presented.

Chapter 5: Rheological study and pre-screening of effective ingredients on leveling of AF coatings

In this chapter, a series of rheological studies are conducted to investigate the rheological effects on leveling of different ingredients in the formulation of conventional AF coatings. Various rheological tests are performed to simulate the shear during coating application and the subsequent leveling processes using a Discovery Hybrid Rheometer (DHR-2). The rheological behaviors of different formulation ingredients are analyzed. Following, a pre-screening of effective ingredients on leveling of AF coatings are performed. During this process, drawdown applications are conducted using both flat and spiral applicators and roughness of the dried samples are measured using a mobile roughness measuring instrument (MarSurf PS10 from Mahr GmbH).

Chapter 6: Leveling measurements of AF coatings using an optical 3D profilometer: effects of additives and solvent concentration and type

This chapter presents a study on the effects of various additives (including leveling additives, wetting and dispersing agents, and sagging agents), solvent concentration and type on leveling of AF coatings. A novel approach to quantitatively study leveling process is described. Using this approach, dynamic surface textures during leveling process of selected model AF formulations are obtained using a combination of an optical 3D profilometer and a retrofitted automatic film application system. Evaporation rate experiments are also conducted to obtain the drying kinetics. To evaluate the effects of additives, solvent concentration and type on leveling, a spraying application method is employed.

Chapter 7: Leveling kinetics of coatings with solvent evaporation and non-Newtonian rheology

This chapter provides a study of the leveling kinetics of AF coatings with solvent evaporation involved using both experiments and model simulations. Effects of various physical parameters on leveling are studied, including the average film thickness, the wavelength of surface texture, and the coating

viscosity. Besides, the dynamic values of those parameters during leveling process are obtained from a combination of the profilometer approach and the rheological studies. Based on the experimental data obtained, semi-empirical models describing the leveling process of selected AF coatings are presented.

Chapter 8: Concluding remarks

This chapter summarizes the main conclusions of the thesis and provides suggestions for future work.

2 Literature survey on drag resistance and coating leveling

This chapter presents an overview of biofouling, FCCs, drag resistance on ship hulls and the associated leveling phenomenon. Experimental setups for drag measurements are briefly introduced. Parameters affecting drag resistance are summarized and the effects of FCC surfaces and surface irregularities highlighted. Simulations of the effects of surface irregularities on drag resistance using CFD are also briefly mentioned. Previous leveling studies and challenges (including sagging problem and leveling measurements) are discussed with the aim of later posing a strategy for optimization of leveling of AF coatings. At the end, possible ways to optimize leveling are summarized.

This chapter is aimed to provide necessary background knowledge to the readers to understand the motivations, objectives, and hypotheses of this thesis work as well as the challenges in the field and achievements of the research. A more specific literature review will be presented in the introduction section of each chapter written in manuscript format.

2.1 Biofouling and fouling control coatings (FCCs)

Biofouling is known as the settlement of marine species on any surfaces immersed in seawater, such as bacteria, algae, mussels, and barnacles (see Figure 2.1). This plant and animal growth is undesired because it increases the drag resistance of ships, and leads to higher fuel consumption and emissions of harmful gases.

Figure 2.1 Biofouling on ship hulls. Hard fouling with barnacles (top), plant fouling (bottom left), and soft fouling consisting of slime (bottom right). Courtesy of Hempel A/S.

Consequently, ships are usually applied with various layers of functionalized coatings on their outer surfaces to prevent corrosion and biofouling in the aggressive marine environment. A schematic illustration and a microscopic image of coating layers on ship hulls are shown in Figure 2.2. Typically, the outmost layers consist of FCCs which prevent (or at least deter) marine organisms from attaching to the ship surface. The bottom layers are anticorrosive coatings. For FCCs, a tie-coat is needed to ensure good adhesion to the underlying anticorrosive coatings.

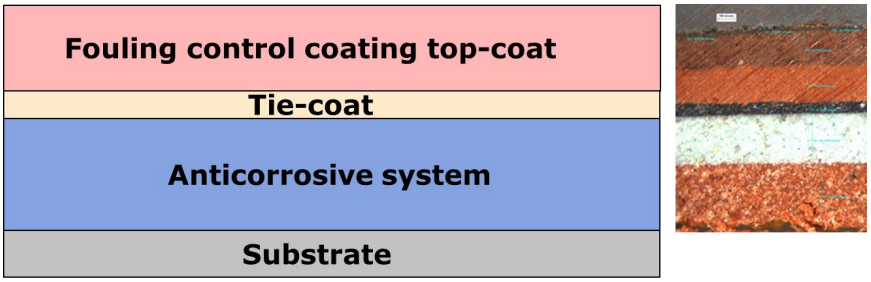

Figure 2.2 Schematic illustration (left) and microscopic image (right) of coating layers on ship hulls. Right hand figure: the two bottom layers are anticorrosive coatings; the middle black layer is a tie-coat; the top two layers are FCCs. Courtesy of Hempel A/S.

Two main types of FCCs have been developed with different antifouling mechanisms as demonstrated in Figure 2.3.[6] One is the conventional biocide-based antifouling (AF) coatings. These are normally highly pigmented coatings containing biocides that are released into seawater to combat biofouling in a controlled manner. The other type is so-called fouling release (FR) coatings which possess smooth surfaces with low surface energy (traditional FR coating feature) and adequate elasticity that make it difficult for marine organisms to adhere under the assistance of hydrodynamic force during sailing.[7] Notice from Figure 2.3 that AF coatings normally have rougher surfaces than FR coatings due to the high pigment amount.

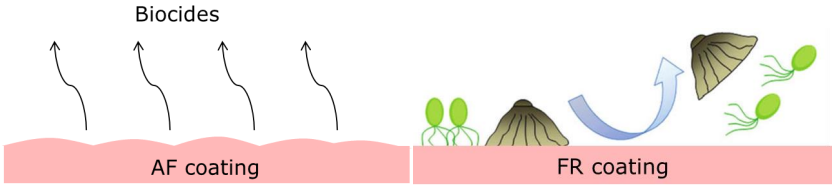

Figure 2.3 Simplified illustrations of the working mechanisms of conventional AF coatings (left) and FR coatings (right). The right hand figure was modified with permission from Lejars *et al.*[6] Copyright © 2012 American Chemical Society.

For AF coatings, after immersion, water will penetrate into the coating film and dissolve the soluble ingredients. Following, the biocides are leached together with the soluble parts and released into

seawater. Consequently, a leached layer is formed on top and it will gradually be eroded or polished away so that a new front can be exposed to seawater.[1] It is crucial that the biocide leaching rate is well controlled for AF coatings to ensure effective antifouling performance and desired lifetime of the applied coating layers.

Various types of biocide-based AF coatings have been developed based on different binder technologies.[8] One type is called self-polishing copolymer (SPC) coatings which have stable biocide release rates and the leaching rate increases linearly with the sailing speed, up to 15 μm per month.[9] In addition, the leached layer is fairly thin and the thickness of the leached layer is quite stable, typically within 10 and 20 μm.[1,10] The main ingredients in AF coating formulations and their functions are summarized in Table 2.1.

Table 2.1 Typical ingredients and their functions in AF coating formulations.

Ingredients	**Functions**
Binders	Combine all ingredients together to form a network
Rosins	Prevent cracking and increase flexibility of the dried film
	Control the polishing rate
Pigments	Most are biocides to prevent biofouling
	Provide color effects
Solvents	Dissolve rosins and other soluble ingredients
	Wet pigments and other insoluble ingredients
Additives	Impart rheological, wetting and dispersing effects

FR coatings were developed later than AF coatings and they are still evolving. The traditional FR coatings typically have low surface energy and high elasticity, which makes it hard for marine organisms to remain (but still possible to attach) with the help from hydrodynamic force during sailing. Although macro-fouling organisms cannot easily adhere to FR coating surfaces, these surfaces are vulnerable to the build-up of a slime layer which is mainly composed of diatoms and bacteria. Diatoms are known to attach strongly to hydrophobic surfaces and be difficult to remove even at high hydrodynamic stress withstanding water speeds up to 30 knots. Therefore, to combat slime fouling, new FR coating technologies have been developed with high surface energy, which makes it hard for marine organisms to attach under the assistance of hydrodynamic force.[11] It should be noticed that the hydrodynamic force is of great importance for FR coatings to limit biofouling. As a result, the antifouling efficiency of FR

coatings is normally low when marine vessels are slow steaming (sailing at speeds significantly below the original design speed, maximum 18 knots for container vessels), especially during idle period.

Consequently, researches have been focusing on improving FR coatings efficiency against slime fouling and antifouling performance at low speeds or during idle period, particularly in the development of fluoro-based polymers and hybrid FR coatings (combining AF coatings and traditional FR coatings).[6] Recently, FR coating products containing small amounts of biocides have become commercially available.[12] Besides, grooming (frequent and gentle wiping the hull surface) has been proved to be an effective method in controlling biofouling and a recent study showed that the drag resistance associated with groomed biofilms on FR coating was much less than the ungroomed one.[13]

In addition, FR coatings have poor adhesion, and a tie-coat is necessary to provide good adhesion between the FR top-coat and the epoxy-based anticorrosive sublayer. However, the main disadvantage of FR coatings is that they are soft and vulnerable to mechanical damage due to their low elastic modulus.[6] Although conventional AF coatings also face the same challenge, they do not rely solely on the surface properties for their efficiency.[14] Furthermore, FR coatings are more expensive than AF coatings though they are more environmentally friendly with less (or no) release of toxic compounds to the marine environment.[15] The market penetration of FR coatings has been limited (<10%) due to the high initial cost and the fact that the majority of the world's fleet do not operate at sufficiently high speeds for the current FR coatings to perform at their best.[16]

The antifouling performance of biocide-based AF coatings is typically assessed by static immersion tests in the field by evaluating the types and amounts of micro- and macro-organisms growing on the test panels. For FR coatings, the analysis is usually supplemented by a measurement of adhesion strength of barnacles in shear because barnacles are macro-fouling organisms which will eventually attach firmly to the surface.[6] Further details about two FCC technologies and comparison of antifouling performance between AF and FR coatings can be found in the open literature[1,8,10,17,18]

2.2 Drag resistance of ship hulls

The fuel efficiency of a ship is directly related to the drag resistance arising from the motion of seawater over the ship surface. The drag resistance (F_T) consists of frictional resistance (F_F) which is defined as the forces opposing a viscous fluid flow across a surface and residuary resistance (F_R) which is due to wave and eddy formation during the movement, as presented in Equation (2.1). Air resistance (F_A) represents a minor portion of the total resistance, no more than 2% for slow steaming vessels like oil tankers and no more than 10% for fast trading ships like container vessels.[19,20]

$$F_T = F_F + F_R + F_A \tag{2.1}$$

Frictional resistance accounts for a considerable part of a ship's total drag resistance. For instance, frictional resistance causes 70 to 90% of the total drag resistance for slow steaming vessels and less than 40% for fast trading ships.[19] The first quarter of the underwater hull (from the bow) contributes most to the overall frictional drag and the contribution diminish gradually from fore to aft.[21] The residuary resistance is determined by the length of the ship and the ratio of width to the vertical distance from the bottom of the hull to the waterline.[22] After a ship has been built, it is barely feasible to decrease the residuary resistance. Therefore, it is rather feasible to reduce the frictional resistance and thereby the drag resistance and fuel consumption to achieve higher fuel efficiency. Theoretically, the total drag resistance that a marine vessel is subjected to can be calculated. The approach for this can be found in appendix A.

2.2.1 Experimental setups for drag measurements

Various setups can be used to determine drag resistance, such as towing tank, rotating cylinders, water tunnels, and pipes. Comparisons among them have been elaborated in a previous review work.[8] Their advantages and disadvantages are summarized in Table 2.2.

In the present work, a rotating cylinder that provides a simple and accurate method to estimate drag resistance (or more precisely torque) has been used (more elaboration in the chapter 4). This type of setup has been applied to test and develop FCCs and has often been used in some form in hull coating industries and at scientific institutes.[23,24]

This pilot-scale setup (see Figure 2.4) consists of two concentric cylinders where the inner one is applied with coating samples and rotates. Both of them are immersed into a tank containing around 600 liters of artificial seawater where the temperature is controlled by a heat exchanger. A typical composition of the artificial seawater has been used according to the recommendation of Grasshoff.[25] A torque sensor installed on the shaft records the torque during rotation. The rotation speed, revolutions per minute (RPM), can be controlled. More detailed description of this setup and experimental uncertainties can be found in previous work[2,17]

Table 2.2 Advantages and disadvantages of experimental setups for drag measurements. Modified from Lindholdt *et al.*[8] Copyright © 2015 American Coatings Association

Test setups	Advantages	Disadvantages
Rotating disk[26]	Small size Easy application of coatings Fairly low cost	Varying shear stress over the test surface
Rotating cylinder[24]	Small size Fairly low cost	Complex interpretation of friction coefficient
Towing tank[27]	No pressure gradient Resemblance to ship geometry	Large tank necessary Limited maximum speed and Reynolds number
Water tunnel[28]	Small size Controlled flow	Complicated flow stability to two- and three-dimensional controlled disturbances
Static and dynamic panel exposure tested on a boat[29]	Flexible immersion conditions (static and/or dynamic)	Dynamic immersion could deviate some from actual hull conditions of a moving ship
Pipes[30]	Vast amount of literature for flow in pipes	Large uncertainty Complicated visual inspection
Optical methods for drag measurements[31]	Accurate flow pattern measurements	Expensive equipment Indirect drag evaluation

As presented in Table 2.2, this setup has many advantages, such as low operating cost, easy maintenance, and simple construction. However, it also has some disadvantages. One disadvantage is the difficulty in applying coatings on the cylindrical surfaces to obtain the same smoothness as applying on flat or plane surfaces which provide better similarities to the real hull surfaces.[23] Another disadvantage is the end effects which are present at the top and bottom of the cylinder. The flow regimes at the top and bottom are different from those at the periphery surface.[8] Besides, the friction from the bearings also contributes to the measured torque. Both the torque from the top and bottom and the bearings should be subtracted from the total measured torque afterwards. The detailed conversion of torque values to frictional coefficient can be found in appendix B.

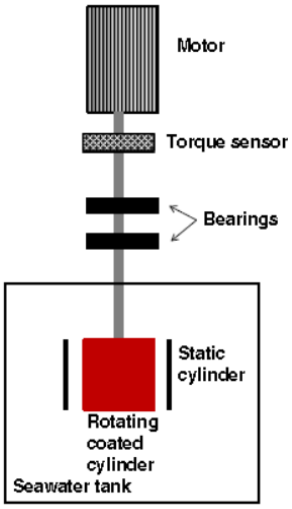

Figure 2.4 The schematic of the pilot-scale rotary setup. Reprinted from Lindholdt *et al.*[2] Copyright © 2015 American Coatings Association

To evaluate the drag performance of FCCs with biofouling process involved, both static and dynamic exposures have been conducted.[32] Swain *et al.*[29] developed an approach to combine static and dynamic exposures of panels and drag measurements afterwards. After static immersion in natural seawater condition, the panels were exposed in a dynamic test tank. After exposures, drag measurements of the panels were performed using a hydrodynamic testing facility similar to a boat with a drag meter.

Accurately converting lab-scale frictional coefficients to full-scale values is complex for both clean and bio-fouled FCCs. Even if the lab-scale results are considered to be accurate, the real-life fouling pattern is heterogeneous, which complicates scaling-up. Nevertheless, lab-scale tests can still indicate the drag resistance of different FCCs in full-scale condition.[8]

2.2.2 Parameters that affect drag performance

Ship design (geometry); propulsion system (propeller and engine); and hull surface condition (such as coating surface roughness and waviness, mechanical damage, welding seams and biofouling) are three main parameters that affect the overall drag performance and fuel efficiency of a ship. An imprint of a welding seam from a ship hull is illustrated in Figure 2.5. In order to minimize drag resistance and fuel consumption, these three parameters should be considered for the newly designed ships. However, for the existing ships, the hull surface condition is the dominating parameter because the ship geometry and propulsion system can barely be changed after a ship has been built. Besides, drag resistance can also be influenced by sailing speed, seawater conditions (i.e., temperature and salinity of seawater), weather conditions (i.e., wind, waves and currents). The detailed description of them can be found in the references[8,17,33,34] and will not be covered here.

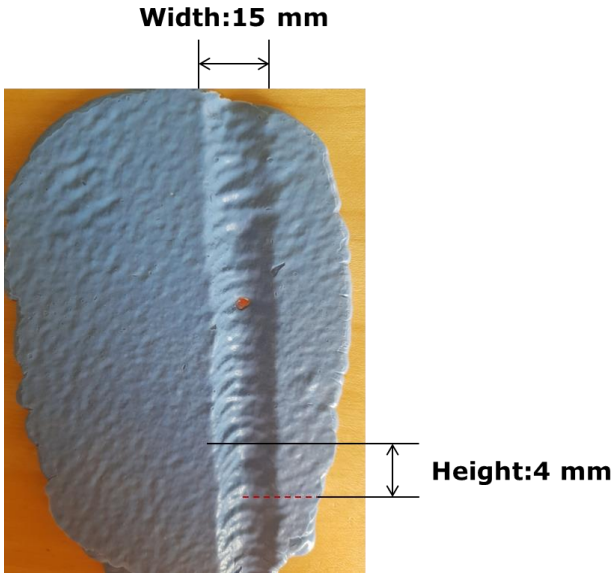

Figure 2.5 An imprint of a typical welding seam on a ship hull with seam width 15 mm and seam height 4 mm. Courtesy of Hempel A/S.

The hull surface condition can be classified into three cases: smooth, mechanically rough and bio-fouled. A relatively smooth surface condition is typically the condition after dry-docking or the newly

applied coating surfaces without biofouling. The mechanical roughness can be interpreted as surface irregularities due to structural defects (welding seams and substrate waviness),[8] mechanical damage, corrosion and poor coating conditions (e.g., over spraying, and dry spraying). Those large scale irregularities were found to have influences on drag performance. More details can be found in previous work.[24]

For the relatively smooth surface condition, the hull surface profile can be categorized into roughness (micro-roughness) profile and waviness (macro-roughness) profile. Normally, waviness profile is superimposed on top of the roughness profile. To focus on the profiles of interest, different cut-off lengths for filtering should be selected. In the present work, waviness was considered to be more relevant to drag reduction. A cut-off length shorter than the waviness wavelength will eliminate waviness characteristics and only include roughness characteristics. A long-pass filter (short wavelength cut-off) allows the long wavelength components through, thereby excluding the waviness profile. A short-pass filter (long wavelength cut-off) allows the short wavelength components through, thereby excluding the roughness profile.

Those principles are widely used in various methods available to measure surface profiles (not presented here), such as stylus methods[24] and optical methods.[17,23,35] The stylus methods apply a probe to go through a surface, which means that they are only applicable to a dry surface. Moreover, the short wavelength cut-off in stylus-based roughness measurement equipment is fixed by the ball diameter of the stylus.[35] Based on International Organization for Standardization (ISO) standards, the standard cut-off lengths are 8 mm, 2.5 mm, 0.8 mm, 0.25 mm, and 0.08 mm. However, they may not be enough in some cases, for instance, when the wavelength of the surface profile goes up to 30 mm. In addition, it is difficult to choose a suitable cut-off length to have comparable results with different investigations. Normally, choosing cut-off lengths depends on the specific case. All reported cut-off lengths in previous studies are more than 2.5 mm and many of them are more than 10 mm. None of these studies used any of the cut-off lengths as specified by ISO standard.[35] Therefore, in this project, different cut-off lengths have been used according to the specific surface textures and measuring instrument techniques. The reasons for choosing those cut-off lengths will be explained in the corresponding context.

Various surface texture parameters can be used to compare surface profiles complying with the ISO standards. The most commonly used ones are briefly mentioned here. Arithmetic average roughness *Ra* (or waviness *Wa*) is the average value of the absolute values of all points of the profile, which is the universally recognized and most commonly used international parameter. *Rz* (or *Wz*) is the average height between five (typically) or six highest peaks and five lowest valleys within the evaluation length. Maximum peak to valley roughness *Rt* is the height between the maximum peak and lowest valley within the evaluation length.[8] One of the fundamental difficulties in defining surface texture is the fact

that a non-smooth surface cannot be described solely by a single surface texture parameter. Normally, several parameters are needed.[36] Even with these parameters defined, the drag characterization can still be complicated.[30]

In practice, to obtain an initial assessment of surface condition (thereby drag performance) of different FCCs, a quick and simple method is to measure the widely used hull roughness parameter *Rt(50)* which is defined as the height between the maximum peak and the lowest valley in any given length of 50 mm along the ship hull.[8] However, *Rt(50)* cannot be used to characterize a fouled surface.[36] Normally, the average hull roughness (AHR) is defined by conducting a number of mechanical roughness measurements (e.g., 100) of *Rt(50)* over the hull using a hull roughness gauge. However, the measured values of roughness parameters are subject to large variations due to random sampling (non-uniformity of roughness). Therefore, sufficient number of measurements should be done to obtain an accurate AHR.[37] Overall, it is still challenging to measure the hull roughness with fouling accurately.[38]

In summary, the effects of hull surface condition (including welding seams, coating surface condition with a focus on waviness) on drag resistance are the core of the present work. Their scales on a ship hull are illustrated in Figure 2.6. The welding seam height is normally within 3-9 mm with a width of about 15 mm. Waviness and roughness are differentiated using a cut-off wavelength (2.5 mm used in the figure). The waviness (height) is typically more than 0.1 mm and roughness (height) is below 0.1 mm.

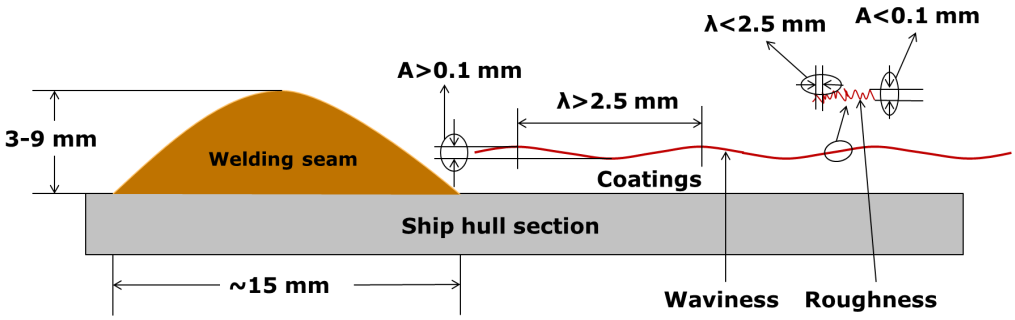

Figure 2.6 Schematic illustration of welding seam, coating surface waviness and roughness on a ship hull section and their approximate dimensions in reality. λ is the profile wavelength and A is the peak-to-valley height.

2.2.3 Effects on drag resistance of FCC surface condition

The FCC surface condition affects frictional resistance and thereby the drag resistance when the coating surface is still free of biofouling. Feedback from ship owners have shown that in real life they observe differences in drag and fuel consumption between newly applied AF and FR coatings after short sailing period (a few weeks without biofouling). Numerous studies have been conducted to compare their drag resistances.

Due to good spreading characteristics of the silicone elastomer, the surface texture of a FR coating is much less 'spiky' and it has lower peak-to-valley height compared to conventional AF coatings.[8] Besides, the tie-coat of FR coatings is already effectively leveling out the sharp characteristics of the anticorrosive sublayer before the surface texture is further decreased by the subsequent topcoat. Although tie-coats are also used for AF coatings, they are different types. It was also found that FR coatings were less negatively impacted by the substrate roughness compared to AF coatings.[3] Furthermore, Weinell *et al.*[24,39] found that FR coatings possess lower micro-roughness than AF coatings; however, macro-roughness (waviness) originating from the spray application and the subsequent leveling behavior were quite similar.

In addition, FR coatings were reported to have lower surface free energy, critical surface tension and polar components leading to weak interaction with polar molecules like water and an increase in surface hydrophobicity, compared to AF coatings.[16] On the other hand, CFD modeling has shown that turbulence caused by FR coatings is significantly less than AF coatings.[15] FR surfaces are capable of delaying transition from laminar to turbulent flow regime and reducing drag in turbulent flows by dampening turbulence production in the boundary layer.[6] CFD simulations were seen as a valuable tool to study the effects of hull surface irregularities on drag performance and it will be introduced further in a later section including the turbulent boundary layer.

Furthermore, it was found that FR coatings exhibited less drag in newly applied condition.[2,8] However, some studies reported that FR coatings led to higher drag than AF coatings, though the measured roughness of FR coatings was considerably lower than that of AF coatings.[26,40,41] The proposed reasons were the experimental uncertainties and the application method. Swain *et al.*[29] also revealed that the exposure conditions have influences on the drag performance and thereby the comparison between two FCC technologies. Therefore, due to different experimental conditions and uncertainties, the previous results were not comparable.

Meanwhile, various challenges exist in evaluating the drag performance of different FCCs in full-scale. One challenge is because it is rather time-consuming to perform full-scale measurements. Another

challenge in achieving a fair comparison of drag resistance among different FCCs in full-scale is due to that the exposure conditions a ship experiences is ever-changing. Furthermore, the surface conditions of newly applied FCCs have been shown to be poor predictors of long-term drag performance because it only reflects the drag performance without biofouling involved. This makes it more difficult to predict long-term drag performance in full-scale based on the lab-scale drag measurements of newly applied coatings.

2.2.4 Effects on drag resistance of surface irregularities on ship hull using CFD simulation

CFD simulation is an effective approach to investigate the effects of hull surface irregularities on drag resistance. However, relevant studies are rare and therefore only a basic overview is introduced here. In the early 2000s, strip theory was used for 80% of all seakeeping computations with its particular advantages.[42] The flow pattern around a ship hull could be simulated numerically and validated with experimental data by means of Reynolds Averaged Navier-Stokes (RANS), Large Eddy Simulation (LES) and Direct Numerical Solution (DNS). RANS has been widely used by shipbuilding industries.[43] Besides, various turbulence models are available, such as standard and realizable k-ε, standard k-ω, shear-stress transport k-ω (SST), and Spalart-Allmaras.

The experimental investigation was usually carried out using a flat plate based on the assumption of Froude[44] that the skin friction of a hull equals to a flat plate with the same length and wetted surface area. Recently, the effects of welding seams on drag resistance were studied by Ciortan and Bertram using CFD simulation approach.[45] Meshing and flow simulation were performed by using RANS solver in Star CCM+ CFD program. Unstructured mesh was mostly used though structured mesh may provide more precise results than unstructured mesh[46] because it is more complex to form structured meshes, especially when the geometry is complicated.

Turbulent boundary layer

At the hull (or wall), there is no relative motion between the fluid and the wall (the fluid velocity is zero), which is called no-slip condition. At some distance away from the wall, the mean velocity reaches its freestream value. Consequently, a velocity gradient is generated due to these two boundary conditions. The region in which this velocity gradient exists is called the boundary layer. Normally, a boundary layer is formed around a ship when it is in motion.

The concept of a turbulent boundary layer is essential to understand the flow patterns around a ship hull. Figure 2.7 shows a typical development of a turbulent boundary layer over a flat surface. In the boundary layer, the mean velocity U reaches the free-stream-velocity U_∞ asymptotically. The boundary layer thickness is conventionally defined as the distance from the wall where the local mean velocity U reaches $0.99U_\infty$. The flow is laminar at the first portion of a flat plate. When the flow continues across the plate or the ship hull, the flow becomes more and more turbulent in the short transition region. Eventually, the downward stream develops a highly turbulent region where the boundary layer thickness is steadily increased.

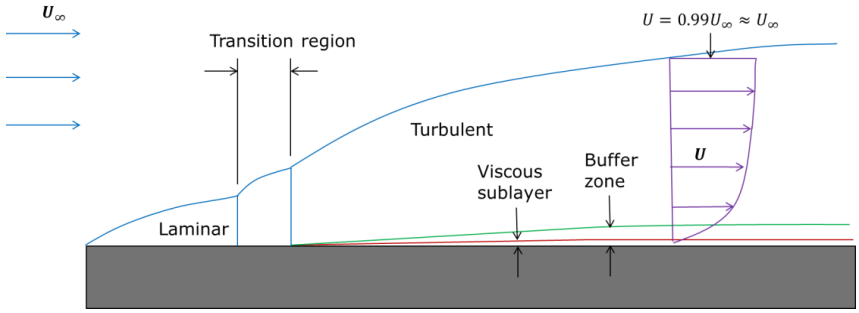

Figure 2.7 A typical development of a turbulent boundary layer over a flat surface. Modified from Demirel *et al.*[44]

Two main regions are assumed to be included in a turbulent boundary layer: an inner region and an outer region as shown in Figure 2.8. The inner region is composed of a viscous sublayer and a log-law region which only occupy 10 to 20% of the entire boundary layer thickness. Only the flow in the inner region can be affected by surface roughness. The average velocity in the inner region depends on wall shear stress, fluid density, kinematic viscosity and the distance from the wall.[44] The details about the theories of wall functions can be found in literature[41,47–49] and will not be covered here. The effects of surface roughness on turbulent boundary layers can be found in earlier work[20,44,50–52]

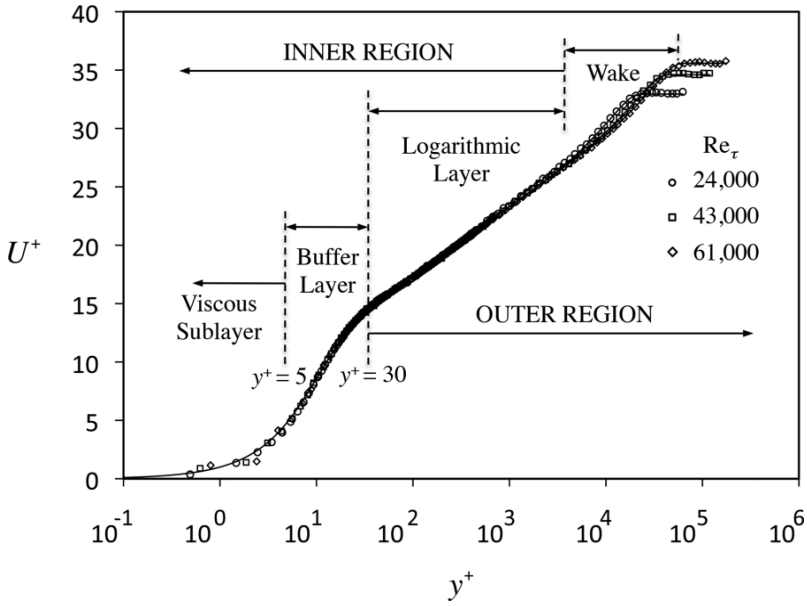

Figure 2.8 Velocity profile in a turbulent boundary layer. U^+ is the non-dimensional mean velocity and y^+ is the non-dimensional normal distance from the wall. Reprinted from Perlin *et al.*[53]

2.3 Coating leveling

A liquid film tends to level out itself to minimize its surface area and thereby the free surface energy. This physical phenomenon is called leveling which is driven mainly by the surface tension (the surface force decreasing the surface free energy of liquids and solids by minimizing the surface area to a flat surface). However, it is well known that when a coating is applied to a substrate, the dried coating film will not become completely flat depending on the leveling properties of the coatings as illustrated in Figure 2.9.

Figure 2.9 Dried FCC surfaces with good (left, FR coating) and poor (right, AF coating) leveling properties.

Surface unevenness on cured coating films is undesired not solely due to the poor esthetics. If the function of the coating is protection, an uneven coating may not provide adequate protection because the unevenness will constitute sites of weakness (starting points for corrosion, cracking, and blistering).[5] Furthermore, a rough surface will increase friction between coating surfaces and its surrounding fluids, which may cause unwanted impacts, for instance, cost. For FCCs, smoother coating surface may lead to less biofouling (thereby less drag resistance and fuel consumption), which depends on the preference of different marine organisms.

Therefore, a smoother coating surface could be achieved by improving the leveling properties of the coating. Coating industries are particularly interested in surface leveling properties because they determine the ultimate smoothness of the coating surface. As a result, it is of considerable importance to improve leveling properties of FCCs (especially conventional AF coatings) after application to reduce frictional resistance and the associated fuel consumption for marine vessels. Most FCCs are solvent-based coatings and they are typically applied by spraying in shipyards. Hence, to improve leveling properties of FCCs, those factors should be taken into account.

2.3.1 Review of previous leveling studies

The previous leveling studies are categorized and summarized in this section. The details of each study will not be elaborated much yet the important findings from the studies are briefly discussed below to introduce the reader to the field.

Leveling of non-volatile liquids with Newtonian rheology

After coating application with a brush, the initial brush marks will be left on the surface. After short while, those brush marks will level out and appear flat visually (actually the surface is not absolutely flat). This leveling phenomenon was explained in the well-known brush mark studies of Smith, Orchard and Rhind-Tutt[54] in 1961. Smith *et al.* proposed that leveling is driven mainly by surface tension and retarded by the viscous drag within the coating film. They also stated that the rate of leveling may depend on the geometry of the coating film (film thickness and application wavelength), surface tension and viscosity. Moreover, it was concluded that the influence of gravity may be neglected when the wavelength is less than about three mm.[54,55] Therefore, both high degree of pigmentation and quick drying will lead to poor leveling due to the associated high viscosity. Accordingly, it was inferred that leveling may be improved by adding small amount of high boiling solvent to retard the build-up of viscosity.

To continue studying leveling theoretically, Orchard assumed a sinusoidally structured liquid surface on a smooth substrate. Theoretical derivation based on an idealized sine wave surface profile was accepted as more accurate compared to a circular circumference profile according to the experimental findings, despite the slight inaccuracy introduced by a sine wave profile.[5]

Based on the assumptions of long wavelength, small amplitude, and constant average film thickness, the evolution of the amplitude of a sinusoidal profile from a_0 to a_t is given by Orchard[56] as

$$ln\left(\frac{a_0}{a_t}\right) = \frac{16\pi^4 h^3}{3\lambda^4}\int \frac{\sigma}{\eta} dt \tag{2.2}$$

where a_t and a_0 represent amplitudes at time t and initial time, h is the film thickness, λ is the wavelength, σ is the surface tension, and η is the viscosity of the coating. For an ideal case of constant σ and η, the above Equation (2.2) is simplified to the following Orchard equation

$$ln\left(\frac{a_0}{a_t}\right) = \frac{16\pi^4 \sigma h^3 t}{3\lambda^4 \eta} \tag{2.3}$$

Based on the Equation (2.3), high film thickness, surface tension and low wavelength and viscosity will lead to fast leveling rate and promote leveling. However, Patton[5] demonstrated that longer wavelength can result from higher film thickness as well, which means the wavelength and film thickness are interrelated.

However, the above studies were based only on the steady-state viscosity and did not take thixotropic effects and solvent loss (evaporation) into account. Therefore, their theories are only applicable to non-volatile liquids and Newtonian flow, far from non-Newtonian coatings rheology. Nevertheless, it has been shown experimentally that the Orchard theory is still valid if the ratio between the amplitude of the irregularities and the average film thickness is less than 20%.[55]

Leveling of non-volatile coatings with thixotropic rheology

Cohu and Magnin were the first to take thixotropic effect into account. They developed a five-parameter model by stepwise calculations based on Orchard theory.[55] The detailed model development will not be covered here and only the important findings will be briefly summarized below.

For non-evaporative coatings with thixotropic rheology, the viscosity increases over time during the leveling process for two reasons: 1) when leveling proceeds, the decrease of amplitude leads to the decrease of the stress within the film, which causes the increase of viscosity for shear-thinning fluids; 2) during coating application, high shear rates of about 10^4 to 10^6 s^{-1} may result in a high degree of structural breakdown and after application, the shear rates drop rapidly to 10^{-2}-10^{-1} s^{-1}, where thixotropic recovery occurs causing the increase of viscosity. The rheological properties of thixotropic coatings can be understood by considering the presence of weak networks which will present under zero or low shear rates and will be broken under high shear rates.[55]

Cohu and Magnin studied the thixotropic structural recovery, which occurred during leveling through step shear rate experiments using a Carrimed Weissenberg (shear rate controlled) rheometer. A high pre-shear rate was first imposed to the samples and instantaneously, a very low shear rate was applied as illustrated in Figure 2.10. The revolution of the shear stress was recorded during the low shear rate period to indicate the thixotropic recovery.

According to the obtained results, it was concluded that a pre-shear rate of 100 s^{-1} was enough to provide a structural breakdown and the high shear rate during the real application process would completely destroy any structure within the coatings.[55] They found a competition between structure recover and leveling after application. If the structure recovers too fast, the leveling process will be

stopped by the recovered yield stress. Yield stress can be understood as the lowest stress needed to give a non-zero velocity to the coating or the lowest stress that the coating needed to flow. Nevertheless, the existence of yield stress does not necessarily lead to imperfect leveling.[55] The effects of yield point will be discussed more in a later section.

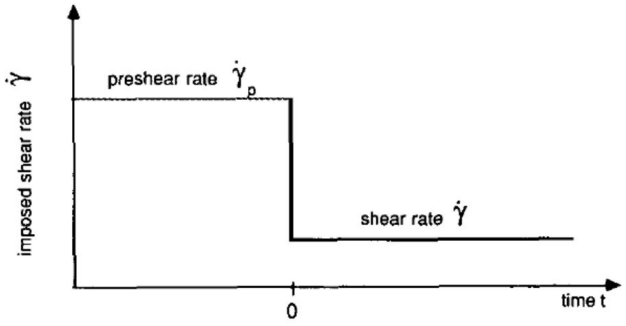

Figure 2.10 Typical step shear rate test. Reprinted from Cohu and Magnin[55]

Few studies regarding leveling of thixotropic liquids have been published. After the first thixotropic study of Cohu and Magnin, one more paper was published recently where the effect of thixotropy in the hydrodynamic behavior of thin films on a horizontal substrate was studied by Livescu *et al.*[57] Most recently, thixotropic effects were included in the leveling studies of automotive coatings[58] and in a systematic leveling study using both experiments and computational simulation,[59] which will be introduced in the later chapters with more details.

Leveling of solvent-based coatings

Overdiep[60] compared the non-volatile mineral oil with evaporative coatings and the experimental results showed a striking difference in leveling behavior between them. For the mineral oil, leveling process ended when the surface became flat which was in good agreement with the Orchard theory. However, the leveling process still continued for the evaporative coatings after the surface became flat, which was the so-called reversal phenomenon and could not be explained by the Orchard theory. As a result, Overdiep[60] proposed the existence of surface-tension-gradient (also called Marangoni effects) which might be caused by the non-uniformities in the concentration of solvent and he derived a model taking solvent evaporation into account.

Overdiep concluded that the increase in viscosity of air-drying coatings immediately after application was mainly controlled by solvent evaporation (physical drying) and to a minor extent by thixotropy.[60] The solvent evaporation profile of coatings was studied by Kiil[61] and the results showed that solvent evaporation rate of coatings was initially controlled by the external mass transport of solvent, and it depended on temperature, wind velocity and solvent concentration in the film and in the surrounding air. Later, the solvent evaporation rate went through a transition period where it rapidly decreased. This was attributed to the arising solvent diffusion resistance in the film due to the solidification of the top surface.

Along solvent evaporation, chemical curing, referring to two or more components react in a volatile solvent mixture, is another aspect that should be considered for leveling of thermoset coatings.[61] In this case, after application, solvent starts to evaporate and low-molecular-weight binders begin to react with curing agents. Crosslinking may occur and the viscosity will be increased due to both crosslinking and solvent evaporation.

Based on the theory of Overdiep, Wilson[62,63] has conducted further studies in leveling of solvent-based coatings to understand the physical mechanism behind. He proposed a systematic explanation of the reversal phenomenon and the surface-tension-gradient effects on leveling as follows.

Typically, solvent-based high-gloss alkyd paints (as a case study) consist of a non-volatile resin dissolved in volatile solvent and pure resin has a higher surface tension than pure solvent. In other words, the surface tension of the film is inversely proportional to the local concentration of solvent. The concentration of the solvent near the peaks relative to the concentration of the solvent near the valleys is higher as the solvent evaporates (the evaporation rate is higher at valleys, therefore the resin concentration increase faster there compared to that at peaks). Consequently, the surface tension at the peaks is lower than that at the valleys. Therefore, the resulting surface-tension-gradient drives the flow from peaks to valleys, which reinforces the leveling process. However, the imbalance in the solvent concentration still exists when the coating surface levels out and thus the observed reverse phenomenon occurs. Even though the initial film thickness is uniform, the reversal phenomenon will still occur if the solvent concentration is not homogeneous. Overall, the reversal phenomenon is caused by the initial non-uniformities in solvent concentration rather than inertia. The uniformity of solvent concentration is an important parameter for good leveling.

In addition, Wilson concluded that surface-tension-gradient effects could lead to a faster initial leveling rate than that due to surface tension effects and surface-tension-gradient effect itself was sufficient to explain the reversal phenomena in solvent-based coating.

Howison and co-workers[64] continued the model development work based on the studies of Wilson. One emphasis has also been given to the importance of achieving uniform solvent distribution at the beginning of the drying process. On the other hand, they proposed that solvent diffusivity was a strongly varying parameter which may change by several orders of magnitude as the solvent concentration varies. Actually, the diffusivity of solvent may decrease several orders of magnitude as the solvent concentration decreases from 1 to 0, which may be accompanied by a rapid increase in viscosity.

Other studies

Improving leveling properties is important not only for liquid coatings, but also for powder coatings.[65,66] The leveling of viscoelastic fluids was studied by Biermann[67] with a conclusion that viscoelasticity always has negative effects on leveling rate and this may partially explain why it is difficult for powder coating to level ideally since powder coatings have high viscoelasticity.

Besides coatings, leveling of other liquids, e.g., colloid suspensions[68] was investigated and leveling of coatings on different substrates, such as porous paper media[69] and curved surfaces[70] were also studied. Furthermore, the effects of surfactants on leveling behavior of thin coating films were discussed by Schwartz *et al.*[71] The presence of surfactants resulting in surface-tension-gradient forces was found to slow down the rate of leveling, which was in contradiction with the previous observations from Overdiep[60] and Wilson.[62,63] The effects of electrostatic charges on leveling of coatings were investigated as well,[72] more details can be found in the references[73,74]

Effects of yield point on leveling

Patton[5] found that the reduction in amplitude was fast at the beginning of leveling, followed by a sudden slowing and finally leveling stopped. The reason why the leveling rate was rapidly decreased was later explained by the high yield value or high viscosities at ultralow shear rates after application. At the beginning, leveling took place at a rate depending on the coefficient of viscosity until the stresses caused by surface tension were nowhere greater than the yield stress of the material.[75,76] In other words, when the shear stress induced by surface tension was below the yield point, leveling stopped. The negative effect of the existence of a yield point in leveling has been investigated by Camina and Howell[77] with conclusion that thixotropic coatings did not produce yield point within 300 s after application. Actually, yield value changes during the leveling process, increasing with the solid content. Therefore, it is rather

complicated and difficult to control yield values and the range of yield values for best leveling was suggested in the previous work.[78,79] In this case, making the system thixotropic might help.

Effects of spraying application on leveling

According to an expert specialized in spraying (Ciaran Dunbar) from Hempel, the following content was summarized (personal communication). During spraying application, some of the droplets touch the surface and bounce back, carried by eddy currents of air; some droplets fall out of the spray pattern under the force of gravity; some droplets miss the object being coated, which is called overspray. Commonly from spraying application, surface roughness may consist of bumps surrounded by valleys rather than ridges and valleys, which will result in the appearance of orange skins, called orange peel. The bumps are larger than spray droplets. The cause of orange peel appearance was found to be due to improper application and/or imbalanced formulation which gave rise to rapid evaporation generating strong convection currents in the coating film. Most commonly, it occurs when spray coatings have solvents with high evaporation rates.

Therefore, the above issues during spraying application may affect leveling performance and it is hard to completely avoid them practically. Besides, in real spraying application, the leveling performance can be affected by the operator's technique, the nozzle type, spraying speed, the distance between nozzle and the target surface, and weather conditions (such as temperature, humidity). Consequently, uncertainties during spraying application are high and uncontrollable.

2.3.2 Leveling related sagging problem

A liquid coating applied to a vertical surface tends to flow downward due to gravity, which is referred to the undesired sagging, running, draining and curtaining.[5] In terms of improving surface condition, sagging problem should also be considered because it may affect drag resistance more than leveling. As a result, it should always be minimized.

When a liquid coating is applied to a vertical surface, the coating film can be regarded as consisting of large quantities of thin layers. Each layer has a thickness of dx and the coating that is trying to slide down has a total film thickness of x and a surface area of one cm^2. The schematic diagrams of the sagging process after application are illustrated in Figure 2.11.[5]

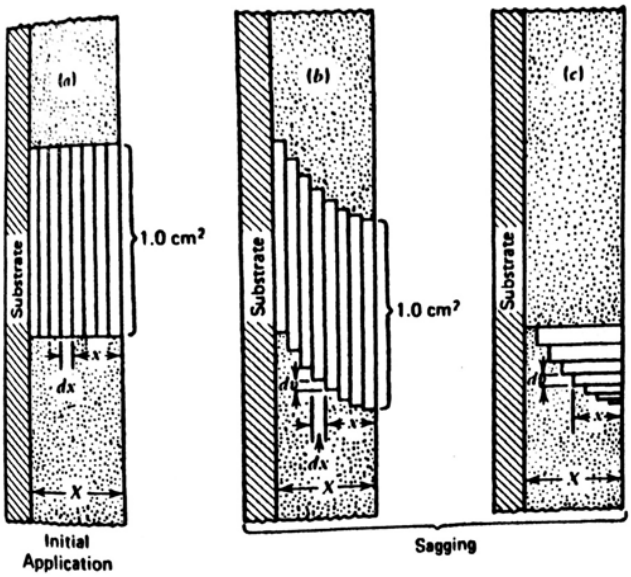

Figure 2.11 Schematic diagrams illustrating (a) coating surface geometry initially applied with uniform thickness to a vertical substrate, (b) coating geometry after sagging, (c) the incremental volumes of coating that sagged during sagging. Reprinted from Patton[5]

The driving force of sagging is gravity. The velocity of coating sagging on a surface v_0 can be approximated by

$$v_0 = \frac{\rho g X^2}{2\eta} \tag{2.4}$$

where ρ is the coating density, g is the acceleration of gravity, X is the total thickness of the applied coating film, η is the coating viscosity. The total volume of coating that sags V_s over a unit cross section of the film during time t is given as

$$V_s = \frac{\rho g t X^3}{3\eta} \tag{2.5}$$

On one hand, it can be seen from equation (2.5) that high film thickness and low viscosity will promote sagging. As presented in the previous section, high film thickness and low viscosity will promote leveling

as well. On the other hand, as aforementioned, during spraying application, the shear rate of coatings may go up to 10^4-10^6 s^{-1}. Immediately after application, coatings are subjected to a low shear rate range from less than 10^{-2} s^{-1} to 10^{-1} s^{-1}, where leveling occurs. Meanwhile, if the coating is applied to a vertical surface, sagging, due to gravitational effects, can also be important because the corresponding shear rate range where sagging takes place (about 10^{-2} to 1 s^{-1}) can overlap with that of leveling.[80] As a result, leveling (desired) and sagging (undesired) phenomena are coupled.

Consequently, the best way to improve leveling without causing sagging problem is to allow the viscosity to remain low for a short time while leveling forces predominate and the viscosity should build up rapidly when the leveling stress becomes lower than the sagging stress. In practice, this can be achieved by adjusting solvent evaporation rate or through thixotropic properties.[54] Hence, it is necessary to make the system thixotropic to obtain satisfactory leveling without excessive sagging, which can be obtained by adding coating additives that impart thixotropic effect. A moderate rate of thixotropic build-up is necessary to have good leveling and sagging properties. On the other hand, it has been concluded that shear-thinning systems are the most desirable ones for sagging control, leveling, and spray ability simultaneously. Even Newtonian systems fail to provide good sagging control and spray ability.[5]

2.3.3 Leveling measurements

The measurement of leveling has long been a challenge. Visual inspection or other subjective evaluations may easily be distorted by differences in hiding power and gloss[81] and it is a very qualitative way. Another method for qualitatively measuring the amplitude of the surface ripples on a liquid film was introduced by Camina and Howell[77] and used by Overdiep,[60] which will not be detailed here. The most commonly used methods are briefly discussed below.

One indirect approach for evaluating leveling is to study the rheological behavior (mainly viscosity profile) during leveling after application. In this case, the shear rates to which the coating is subjected in the actual application process and the subsequent leveling process should be duplicated. For instance, to obtain the viscosity changing profile during leveling, the shear rates should be changed from about 10^4 s^{-1} (representing spraying) down to 10^{-2}-10^{-1} s^{-1} (representing leveling). One example is the aforementioned work from Cohu and Magnin. However, it is difficult to obtain the actual viscosity changing profile during leveling because the shear rates during leveling are not constant and unknown. Moreover, measurement of viscosity as a function of time under those shear rates should also be feasible. Another challenge for viscosity measurement is that all tested samples should be subjected to the same shear

history, which is difficult to achieve because coatings are sensitive to pre-shear. For example, a pre-mixing of the coating sample before viscosity measurement will impose pre-shear to the sample which cannot be identical.

Another quantitative way to evaluate the final leveling performance is surface measurements using roughness measuring instruments by contacting the final dried surface. For instance, the dried surface profile can be measured with a Talysurf 4 instrument (or similar type of instruments) which is capable of measuring surface texture to a resolution of at least 0.025 μm.[81] However, this type of equipment is only feasible for dried film and can only evaluate the final leveling condition.

Dodge[81] used a threaded drawdown bar to achieve sufficiently high shear rates to represent real application. This drawdown technique was combined with profile measurement of the dried coating film, which was believed to provide not only a close duplication of the application and leveling processes but also a quantitative measurement of leveling free from the subjective factors of gloss and hiding power. However, it was still not possible to monitor the leveling process. The rheological technique using the Weissenberg Rheogoniometer was thought to provide a good way to measure the viscosity build-up following the high shear rate from application. However, this equipment was limited on the upper shear rate which can be used (centrifugation of coating from the cone and plate gap for shear rates greater than 2600 s^{-1} was observed). Nevertheless, more advanced rheometers were developed afterwards and are available commercially. By combining those techniques, Dodge concluded that any leveling process was nearly completed within 10-30 seconds after application. However, it has been pointed out that rotational rheometer does not provide a perfect simulation of leveling flows because the rotated rheometers impose large strains to samples and prevent the structure recovery during leveling.[55]

In addition, laser displacement transducer was used by Cohu and Magnin to measure the decay of film disturbances, film thickness and profiles, which may be a useful tool for leveling study.[55]

2.3.4 Summary

Within the evolution of leveling studies, the leveling phenomenon has become better understood, and it has been shown that more factors than previously thought influence the process. Due to the complexity of the leveling process and various intricate effects (such as solvent evaporation process and rheological effects) needed to be considered and involved in the mathematic models, it is not surprising that most of the previous studies have been focusing on one or a couple of effects on leveling.[82] In addition, sagging problem should always be controlled during leveling optimization, which reduces further the

possibilities of improving leveling. Furthermore, quantifying leveling properties and obtaining transient changes of each affecting parameter during leveling process has been a challenge. Consequently, it is rather challenging to improve leveling properties.

Nevertheless, there are still possible ways to optimize leveling. In summary, to improve leveling properties of AF coatings (most are solvent-based coatings with non-Newtonian rheology) which are applied by spraying application in shipyard without causing sagging problems, the following practical aspects should be considered:

- An offset should be found between film thickness and wavelength. Basically, the wavelength of the disturbance depends mainly on the application speed.[56]
- Higher solid content will lead to higher surface tension (only a few percent) for better leveling of solvent-based coatings; however, it will increase the viscosity which retards leveling. Therefore, it is barely feasible to increase surface tension.
- The initial solvent distribution should be as uniform as possible.
- Viscosity is the critical parameter which is possible to adjust. Overall, viscosity increases over time during leveling due to (a) solvent evaporation and (b) thixotropic effects (including shear-thinning behavior and thixotropic recovery). No chemical curing (crosslinking) occurs in conventional AF coatings. However, it is not clear what the controlling factor is. It is more likely these factors are interrelated and it would not be easy to isolate individual influences on leveling. Furthermore, solvent evaporation is also affected by temperature and weather conditions which are not controllable in practice (ambient temperature).

Practically, the principle control is viscosity. In this case, thixotropic effects are always desirable for controlling sagging and leveling. Meanwhile, thixotropic effects may offset the negative effects of yield point. On the other hand, the solvent evaporation rate can also be adjusted for viscosity build-up and thereby for better leveling performance.

Overall, the controlling of thixotropic effects and solvent evaporation should be optimized according to practical conditions and verified by large amounts of trial experiments. As a result, better leveling properties through optimizing coating formulation and/or spraying conditions for a particular AF coating can be finally identified. Although, challenging work needs to be done, it is still a very promising target to achieve optimum leveling conditions for AF coatings.

2.4 Conclusions

Based on the presented literature survey, the following conclusions can be drawn:

- Drag resistance is the main resource of fuel consumption and it should be minimized. Only the frictional resistance can be changed after the ship has been built and it can constitute up to 90% of the total drag resistance for marine vessels sailing at low speeds. Therefore, it is of significant importance to decrease the frictional resistance.
- Rough FCC surfaces (especially AF coatings) make substantial contribution to the frictional resistance. Hence, a main possibility to reduce frictional resistance is to improve the coating surface condition (mainly surface waviness).
- The effects of surface irregularities on drag resistance (e.g., welding seams) should be further investigated and CFD simulation may be a useful approach.
- Optimizing leveling is a potential approach to improve the coating surface condition. Although leveling process is rather complex, and some constraints in leveling measurements and the associated sagging problem exist, it is still possible to optimize leveling by controlling the relevant factors, mainly the viscosity.

3 Scientific hypotheses

This short chapter summarizes the scientific hypotheses of the research and the motivations and ideas behind those hypotheses based on the literature survey and practical interests of the companies. The overall hypothesis behind this project is that improving leveling properties of AF coatings leads to a lower coating surface waviness and thereby less drag resistance.

3.1 Hypotheses in drag force studies

To estimate the value of optimizing the AF coating surface conditions, *via* better leveling properties, it is necessary to study the drag resistance arising from the coating surface and correlate drag resistance with coating surface condition. Besides, it is well known that FR coatings have smoother surfaces than AF coatings, which indicates that FR coating surface condition can be an ideal target for improving leveling of AF coatings. Therefore, both FCC technologies should be investigated and compared in terms of drag resistance. Moreover, it is also important to determine the drag resistance arising from large surface irregularities to evaluate which source is the dominating one. Consequently, the following hypotheses were formulated:

(1) A pilot-scale rotary setup is sufficiently sensitive to detect the differences in drag resistance between AF and FR coating surfaces.

(2) Coating water absorption influences the FCC surfaces and thereby the drag resistance of FCCs.

(3) The effects on the overall drag resistance of welding seams on a ship hull are significant and comparable to those of FCC surfaces.

The first hypothesis originates from an idea of using the existing pilot-scale rotary setup for measuring drag forces (or more precisely torque values) and thereby enables a comparison of the drag resistances of two FCC technologies during various exposure scenarios.

Water absorption, to some extent, inevitably takes place in both AF and FR coatings. However, it is unknown how water absorption, which typically takes about a week to reach saturation, affects the FCC

surfaces and the drag resistance. If water absorption could change the FCC surfaces towards worse conditions, then improving the initial condition of the coating surface through optimizing leveling would become insignificant. Besides, the coatings are immersed in seawater for most of their lifetimes. Those facts led to the formulation of the second hypothesis and experiments with artificial seawater immersion and standard water absorption tests.

The third hypothesis concerns the overall drag resistance of a ship hull which arises not only due to coating surfaces but also surface irregularities. According to previous investigations from Weinell *et al.*,[24] large surface irregularities may actually affect drag resistance in a more severe way compared to coating surfaces. Thus, it was part of the present work, using a specially-designed flexible cylinder in the pilot plant, to study systematically the effects of welding seams (including both seam height and density) on drag resistance; and comparing the results with those obtained for FCC surfaces to identify which source is the dominating one to the drag resistance. To supplement the experiments, CFD simulations of weld seams were also conducted.

Overall, the above hypotheses and the corresponding investigations were seen to be essential for the following leveling studies because they helped to identify the importance and value of improving AF coating surface conditions through optimizing leveling.

3.2 Hypotheses in leveling studies

With respect to leveling studies, the following hypotheses were formulated:

(4) Coating formulation ingredients affect leveling properties of AF coatings.

(5) Leveling kinetics of AF coatings is mainly controlled by solvent evaporation and the simultaneous viscosity build-up.

(6) Leveling kinetics of AF coatings can be quantified using a universal mathematical model.

Coating leveling properties are expected to be related to rheological properties of the coating which are again affected by formulation ingredients. This can be confirmed via hypothesis (4). The ingredients considered in the present study were: binders and rosins, thixotropic agents, pigments, leveling additives, wetting agents, and solvents. The reason for studying binders and rosins, thixotropic agents, and pigments was that they may have direct influences on rheological properties of AF coatings. Therefore, their rheological effects were investigated. On the other hand, theoretically, wetting agents may help with pigment and solvent distribution in the coating matrix, which may promote leveling;

leveling additives may improve the flow ability of AF coatings and thereby leveling; less volatile (high boiling) solvents should slow down the build-up of viscosity and therefore leave more time for leveling.

Hypothesis (5) was stated considering that AF coatings are solvent-borne and no curing (crosslinking) occurs during the drying process. To test the hypothesis, solvent evaporation experiments were conducted.

In general, leveling is a physical phenomenon potentially affected by various coating and application parameters. It was of interest to study this experimentally, but also to see if it is possible to quantify the leveling kinetics by considering the driving forces and affecting parameters of the leveling process. As a result, hypothesis (6) was formulated.

4 Drag resistance of ship hulls with FCCs and welding seams

This chapter is composed of two parts. The first part is an article which has been published in the peer-reviewed journal *Journal of Coatings Technology and Research* as:

Wang, X., Olsen, S.M., Andres Martinez, E., Olsen, K.N., Kiil, S. Drag resistance of ship hulls: effects of surface roughness of newly applied fouling control coatings, coating water absorption, and welding seams. *Journal of Coatings Technology and Research* 2018, *15*(4), 657-669. DOI: 10.1007/s11998-018-0054-7

In addition, the effects of welding seams on drag resistance were further studied using CFD simulation approach, which is presented at the end of this chapter as the second part.

Abstract

Fouling control coatings (FCCs) and irregularities (e.g. welding seams) on ship hull surfaces have significant effects on the overall drag performance of ships. In this work, skin frictions of four newly applied FCCs were compared using a pilot-scale rotary setup. Particular attention was given to the effects of coating water absorption on skin friction. Furthermore, to investigate the effects of welding seam height and density (number of welding seams per five meters of ship side) on drag resistance, a new flexible rotor was designed and used for experimentation.

It was found, under the conditions selected, that a so-called fouling release (FR) coating caused approximately 5.6% less skin friction (torque) over time than traditional biocide-based antifouling (AF) coatings at a tangential speed of 12 knots. Furthermore, results of immersion experiments and supporting "standard" water absorption experiments showed that water absorption of the FR coating did not result in any significant impacts on skin friction. On the other hand, water absorption was found to actually lower the skin friction of AF coatings. This may be attributed to a smoothening of the coating surface.

The effects of welding seam height and density on drag resistance were found to be substantial when welding seam height is above 5 mm, especially at high tangential speeds (above 15 knots). Using an interpolation approach, the pilot-scale welding seam drag data could be used to estimate the drag resistance at approximated full-scale conditions, equivalent to about one welding seam per five meters of ship side. It was shown, in this case, that the contribution of welding seams to ship skin friction could very well be less significant than those of FCCs when the welding seam height is below 5 mm, a representative value for full-scale welding seam height.

4.1 Introduction

Marine biofouling is known as the undesirable accumulation of marine species, such as bacteria, algae, slime, seaweed, barnacles and tubeworms, on any surfaces immersed into seawater. It has long been a global challenge, in particular for the naval industry, because of both economic and environmental issues.[4,83,84] Consequences of biofouling have been elucidated in previous reports,[1,4,6] and one of the most important is the increased drag resistance which leads to a higher fuel consumption.

Drag resistance has been studied since the 1970s[23,24,39,51,85] and recently reviewed.[8] Previous investigations related to drag resistance have been mainly focused on evaluation of drag penalties,[86] prediction of drag resistance,[2] and drag characterization methods.[24,26,51,87] Among all, prediction of drag resistance is still a crucial topic.[2,46] The total drag resistance for a marine vessel is composed of three parts. The major part is skin friction, which accounts for 70-90% of the total drag resistance for slow trading ships (e.g. tankers) and typically less than 40% for faster trading ships (e.g. container ships).[8] The remaining part is primarily attributed to wave and eddy formation, the so-called residuary resistance. Air resistance, above the waterline, normally constitutes a minor portion of the total drag resistance, often 2% or less for slow trading ships and 10% or less for faster trading ships.[19] Schultz reported that the hull conditions, including coating roughness and biofouling, have direct effects on skin friction while the influence on residuary resistance is negligible.[88]

To prevent biofouling, a large number of potential methods have been investigated (see e.g. Swain[7], Callow[89]). However, so far, the most successful approach has been to apply FCCs to underwater ship hull surfaces. Two major fouling control coating technologies have been developed over the years. The conventional biocide based antifouling (AF) coatings release active compounds into seawater in a controlled manner; whereas the so-called fouling release (FR) coatings, which possess low surface energy, flexible mechanical properties and have smooth surfaces, minimize the adhesion between marine organisms and coating surface so that the marine organisms can be removed by hydrodynamic

forces during sailing or an occasional scrubbing. Their developing history and working mechanisms have been described in previous reviews[1,6,84] and will not be discussed in detail here. Recent findings on fouling control technologies are provided by e.g. Oikonomou *et al.*,[90] Yonehara *et al.*[91]

The newly applied FCC surface roughness is of primary importance to the drag performance of marine vehicles and the effects of coating surface roughness on skin friction have been investigated in previous studies[21,51] and detailed by Schultz and co-workers.[48,88,92] Schultz *et al.* also reported that skin friction can account for 90% of the total drag resistance when the coating surface is still free of fouling.[4] Therefore, it is of great interest to compare the effects of surface roughness of different newly applied FCCs on skin friction. Few relevant works have been published so far. Lindholdt *et al.*[2] mentioned that the skin friction difference is significant. Moreover, from ship owners, we have been informed that fuel consumption differences between two FCC technologies have been observed: ships applied with FR coatings consume less fuel than those with AF coatings and the effect can last for months until biofouling growth becomes decisive for the fuel consumption. Therefore, in this work, the skin friction among different newly applied FCCs will be compared and the influence of the difference will be evaluated economically.

Meanwhile, it is important to point out, that water absorption of FCCs is inevitable. Consequently, the drag performance of FCCs may be affected by water absorption of the coating film. However, no relevant studies have been reported so far. Therefore, to verify the hypothesis, the effects of water absorption of newly applied FCCs on skin friction will be investigated in the present work by conducting both immersion experiments and "standard" water absorption tests. From the immersion experiments, the effects of coating surface roughness of two FCC technologies on skin friction can be compared.

Another source of drag resistance is large surface irregularities formed on ship hull surfaces during the ship construction process. Compared to the effects of coating surface roughness on skin friction, large surface irregularities may affect drag resistance more significantly in a different way. An investigation by Weinell *et al.* showed that the contribution of hull coatings to skin friction is negligible compared to large surface irregularities.[24] Therefore, it is important to compare the contribution of coating surface roughness to the overall drag resistance with that of large surface irregularities. One common surface irregularity is welding seams which are normally formed on the ship hull surfaces when two steel plates are welded together, typically ending up with irregular shapes, even though welding seams are constructed according to different standards. The quality of welding seams varies, mainly depending on the welding seam height (from 3 to 9 mm) and welding seam density on the ship hull surfaces. Previously, the effects of welding seam height on drag resistance have been investigated using an approach of computational simulation.[45] However, no experimental work has been reported so far. Therefore, in the present work, the effects of both welding seam height and density on drag resistance

will be studied through an experimental approach. The effects of coating surface roughness on drag resistance will be compared to those of welding seams.

Experimental equipment for estimating drag resistance was summarized in the review by Lindholdt *et al.*[8] Setups with rotating cylinders have been used to estimate drag resistance[2,10,23,24] and will also be used in the present work. One of the main hypotheses is that the rotary setup is sensitive enough to small surface roughness changes so that the corresponding changes in skin friction of different FCCs, after water immersion, can be estimated and compared. The biofouling process will not be part of this work and only welding seams perpendicular to the water surface was considered because the horizontal welding seams have less significant effects on drag resistance.

4.2 Experimental setup

All drag resistance investigations were performed using a pilot-scale rotary setup as shown in Figure 4.1 (left), which contains two concentric cylinders with the inner cylinder rotating. The purpose is to create a close approximation to Couette-flow between two parallel walls of the two cylinders. In this case, one wall moves at a constant velocity and the wall shear stress is comparable to that of a real ship.[17] For further details on the setup see Weinell *et al.*[24] and Lindholdt *et al.*[2,8]

In the present investigation, fouling control coating samples were applied to the outer surface of cylindrical rotors as shown in Figure 4.1 (middle). Subsequently, the coated rotors were mounted onto the shaft of the rotary setup and then immersed into a tank (the diameter of the tank is 0.82 m) containing 600 liters of artificial seawater, following the preparation method descried by Lyman and Fleming.[93] This method was chosen as it is one of the most widely used recipes for artificial seawater. Demineralized water was added every week to the tank to compensate for water evaporation. A KEB frequency converter (type 12.F4.SIE-3440) was used to adjust the rotation speed. Due to heat generated from rotation of the rotor, the temperature of the seawater may increase, and this was avoided using water bath cooling. Isothermal conditions were attained by a cold water bath, which removed the heat generated from rotation of the rotor. The cold water bath is connected to a spiral pipe mounted near the inside wall of the tank. A torque sensor installed on the shaft recorded the torque values generated during the rotation. These values were used to estimate the drag resistance.

Torque measurements have been used to estimate drag resistance of objects and surfaces since the 1970s.[8,87] The conversion from values of torque to skin friction coefficients can be done using equations for wall shear stress, and an assumption of torque values being directly related to the wall shear stress.[2]

Therefore, even though no actual towing tank (“drag”) experiments were done in this work, we use the term “drag resistance” when we discuss the results.

Due to the fact that it was not possible to correct for the contribution to the torque from top and bottom surfaces, the outer shaft surface, and the presence of bearings for the welding seam rotor (introduced below), the total torque only was measured and later presented. This means that relative comparisons are possible. However the absolute drag (torque) values for the individual coatings and welding seams cannot be extracted.

Figure 4.1 The full pilot-scale rotary setup for drag resistance measurements (left), cylindrical rotor (made of polyvinyl chloride) used in the rotary setup (shown without a coating applied) (middle) and the flexible rotor (made of polyoxymethylen) with six artificial welding seams (made of polyvinyl chloride, the grey parts in the photo) on the outer surface (right).

4.2.1 Flexible cylinder

A flexible cylinder as shown in Figure 4.1 (right), was designed to simulate welding seams on ship hull surfaces. The dimension of the flexible cylinder is 0.3 m in diameter and 0.31 m in height. The diameter of the outer static cylinder (not shown) mounted inside the tank is 0.38 m. Therefore, the gap between the flexible cylinder and the outer static cylinder is 40 mm. The artificial welding seams were constructed with a width of 15 mm according to the information provided by A.P. Møller - Mærsk A/S. Four welding seam heights (0, 3, 5 and 9 mm) were used in the study. The cylinder without welding seams (height=0 mm) was used as reference. The artificial welding seams were attached to the cylinder

via grooves cut into the cylinder and with two fixation bolts at each end. A maximum of eight welding seams can be used on the cylinder. The materials of the flexible cylinder and the artificial welding seams are polyoxymethylen and polyvinyl chloride (PVC), respectively.

The flexible rotor allows investigating the effects of both welding seam height and density on drag resistance. Basically, the density of the welding seams was controlled by the number of welding seams mounted on the outer cylinder surface. For reasons of balance, the number of welding seams on the rotor could be 0, 2, 4, 6 and 8, corresponding to welding seam densities of 0, 10, 20, 30 and 40 welding seams per 5 m ship side, respectively. The unit for welding seam density was chosen for convenience of comparison between lab-scale and full-scale. The aforementioned welding seam densities (except zero) are much higher than that on full-scale ships (typically one welding seam per 5 m ship side) because the welding seam density is limited by the relative short circumference of the rotor cylinder. However, as it will be further discussed in the results and discussion section, it is possible to interpolate between data points to find the relevant full-scale drag resistance values. Note, that the welding seam density in the ship bow region can be high with 2 to 3 welding seams per 5 m.

The somewhat irregular welding seams found on real ship hull surfaces were approximated by an arc shape as shown in Figure 4.1 (right). It was assumed that the welding seams on the flexible rotor do not affect each other and that the cylindrical geometry has no effect on drag resistance (relative to flat plate geometry as on ships). The latter assumption is reasonable as discussed in Lindholdt *et al.*[8] However, the former is questionable when going to high welding seam densities[94] and will be discussed further in a later paragraph. During the experiments with welding seams, no coating was applied on the flexible rotor cylinder surfaces.

4.3 Materials and experimental procedures

4.3.1 Seawater immersion experiments

Four commercial fouling control coating formulas were investigated, as listed in Table 4.1, with the purpose of comparing two fouling control coating technologies (AF and FR coatings) and investigating the effects of water absorption on skin friction using the pilot-scale rotary setup. Hempaguard X7 acts as a FR coating, while the other three are AF coatings. In all coatings used, xylene was the main solvent. Acrylic binders and rosins were used in three AF coatings. Besides, three AF coatings contain bioactive pigments (mainly cuprous oxide) and coloring pigments (mainly iron oxide). Hempaguard X7 contains silicone as binder and a small amount of copper pyrithione as bioactive pigment. The sample of Hempaguard X7 was composed of two layers of coatings, one layer of tie-coat followed by one layer of

silicone topcoat. The sample of Dynamic was comprised of one layer of tie-coat followed by two layers of antifouling topcoat. Globic 9000 and Olympic+ included one layer of tie-coat and one layer of antifouling topcoat. The temperature was controlled by a water cooling bath and fluctuated ±2°C during the experiments. It was assumed that the temperature fluctuation was too small to affect the measurements.

Table 4.1 Immersion conditions for each of the studied commercial FCCs.

Fouling control coating samples	Tangential speed (RPM)	Temperature (°C)	Immersion time (Days)
Hempaguard X7 89900 (FR)	400±1	20±2	49
Hempel's Antifouling Dynamic 79580 (AF)	400±1	20±2	49
Hempel's Antifouling Globic 9000 78900 (AF)	400±1	19±2	50
Hempel's Antifouling Olympic+ 72900 (AF)	400±1	19±2	50

The four fouling control coating samples were sprayed (airless) manually on four PVC cylinders by the same person and left to dry at room temperature. The immersion started after they were fully dried/cured (approximately one week). Once immersed, the initial skin frictions were measured immediately and their torque values at various tangential speeds were obtained. After the first measurement, each sample was measured almost once per day in the first week. Afterwards, each sample was measured every two or three days. All the rotors were immersed statically and rotated only when measurements took place. Notice, that only one cylinder for each coating was prepared and at least three repetitions were done for each coated cylinder to obtain standard deviations for the daily measurements.

4.3.2 "Standard" water absorption tests

Water absorption experiments were conducted for samples Hempaguard X7, Dynamic and Globic 9000. The coating samples of Dynamic and Globic 9000 were applied on polycarbonate panels without primer by a Doctor Blade applicator. The sample of Hempaguard X7 was applied with a primer. The gap of the applicator blade used was 300 μm for all samples. Afterwards, for the Dynamic and Globic 9000 coating samples, the panels were dried for 24 h at room temperature followed by 72 h at 45°C; for the Hempaguard X7 coating sample, the panel was dried for several days at room temperature followed by

72 h at 45°C. For each coating formula, three replicates were conducted. A blank panel was used as reference because the panel itself absorbs water. Artificial seawater (the same as used in the above mentioned immersion experiments) was used for all the experiments. The temperature used for absorption was 23°C and for desorption it was 60°C.

The principle of the water absorption experiments is to weigh the panels regularly to calculate the water uptake. It should be noticed that soluble ingredients in AF coatings (e.g. cuprous oxide) will dissolve and be released during the immersion. All the panels were immersed statically for 28 days in total and weighed once per day in the first three days. After one week, the coated samples were weighed only once a week. For convenience of comparison, the unit of the water absorption was taken as g/(m^2 of coating).

4.3.3 Welding seam experiments

To determine the effects of welding seam height and density on drag resistance and compare with the effects of FCCs, a series of welding seam experiments were performed using the new flexible cylinder with the pilot-scale setup (Table 4.2).

For each welding seam height experiment, 2, 4, 6 and 8 welding seams were attached to the flexible cylinder and studied individually. Non-used empty grooves were filled with welding seams of zero mm height as shown for one of the seams in Figure 4.1 (right). For welding height of zero mm, all 8 welding seams must be attached. For verification, the original intact cylinder with a smooth surface before cutting was also measured at each speed. The differences between the intact cylinder and the cylinder with 8 welding seams of zero mm are the joint lines after welding seams are mounted into grooves.

Table 4.2 The experimental series for the flexible rotor under conditions of approximated Couette-flow (14 experiments).

Welding height (mm)	Welding seam numbers			
0	0 (the intact cylinder)		8	
3	2	4	6	8
5	2	4	6	8
9	2	4	6	8

For each experiment, various tangential speeds were applied up to 20 knots and three replicates were performed at each speed. Note that speed indications refer to tangential speeds rather than ship speeds. The Reynolds number for approximated Couette-flow at 20°C was calculated based on the equation described by Arpaci and Larsen[95] and found to be 59810 for 100 RPM (corresponding to a tangential speed of 1.57 m/s or 3.05 knots). Therefore, the flow is turbulent.[96]

The gap between the parallel walls of the two cylinders is 40 mm which is relatively small considering the highest welding height of 9 mm. For further validation, the effects of FCCs measured under approximated Couette-flow condition were compared with experiments performed in the absence of the outer cylinder (Table 4.3), in which case the distance from the tank wall to the cylinder wall was 0.26 m.

Table 4.3 The experimental series for the flexible rotor without the outer cylinder (5 experiments).

Welding height (mm)	Welding seams numbers	
0	8	
5	2	8
9	2	8

4.4 Results and discussion

In this section, the transient effects of water absorption of FCCs on skin friction are presented and discussed. In addition, skin friction of two commercialized fouling control technologies is compared at newly applied coating conditions. Furthermore, the effects of welding seam height and density on drag resistance are demonstrated and discussed. Finally, the effects of welding seams and FCCs on drag resistance are compared at full-scale conditions.

4.4.1 Seawater immersion experiments and "standard" water absorption tests

To investigate the effects of water absorption of FCCs on skin friction and compare the skin friction of two commercialized antifouling technologies, seawater immersion experiments and "standard" water absorption tests were conducted. Results of the seawater immersion experiments are shown in Figures 4.2 and 4.3 and those of water absorption tests in Figure 4.4. Each data point is the average of three replicates and the standard deviations from the three replicates are indicated by the error bars shown in

Figure 4.4. The standard deviations represented by error bars as shown in Figure 4.2 and 4.3 are from three repetitions of the torque measurements.

Figure 4.2 shows that Hempaguard X7 gives a smaller torque than Dynamic and the average torque value of Hempaguard X7 over time (around 5.1 Nm) is approximately 5.6% less than that of Dynamic (around 5.4 Nm) at a tangential speed of 12 knots. Therefore, it can be roughly estimated that in real life conditions, newly applied FR coatings cause less skin friction than newly applied AF coatings at the same sailing speed, which is also in agreement with observations from Lindholdt *et al.*[2] and Mirabedini *et al.*[16]

Furthermore, it can be seen in Figure 4.2 that the torque values of Hempaguard X7 did not vary significantly during immersion despite of some fluctuations. On the other hand, the water absorption amount of Hempaguard X7 is substantial as shown in Figure 4.4. Therefore, it can be inferred that although water absorption of newly applied FR coatings occurs, the surface of FR coatings will not be subjected to prominent changes and the skin friction will not be significantly affected.

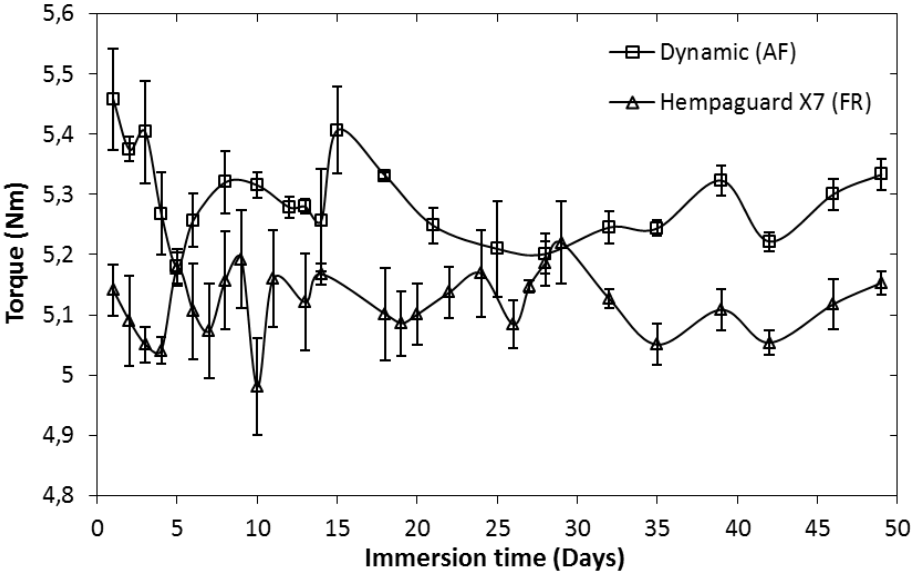

Figure 4.2 The average torque values of daily measurements for the newly applied Hempaguard X7 and Dynamic coatings during their entire immersion periods at a temperature of 20±2°C and a tangential speed of 400±1 RPM (approximately 12 knots). The error bars shown represent the standard deviations of the torque measurements (at least three repetitions were used for each coated cylinder).

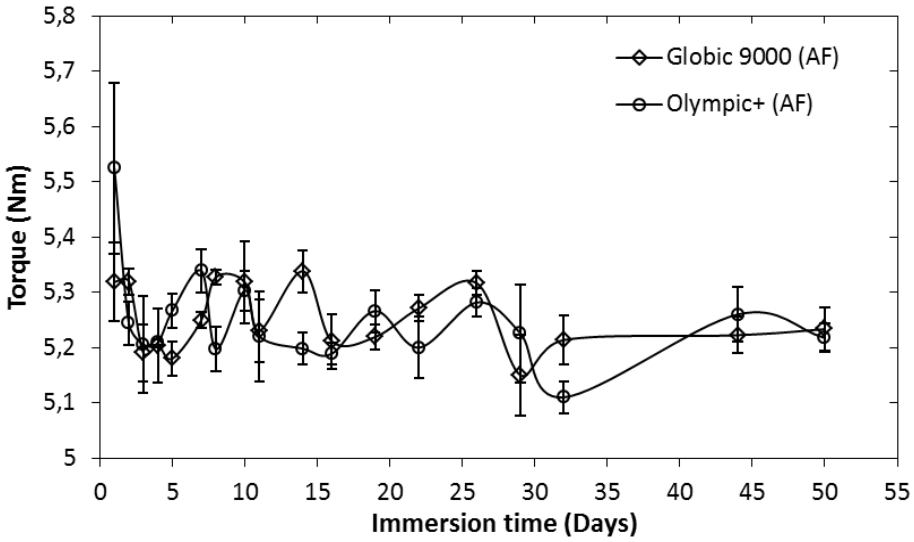

Figure 4.3 The average torque values of daily measurements for the newly applied Globic 9000 and Olympic+ coatings during their entire immersion periods at a temperature of 19±2°C and a tangential speed of 400±1 RPM (approximately 12 knots). The error bars shown represent the standard deviations of the torque measurements (at least three repetitions were used for each coated cylinder).

However, a torque drop (around 0.3 Nm) is observed during the first five immersion days for the three AF coating samples as shown in Figures 4.2 and 4.3. This can be seen as a self-smoothening process. Meanwhile, the amount of water absorption of the AF coatings was found to be prominent in the first week of immersion as shown in Figure 4.4. Therefore, we believe that water absorption most likely acted as the trigger for the reduction in torque. Water absorption may cause swelling of the wetted coating surface, which may smooth the initial surface imperfections. Another possible reason could be that water absorption triggers the polishing process, as explained below, and that the polishing can have a higher impact on the more exposed areas.

After immersion, water will penetrate into the AF coating film and soluble compounds of AF coatings will be gradually dissolved and released into water. Hence, the increasing amount of absorbed water in the first week of immersion observed in Figure 4.4 may be attributed to the water absorption amount being accumulated faster than the release of soluble compounds. After one week, the paths inside the

coating film available for water to penetrate are saturated and therefore further water absorption stops. Water absorption and the release of soluble compounds may equilibrate.

Furthermore, after the release of the soluble compounds from the AF coating film, a porous leached layer will be formed gradually at the coating-water interface.[10] During the rotation in the immersion experiments, the leached layer formed may be polished away if sufficiently vulnerable because of the velocity-dependency.[9,17] After polishing, a new front layer will be exposed to seawater. No polishing is expected in the "standard" water absorption experiments because the samples were immersed stagnantly in seawater.

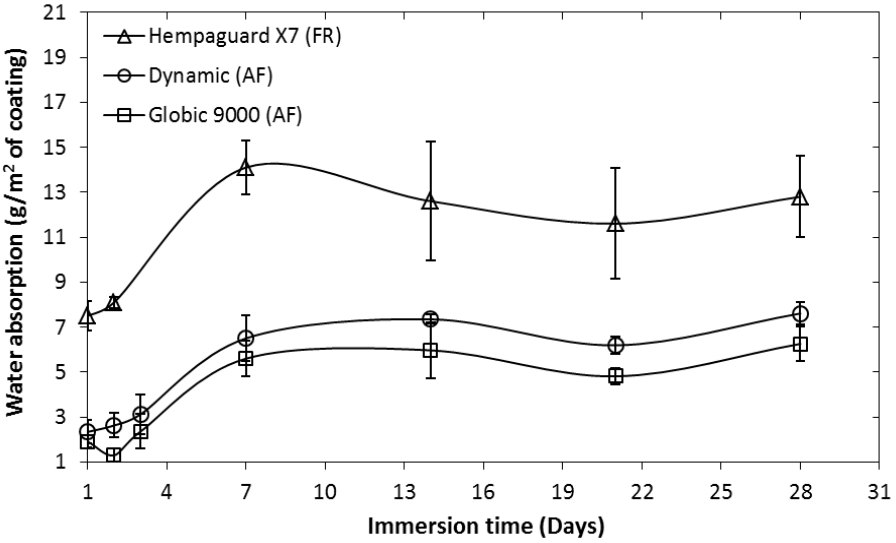

Figure 4.4 Water absorption of Hempaguard X7, Dynamic and Globic 9000 coatings as a function of immersion time. Each data point is the average value of three replicates. The error bar for each data point shown is obtained from the standard deviation of three replicates.

As mentioned earlier, Hempaguard X7 contains small amount of biocides which have extremely low solubility in artificial seawater where the samples were immersed. Consequently, most of the biocides in Hempaguard X7 will not dissolve during the experimentation period. That is one of the reasons why it has higher water absorption compared to the two AF coatings as shown in Figure 4.4. However, the main reason for the big difference in water absorption is a distinct difference in the binders and generic

technologies between FR and AF coatings. After the first week of immersion, Hempaguard X7 reached the maximum water absorption (saturation), and no further water ingress took place.

4.4.2 Welding seam experiments

To determine the effects of welding seam height and density on drag resistance and compare with the effects of FCCs, a series of welding seam experiments were performed using the flexible cylinder. The results are shown in Figures 4.5-4.12. Each data point is the average of three replicates and the standard deviations from the three replicates are indicated by error bars shown in Figures 4.5-4.8 and 4.10, however, note that most error bars are too small to be seen.

Two experiments were performed for a welding height of zero mm to allow comparison with a smooth reference and to evaluate any effects on drag resistance of the new joint lines after the welding seams were mounted into the grooves. The first experiment was conducted using the intact rotor cylinder before the grooves were cut and the second was performed using the rotor cylinder after mounting eight welding seams with welding height of zero mm to the grooves. The results of the two experiments are shown in Figure 4.5.

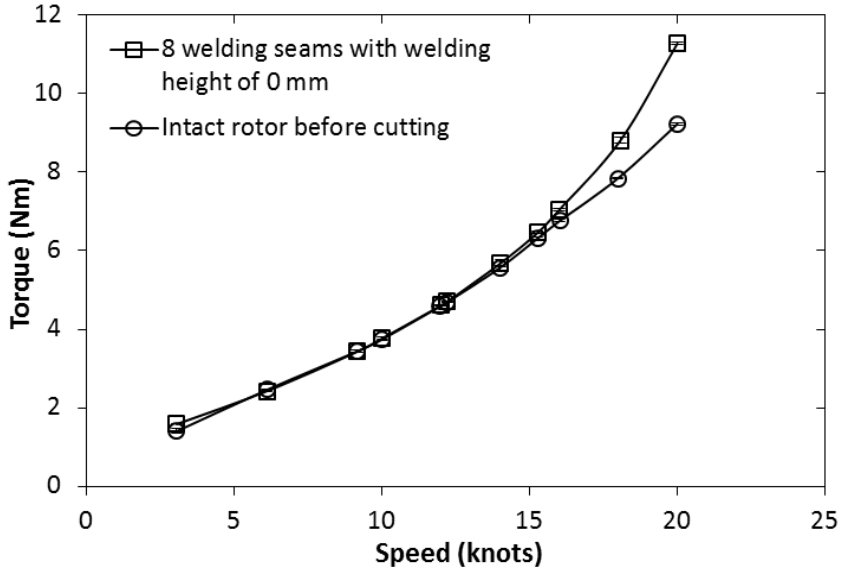

Figure 4.5 Comparison of torque values between the two experiments for a welding height of zero mm.

It can be seen in Figure 4.5 that the torque values are nearly the same in the two experiments when the tangential speed is within the range of 5-15 knots, while some deviations are evident at higher speeds. Therefore, the rotary setup is sensitive to very small surface changes. Furthermore, the impact of surface obstacles on torque becomes more significant at high speeds.

The effects of welding height on torque measurements are shown in Figure 4.6. Clearly, torque values increase when the welding height and the tangential speed are increased. Similar results were found for welding seam numbers of 2, 4, and 6 (not shown).

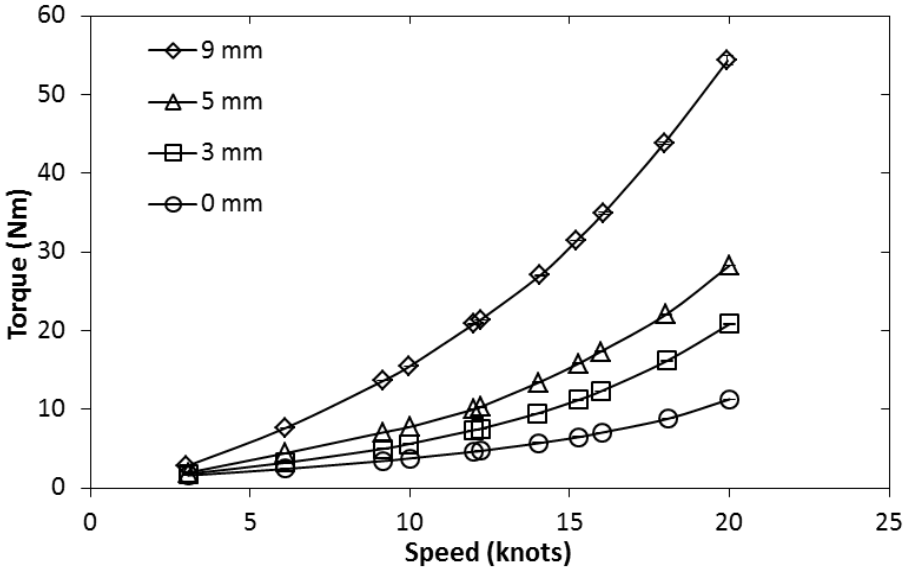

Figure 4.6 Torque values measured for different welding seam heights (0, 3, 5, 9 mm) with 8 welding seams mounted as a function of tangential speed.

The effects of welding seam density on drag resistance were studied as well and the results are shown in Figure 4.7 for a welding height of 9 mm (left) and 3 mm (right). Density is seen to have a strong influence on the torque values, especially at high speeds. Furthermore, when the welding height is 9 mm, the effect of welding seam density is most significant when welding seam density is increased from 10 to 20 welding seams per 5 m, which can also be seen in Figure 4.8. However, when the welding height is decreased to 3 mm, the incremental of torque is consistent when the welding seam density is

increased linearly. This can be explained by the welding seams interacting with each other as the seam density is increased. When the welding seam height is 9 mm, there is a clear "shielding effect" (i.e. each welding seam shields the one behind it). When the welding height is decreased to 3 mm, the "shielding effect" is weakened. Therefore, the aforementioned assumption, that the welding seams do not affect each other, is not very important when the welding seam height is ≤ 5 mm.

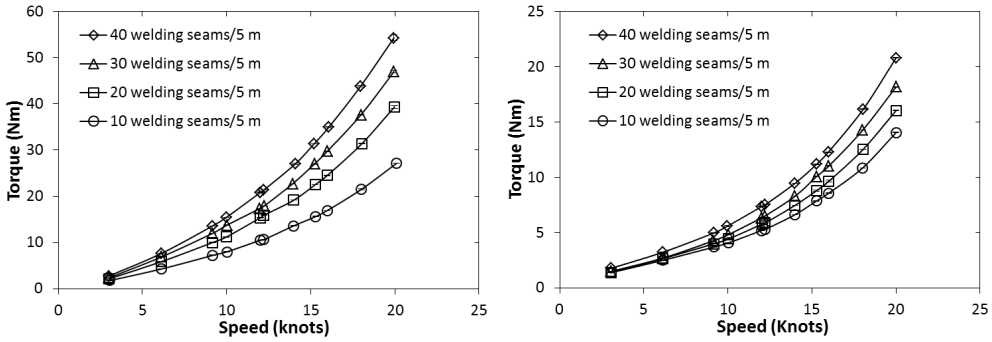

Figure 4.7 Torque values of different welding seam densities (10, 20, 30 and 40 welding seams/5 m) with a welding height of 9 mm (left) and 3 mm (right) as a function of tangential speed.

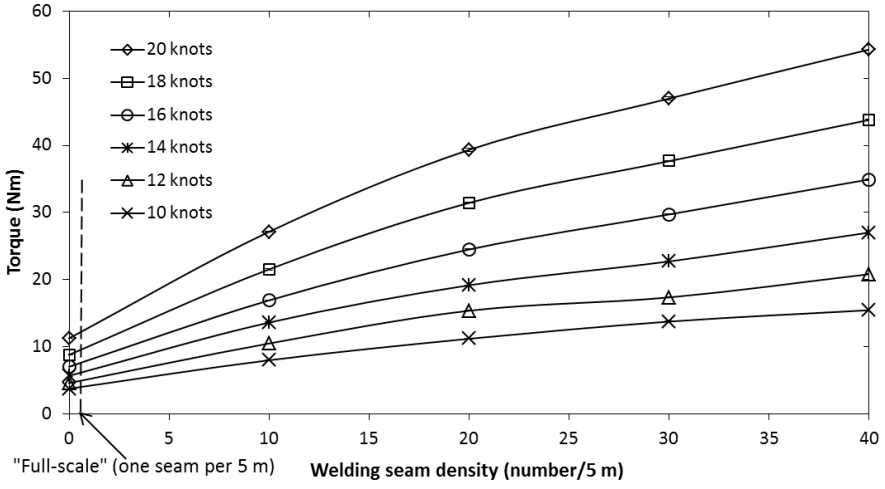

Figure 4.8 Torque values at different tangential speeds for a welding height of 9 mm as a function of welding seam density. The dashed line indicates a welding seam density of one welding seam per 5 m ship side, corresponding to a typical full-scale value.

To obtain torque values estimating typical full-scale conditions, the data from Figure 4.7 have been plotted with welding seam density on the x-axis as shown in Figure 4.8. Using an interpolation approach and assuming a linear curve between 0 and 10 welding seams per 5 m, the "full-scale" values can be very crudely estimated, as indicated in the figure, where the vertical dashed line intersects the different curves. This was also done for welding heights of 3 and 5 mm and the interpolated data are shown in Figure 4.9. The effects of welding seam height on torque are not significant when the height is below 5 mm, which is consistent with the results shown in Figure 4.6. If the welding seam height is decreased from 9 to 5 mm, the torque value is decreased 8.4% at a tangential speed of 20 knots.

It should be noted that this interpolation approach can only give a crude and qualitative estimate of the full-scale values. A quantitative approach requires the same geometry of the object (cylindrical or flat ship side) and a similarity analysis that ensures the same flow conditions over the surface. It is not possible to exactly meet those requirements with the cylindrical rotary setup.

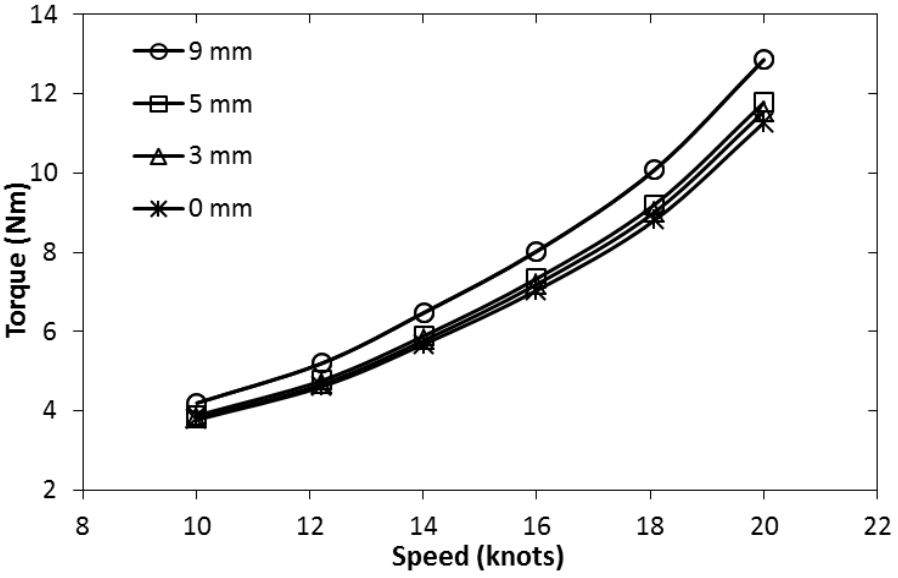

Figure 4.9 Interpolated torque values of different welding seam heights at full-scale welding seam density (one welding seam per 5 m ship side) as a function of tangential speed.

As discussed previously for Figure 4.7, the assumption of individual welding seams not affecting the flow around other seams becomes questionable when the welding seam density is increased to high numbers. This could be the reason why the slopes of the lines in Figure 4.8 start to decrease from somewhere between 10 and 15 seams/(5 m). Interaction effects should lead to less friction because the seams "shield" each other. However, this was not investigated any further because the most interesting part of the plot is the approximated full-scale conditions at very low seam density.

Experimental data for the case where the outer cylinder was absent are compared with those where the outer cylinder was present in Figure 4.10 and 4.11. Figure 4.10 shows that the torque values of all welding seam heights are increased after removing the outer cylinder, which is most likely due to a stronger turbulence effect. The flow is now far from Couette-flow and the rotation speed could not exceed 16 knots for the 9 mm case because of prohibitive turbulence levels. Consequently, the interpolated torque values of all welding seam heights at full-scale welding seam density are increased as shown in Figure 4.11, especially at high speeds.

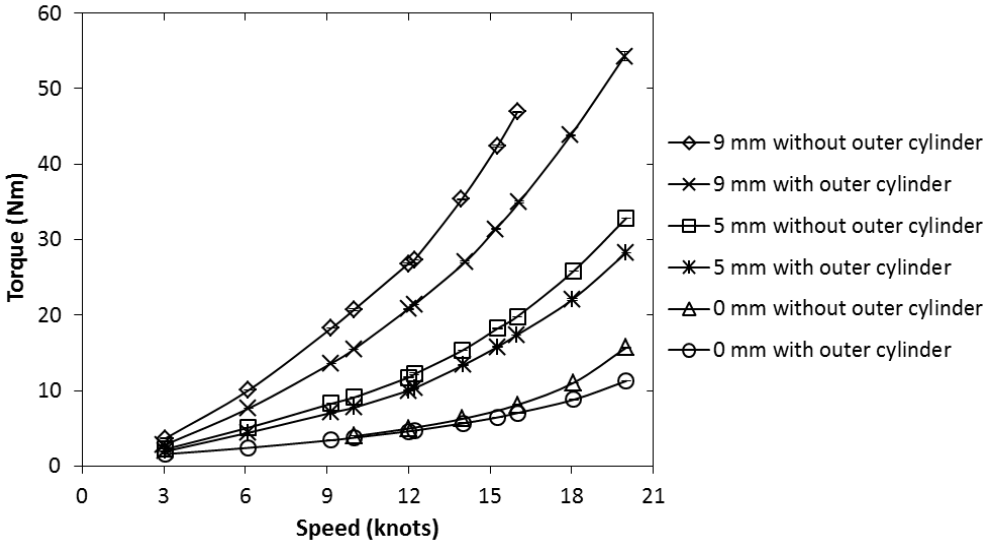

Figure 4.10 Comparison of torque values before and after removing the outer cylinder for welding seam heights of 0, 5 and 9 mm with 8 welding seams mounted as a function of tangential speed.

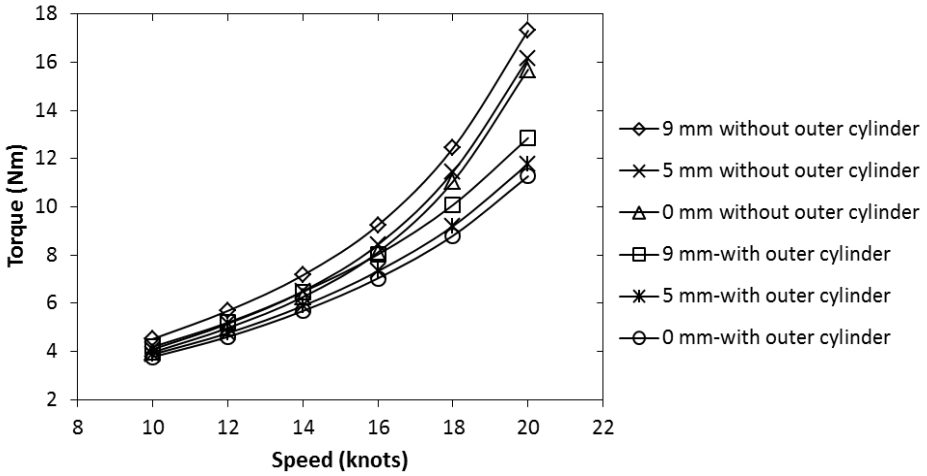

Figure 4.11 Comparison of interpolated torque values (to approximated full-scale conditions) before and after removing the outer cylinder for welding seam heights of 0, 5 and 9 mm at full-scale welding seam density (one welding seam per 5 m ship side) as a function of tangential speed.

4.4.3 Comparison of effects of coatings and welding seams on drag resistance

To compare the effects of welding seams and FCCs on drag resistance, torque values at a tangential speed of 12 knots have been summarized in Figure 4.12. Data points for FCCs were estimated from the results of immersion experiments. It can be seen that at full-scale welding seam density, the torque values of all cylinders with FCCs are higher than those of smooth cylinders with welding seams when welding seam height is below 5 mm. Furthermore, when welding seam height is 9 mm, the torque values of all cylinders with FCCs are still equal to or higher than those of smooth cylinders with welding seams except for Hempaguard X7. Therefore, considering that the welding seam height is normally not above 5 mm, when following the European shipyard standard, both AF coatings and FR coatings will cause more drag resistance than welding seams at full-scale conditions. This is a consequence of the larger surface area taken up by coatings relative to welding seams. Notice that the torque values of FCCs were estimated from the immersion experiments at one speed only and further evidence at other speeds are needed for a more detailed analysis.

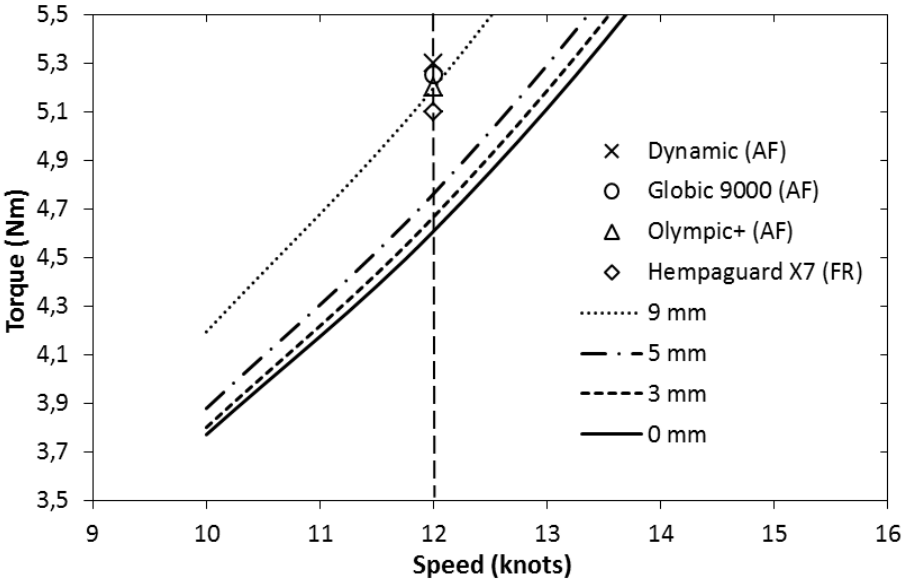

Figure 4.12 Comparison between torque values for different welding seam heights (Couette-flow) at full-scale welding seam density (one welding seam per 5 m ship side) and the experimental torque values of different FCCs (in the absence of welding seams) at a tangential speed of 12 knots (indicated by the dashed line).

4.5 Conclusions

In the present work, the effects of water absorption of FCCs and the presence of welding seams on drag resistance have been investigated using a pilot-scale setup with rotating cylinders. The rotary setup was found to be sufficiently sensitive to detect the impact of small changes in surface morphology on the cylinder on drag resistance and therefore the differences in drag resistance between two fouling control coating technologies were determined. It was found that the newly applied FR coating, over time, caused approximately 5.6% less skin friction (torque) than the newly applied AF coatings at a tangential speed of 12 knots. This means that ship owners, in the initial period of ship use when the ship hull surface is still free of biofouling, can save fuel by using FR coatings instead of AF coatings. Besides, water absorption amounts for both FR and AF coatings were found to be significant. The effects of water absorption of the newly applied FR coating on skin friction were found to be insignificant and water

absorption lowered the skin friction of the newly applied AF coatings, which are crucial for FCCs because they are exposed to seawater for most of their life spans.

A flexible rotating cylinder was used to provide crude estimations of the effects of welding seam height and density on drag resistance at approximate "full-scale" conditions. It was found that the effects of welding height and density on drag resistance were significant, especially at high speeds. Besides, welding seams could interact with each other. Based on the results obtained, it was suggested that welding seam height should be controlled to less than 5 mm when ships are constructed in shipyards. This will minimize the negative effects from both welding seam height and density, especially for ships scheduled to sail at high speeds (more than 15 knots of tangential speed). Accordingly, considerable economic benefits can be achieved. Furthermore, when welding seam height is below 5 mm at full-scale conditions, FCCs were found to result in a higher drag resistance than that of welding seams at a tangential speed of 12 knots. On real ships, to reduce the impacts of welding seams, these can be ground. The economic savings related to drag reduction from grinding will be significant for welding seams of heights above 5 mm.

4.6 Further work with CFD simulations of welding seams on ship hulls

The effects of welding seams on drag resistance of ship hulls were further investigated using CFD simulation and the results are briefly presented in this section of the chapter.

4.6.1 Methods

Sketches of welding seams on the ship hulls were generated using SOLIDWORKS. Structured mesh was adopted for its high accuracy in computation using ICEM CFD 17.0. All numerical simulations were performed using ANSYS CFX 17.0.

A welding seam was represented by an arc of a circle and only butt welds perpendicular to the water flow direction were simulated on a flat plate. A ship hull section was simulated as a plate field of 5000 mm in length and 100 mm in height. The fluid width was 1000 mm to capture the turbulent boundary layer. One welding seam was located in the middle of the plate. The number of plates (thereby welding seams) was duplicated into 2, 3, and 6. Therefore, the distance between two welding seams was 5000 mm which is a typical value for container ships according to the information provided by Maersk Line. Thus, it was the same full-scale seam density (one welding seam per five meters of ship side) as used in the previous experimental investigations. Initially, the welding seam height of 3 mm was taken to

represent a good quality standard like that of North European ship yards. Furthermore, it was increased to 5 and 9 mm which represent medium and poor shipyard standards as found in developing countries.[45] The welding width was unified to 15 mm according to the information provided by ship operators from Maersk Line. The selected sailing speeds were 10, 12, 14, 16, 18 and 20 knots (5.14, 6.17, 7.20, 8.23, 9.26 and 10.29 m/s, respectively). No coating layer was present and simulated on the plate.

All the simulations were run in steady state because no significant transient effect was expected and all simulations converged. The SST turbulence model was applied. A value of $y^+ < 1$ was obtained in all simulations based on proper mesh size (57134 elements in one plate field) to capture separation on rounded structures and thereby to obtain the near wall velocity gradient within the boundary layer. The structured mesh conditions near the welding seam can be seen from Figure 4.13 with fine mesh size near the wall.

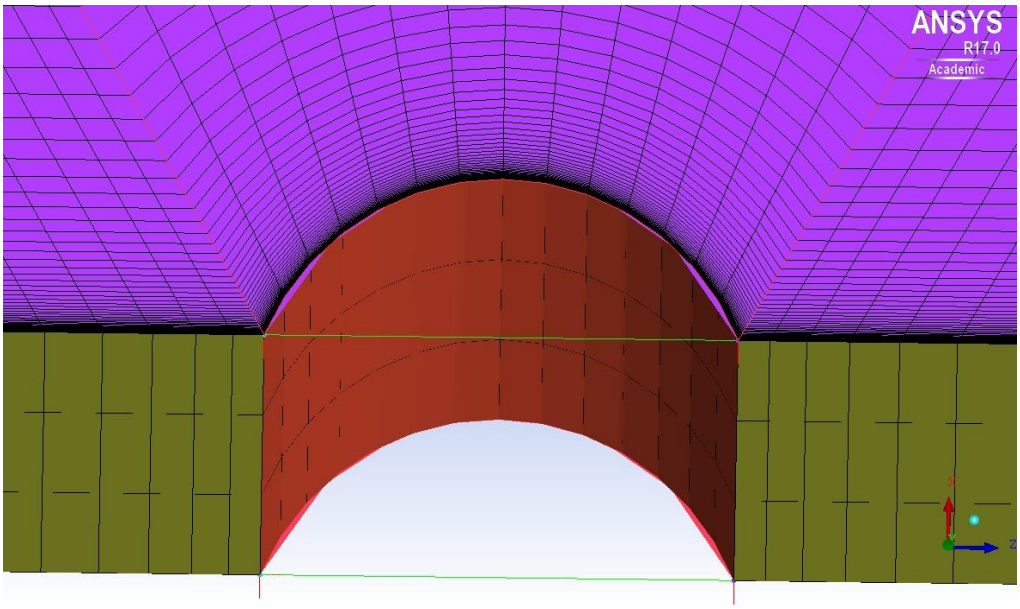

Figure 4.13 Mesh details around a welding seam.

The total resistance F_T was obtained directly from ANSYS CFX 17.0, which can be expressed in the following equation:

$$F_T = \frac{1}{2}\rho C_T U^2 S \tag{4.1}$$

$$C_T = \frac{2\tau_\omega}{\rho U^2} \tag{4.2}$$

where τ_w is wall shear, ρ is water density, C_T is total resistance coefficient, U is free stream velocity, and S is the wetted surface area.

4.6.2 Results and discussion

Table 4.4 presents the obtained resistance values on welding seams and hull surfaces for three welding seam heights with different welding seam numbers. It can be seen that the resistances on both hull surfaces (HR) and welding seams (WR) increased with speed as expected based on Equation (4.1).

Besides, when welding seam height was increased, the resistance increased on welding seams whereas decreased slightly on the hull surfaces. Same observations were found for all the cases with different welding seam numbers. A circular zone was formed behind the welding seam following the flow direction as shown in Figure 4.14, where the turbulence was weakened and the flow velocity and shear stress became low. Besides, on top of the welding seams, a boundary layer separation was observed (see Figure 4.15) and following a pressure drop occurred in the back of the welding seam, which caused the pressure drag (or residuary resistance). Consequently, when the welding height was increased, the pressure drop on the welding seams was increased and thereby the resistance was increased on welding seams. However, the flow velocity and shear stress on the hull surfaces after the welding seam were decreased and thereby the resistance on the hull surfaces was decreased.

On one hand, it can be seen from Table 4.4 that the resistance from welding seams (including both friction and pressure drag) was much lower than that from hull surfaces (mainly friction drag) due to the larger surface area. Therefore, the friction drag is the dominating one for the total resistance and the hull surface condition is more important than the welding seams considering the total resistance a marine vehicle is subjected to. Consequently, the coating surface roughness condition is crucial because it affects the friction drag, which agrees well with the experimental results discussed in the previous section (see Figure 4.12).

Table 4.4 The obtained resistance on welding seams (WR) and hull surfaces (HR) for different welding heights at different speeds with different welding seam numbers (W/T% = force ratio between welding seams and total in percentage). The resistance values on hull surfaces without welding seams are shown as references.

	No seams/ 0 mm	**Welding seam height with two welding seams (plate fields)**								
		3 mm			**5 mm**			**9 mm**		
Speed	HR (N)	HR (N)	WR (N)	W/T%	HR (N)	WR (N)	W/T%	HR (N)	WR (N)	W/T%
10 knots	31,01	30,33	1,08	3,45	29,56	2,66	8,26	28,33	6,34	18,29
12 knots	43,49	42,53	1,51	3,42	41,45	3,74	8,28	39,73	8,98	18,44
14 knots	57,88	56,63	1,99	3,40	55,19	4,98	8,27	52,88	12,06	18,58
16 knots	74,18	72,57	2,53	3,37	70,73	6,35	8,24	67,76	15,58	18,70
18 knots	92,29	90,33	3,12	3,34	88,05	7,85	8,18	84,31	19,53	18,81
20 knots	112,22	109,82	3,76	3,31	107,07	9,44	8,10	102,50	23,89	18,90
	No seams/ 0 mm	**Welding seam height with three welding seams (plate fields)**								
		3mm			**5mm**			**9mm**		
Speed	HR (N)	HR (N)	WR (N)	W/T%	HR (N)	WR (N)	W/T%	HR (N)	WR (N)	W/T%
10 knots	43,96	42,89	1,55	3,48	41,73	3,79	8,33	39,74	8,97	18,42
12 knots	61,70	60,21	2,16	3,46	58,57	5,33	8,34	55,77	12,72	18,57
14 knots	82,19	80,21	2,85	3,43	78,04	7,10	8,34	74,29	17,09	18,70
16 knots	105,36	102,86	3,62	3,40	100,08	9,07	8,31	97,02	21,77	18,32
18 knots	131,17	128,09	4,47	3,38	124,65	11,21	8,25	118,59	27,67	18,92
20 knots	159,55	155,82	5,40	3,35	151,67	13,49	8,17	144,22	33,86	19,01
	No seams/ 0 mm	**Welding seam height with six welding seams (plate fields)**								
		3mm			**5mm**			**9mm**		
Speed	HR (N)	HR (N)	WR (N)	W/T%	HR (N)	WR (N)	W/T%	HR (N)	WR (N)	W/T%
10 knots	80,14	78,01	2,85	3,53	75,75	6,93	8,39	71,61	16,27	18,52
12 knots	112,61	109,65	3,97	3,50	106,46	9,77	8,40	100,65	23,07	18,65
14 knots	150,16	146,25	5,26	3,47	142,00	13,02	8,40	134,20	31,02	18,78
16 knots	192,64	187,70	6,70	3,44	182,26	16,66	8,37	172,20	40,10	18,89
18 knots	240,03	233,93	8,28	3,42	227,20	20,62	8,32	214,55	50,29	18,99
20 knots	292,11	284,76	9,99	3,39	276,65	24,85	8,24	261,11	61,57	19,08

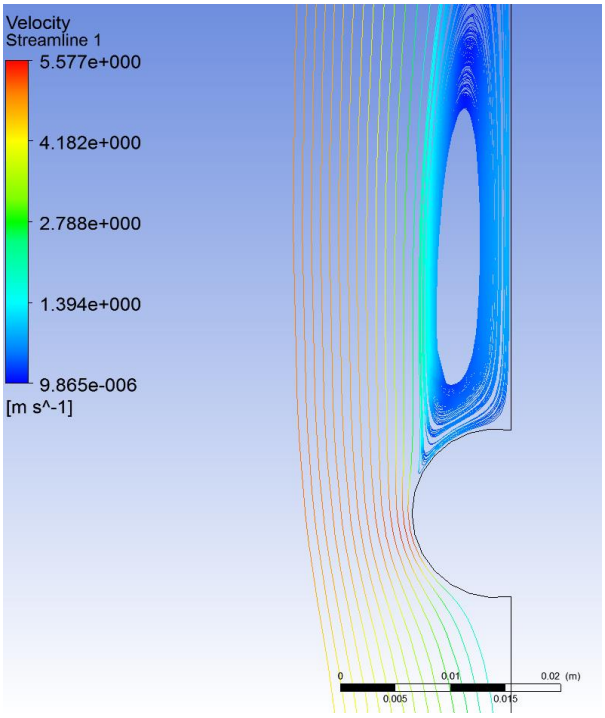

Figure 4.14 The velocity streamline near a welding seam.

On the other hand, the contribution of welding seams to the total resistance (W/T) increased significantly with welding seam height, from about 3.4 to 19% when welding height was increased from 3 to 9 mm, which can be seen in both Table 4.4 and Figure 4.16. Moreover, the contribution of welding seams to the total resistance was independent of the number of plates (or welding seams) and the speed. Therefore, the significant impacts of welding seam height agreed well with the findings from experiments as presented in the previous section of this chapter.

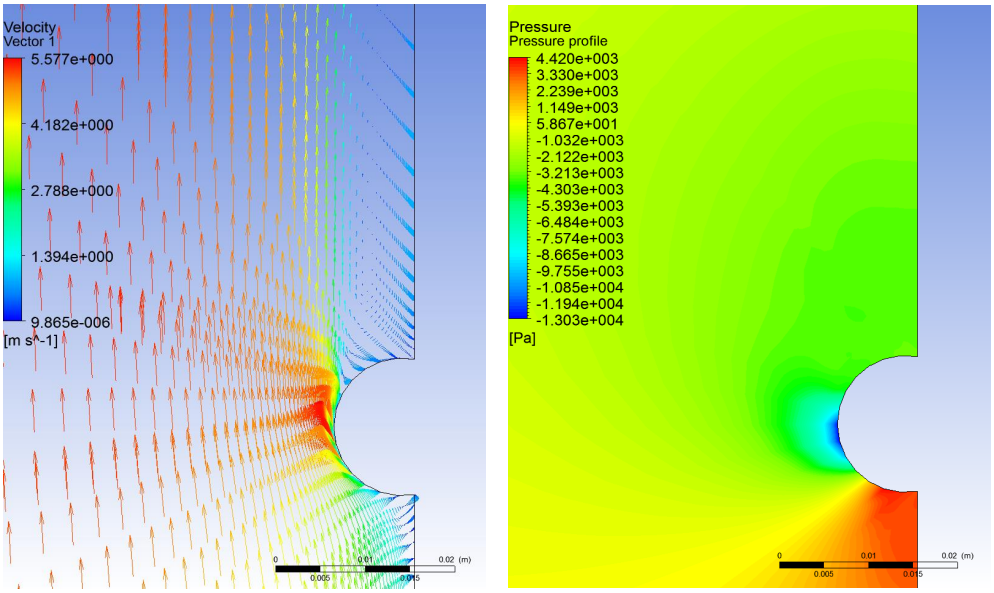

Figure 4.15 The velocity vector (left) and the pressure profile (right) near a welding seam.

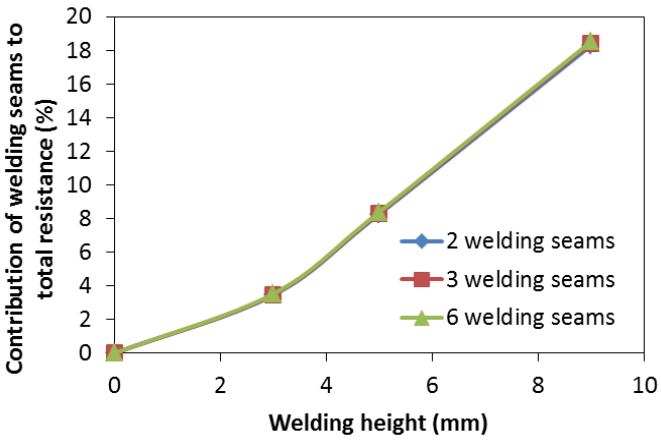

Figure 4.16 Contribution of welding seams to the total resistance in percentage as a function of welding height with different numbers of welding seams.

The advantage of using flat plate geometry was that it simulated the ship surface in full-scale. However, the results (e.g., wall shear) cannot be compared directly with the experimental results from the pilot-scale rotary setup because the flow conditions were different due to the difference in geometry. Therefore, the rotary setup was also considered to be simulated using CFD approach and the geometry domain contained the whole tank with the rotor attached on the shaft. As an initial step, the entire geometry without welding seams on the rotor was simulated successfully. However, after adding two welding seams on the rotor, the following simulation did not converge due to the complexity of the geometry and the tiny size of the welding seams. Consequently, no further simulations of welding seams on the rotor geometry were performed.

4.6.3 Conclusions

Using the CFD simulation approach, the flow conditions near the welding seams were demonstrated and it was found that when welding height was increased, the resistance on the welding seams was increased while the resistance on the hull surfaces was decreased. Moreover, those findings from experimental approach were further verified by the CFD simulation results. On one hand, the significant effects of welding seam height on the total resistance found from experiments were confirmed by the CFD simulation results. Combining the experimental and CFD results, the welding seam height is suggested to be controlled below 5 mm in the ship yards to lower the total resistance and fuel consumption. On the other hand, the dominance of friction drag to the total resistance was observed from CFD simulation. In agreement with the experimental results, the hull surface conditions and thereby the coating surface conditions were proved to be crucial and should be optimized to minimize the friction drag and thereby the total resistance for marine vessels.

5 Rheological study and pre-screening of effective ingredients on leveling of AF coatings

So far, the previous drag force studies have confirmed the importance and value of improving FCC surface conditions through optimizing leveling to the drag resistance. Consequently, the subsequent work is to investigate coating leveling process with a further purpose of exploring methods to reduce coating surface unevenness after application, particularly for AF coatings. As an initial step, effects of formulation ingredients of AF coatings on leveling were studied from rheology perspective because it was seen to be necessary to understand the rheological behaviors of these ingredients during leveling process after application. Within this process, coatings were expected to undergo substantial changes in their rheological properties due to the change of shear.

Therefore, leveling related rheological studies of AF coating ingredients and followed with a pre-screening of effective ingredients on leveling of AF coatings are presented in this chapter. All the ingredients related to leveling of AF coatings are separated into two categories. The first one includes binders and rosins, thickeners/thixotropic agents and pigments; the second one involves leveling additives, wetting agents, and solvents. They were studied separately and presented as two sections of this chapter. Note that, commercial formulations from Hempel A/S are involved in this chapter. Due to the confidentiality, formulation related details are not provided.

5.1 Methodology and uncertainty analysis

Rheological experiments were conducted using a stress-controlled DHR-2 rheometer from TA Instruments with parallel plate geometry. The diameter of the rotating plate is 40 mm. The geometry gap was controlled to be 500 μm. During preliminary experiments, it was observed that pre-shear had significant effects on the repeatability of the results. Hence, the gap closure method was adjusted to exponential type to lower the pre-shear and afterwards more than 3 mins soak time was ensured to dissipate the pre-shear. The experimental temperature was controlled to 25°C. A cover was used to limit solvent evaporation.

5.1.1 Selection of testing methods for rheological study

Four types of rheological tests were considered as shown in Table 5.1. Among all, flow peak hold and flow sweep tests were taken as more relevant for leveling study because they could simulate the application process and the subsequent leveling process. Besides, the build-up process of viscosity during leveling was obtainable as well. The rest of the tests were also performed for selected samples to provide guidelines yet the corresponding results are not shown.

Table 5.1 Analysis of rheological testing methods for coating leveling studies.

Testing methods		Related coating properties	Considerations
Rotational/Flow test (reflecting coating viscous behavior)	Peak Hold	Viscosity building-up during leveling process after application	Possible to make two steps representing application and leveling process, respectively
	Ramp	Yield point, transient viscosity profile vs. shear	Faster in obtaining viscosity profile but less reliable, hard to reach shear rates below 10^{-1} s^{-1}
	Sweep	Steady state viscosity profile vs. shear	More reliable but takes long time, can reach very low shear rates (down to 10^{-4} s^{-1})
Oscillation test (reflecting coating viscoelastic behavior)	Amplitude	Structural strength based on linear viscoelastic region (LVER)	LVER reveals the lowest shear from where structure starts to breakdown

Two steps of flow peak hold tests were performed as shown in Figure 5.1: the first step with constant high shear rate (10^{4} s^{-1} was applied in this case) for 100 s representing application process; followed immediately the second step with constant low shear rate (10^{-2} s^{-1} was applied) for 100 s representing leveling process. On the other hand, logarithmic sweep from low torque to high torque was performed in flow sweep test. The applied torque values varied based on sample conditions and they are specified in the figure captions. In some cases, the structure could not recover after breaking down at high torques. Therefore, the torque was changed from low to high values instead of high to low values. Steady state sensing was activated to obtain steady state viscosity values. For each sample, each test was

performed with three replicates. However, due to that the obtained y-axis values from the replicates did not correspond to the same x-axis values, it was not possible to calculate the average values and the standard deviations from the replicates. Therefore, the results of one replicate were shown in the results section and an overall uncertainty analysis was performed.

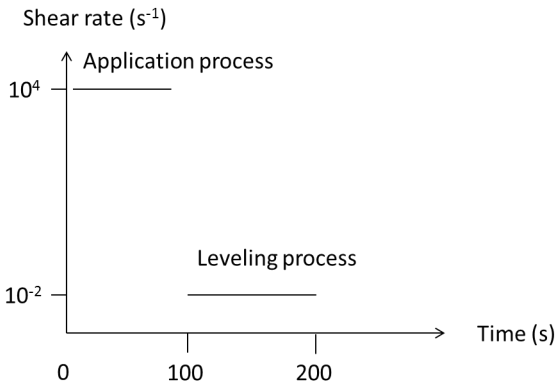

Figure 5.1 Two steps of flow peak hold tests: first step with high shear rate of 10^4 s^{-1} for 100 s representing application process and second step with low shear rate of 10^{-2} s^{-1} for 100 s representing leveling process.

5.1.2 Uncertainty analysis

The equipment uncertainty was evaluated by using silicone putty (poly(dimethyl)siloxane (PDMS)) at 30°C for oscillation frequency test. Before the test, oscillation amplitude test was conducted once to determine the LVER so that the following oscillation frequency tests were performed within LVER (with stress of 50 Pa). The frequency was increased in a logarithmic sweep manner from 1 to 10 rad/s. The same procedure was repeated six times.

The average values of complex viscosity and the error bars representing standard deviations from six repetitions are shown in Figure 5.2. Furthermore, the results of storage modulus and loss modulus were compared with those from Danish Polymer Centre (DPC) as shown in Figure 5.3.

It can be seen that the calculated standard deviations (represented by error bars shown in Figure 5.2) are not high, which means that the repeatability of the experimental procedure using DHR-2 rheometer is high. Meanwhile, the storage modulus and loss modulus curves obtained in this work and previous

work from DPC are overlapping with each other as shown in Figure 5.3. Therefore, the equipment accuracy is high.

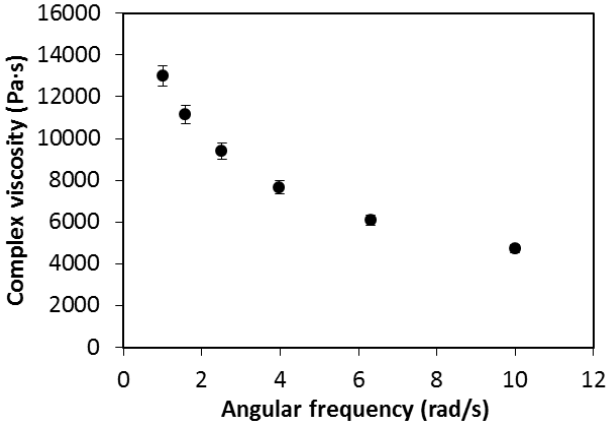

Figure 5.2 Average values of complex viscosity from six repetitions as a function of angular frequency. The error bars represent the standard deviations calculated from six repetitions.

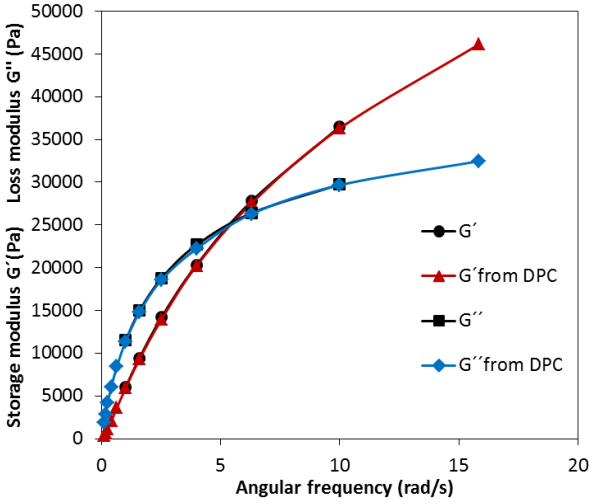

Figure 5.3 Comparisons of storage modulus G' and loss modulus G" as a function of angular frequency of the same sample (silicone putty) obtained in this work and previous work from DPC.

To determine the experimental uncertainties of flow peak hold and flow sweep tests, each test for the same sample was repeated three times. It can be seen from Figures 5.4 and 5.5 that the repeatability of flow peak hold and flow sweep test is high and the experimental uncertainty is low.

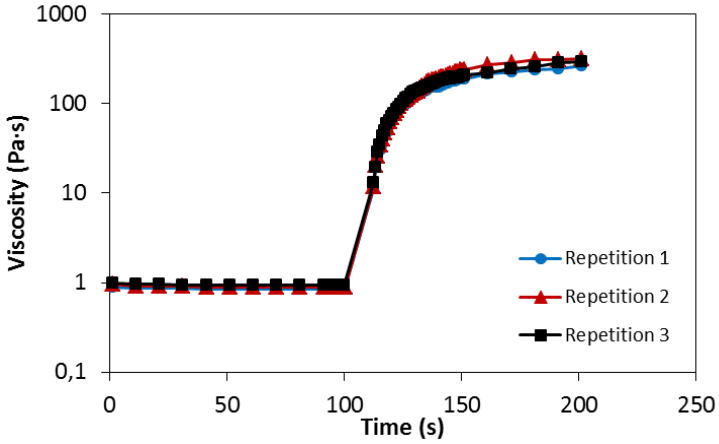

Figure 5.4 Viscosity over time from flow peak hold tests for the same sample with three repetitions: the first 100 s with constant high shear rate (10^4 s^{-1}) and the last 100 s with constant low shear rate (10^{-2} s^{-1}).

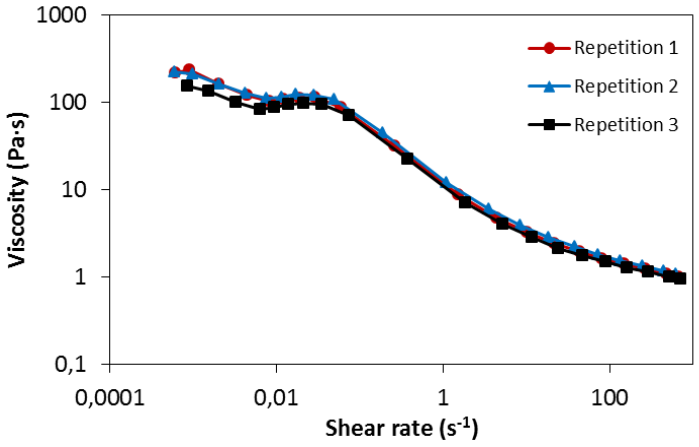

Figure 5.5 Viscosity as a function of shear rate from flow sweep tests for the same sample with three repetitions: from low torque (1 µN·m) to high torque (10^4 µN·m).

Note that, due to the fact that each flow sweep test took around half hour to finish (much longer than flow peak hold test), solvent evaporation might be considerable during the experiment. Therefore, potential changes might occur in the coating samples and extra uncertainty might be added.

5.2 Rheological study of individual ingredient and their mixtures in AF coatings

In this part, the ingredients in the first category (binders and rosins, thickeners/thixotropic agents and pigments) are investigated. The main function of binder system in AF coatings is to create a network among all coating ingredients. Rosins are used in AF coatings to improve cracking resistance and control the rate of biocides release. They constitute the binder system together with other binders. In theory, the addition of thixotropic agents enables to modify rheology by means of thickening without substantial amendment of other coating properties. The network formed by adding thixotropic agents may be destroyed when the coating is subjected to high shear (application), which will lead to lower viscosity and better spray ability. After application, viscosity is increased due to the recovery of the network under low shear (leveling and sagging involved). Pigments in AF coating formulations mainly refer to biocides. Due to the high amount of biocides needed to combat biofouling, the pigment volume concentration of AF coatings is normally high, which may have influence on rheology.

5.2.1 Materials

Because binders are the backbone of a coating formulation, it is important to investigate their rheological behavior separately. The selected binders dissolved in xylene (the main solvent used in AF coatings) and their viscosity ranges are summarized in Table 5.2. Note that, the binders used in sample B6 and B7 were different rosins, which showed very low viscosity after dissolving in xylene. Therefore, their own rheological effects were seen to be very low and not further studied.

Mixtures of binders and rosins (BR), binders, rosins, and thixotropic agents (BRT) with the same ratio as in commercial AF coatings were prepared for comparison. The detailed comparison principles will be explained in the corresponding context. Various commercial AF coating formulations (F) were studied in this work as listed in Table 5.3. The differences between high polishing and low polishing formulations are the binder types and rosin amount (high polishing ones have higher rosin amount compared to low polishing ones).

Table 5.2 The selected binders and their corresponding viscosity ranges determined by the Brookfield test method at 25°C based on ISO standard.[97]

Binder types	Viscosity ranges (Pa·s)
B1 (45% binder 1 in xylene)	1.5-6.0
B2 (50% binder 2 in xylene)	0.25-0.4
B3 (55% binder 3 in xylene)	0.35-0.55
B4 (50% binder 4 in xylene)	1.1-2.3
B5 (65% binder 5 in xylene)	1.0-2.5
B6 (50% binder 6 in xylene)	Very low
B7 (50% binder 7 in xylene)	Very low

Table 5.3 The prepared full formulations (F), binder and rosin mixtures (BR), and binder, rosin, thixotropic agent mixtures (BRT) with the same ratio as in the full formulations. The full formulations were categorized into high polishing and low polishing ones.

	Sample notations			
High polishing	F1-BR1/BRT1	F3-BR3/BRT3	F5-BR5/BRT5	F8*-BR8/BRT8
Low polishing	F2-BR2/BRT2	F4-BR4/BRT4	F6-BR6/BRT6	F7-BR7/BRT7

*An old AF formulation with poor leveling performance as a reference

In addition, to study the effects of thixotropic agents on full formulations, the full formulations without thixotropic agents (w/oT) were prepared as shown in Table 5.4 to compare with the corresponding full formulations with thixotropic agents.

Table 5.4 Samples prepared for full formulations without thixotropic agents (w/oT). The full formulations were categorized into high polishing and low polishing ones. Full formulation 8 was not studied in this part.

	Sample notations			
High polishing	F1- w/oT	F3- w/oT	F5- w/oT	
Low polishing	F2- w/oT	F4- w/oT	F6- w/oT	F7- w/oT

5.2.2 Results and discussion

Rheological information of individual binders

Due to the high amount of plots, the results for individual binders are summarized below without showing the plots. Binders B2, B3, B4 and B5 behaved like Newtonian flow while binder B1 was slightly shear-thinning. From flow sweep tests, B4 and B5 behaved similarly with similar viscosity while B2 and B3 showed similar trend and viscosity. Oscillation amplitude tests showed that, for all binders, viscous characteristic was dominating since the loss modulus was always higher than storage modulus. The loss modulus of B1 was the highest, following B4 and B5, with B2 and B3 the lowest. The storage modulus was same (nearly 0 Pa·s) for all binders, which meant the elasticity of those binders was very low. Therefore, the five binders can be divided into three groups according to their behaviors: B1; B2 and B3; B4 and B5.

In addition, after comparison between low polishing and high polishing formulations, no significant difference was found in their rheological behaviors. Therefore, changing rosin amount and binder combinations did not have significant influence on rheology.

Effects of rosins and thixotropic agents on binders

The effects of rosins and thixotropic agents on binders can be seen from Figures 5.6 and 5.7 of results from flow peak hold and flow sweep tests. The shear-thinning behavior of binder B1 can be seen from Figure 5.6 as well. Compared to pure binder (B1), the presence of rosin (BR3) decreased the overall viscosity as shown in both figures, probably due to the presence of xylene which diluted the mixture. However, the viscosity behavior was not changed much though a slight build-up process appeared after high shear as seen in Figure 5.7, which confirmed that rosin had insignificant rheological effects on the binder system.

However, the addition of thixotropic agents showed large effects on viscosity at low shear rates from both flow peak hold and flow sweep tests. After switching from high to low shear rates, the rapid build-up process of viscosity can be seen for sample BRT3 from both Figures 5.6 and 5.7 due to the imposed thixotropic effects. Consequently, sagging will be prevented and leveling will be impeded. Similar results were found for other formulations (plots are not shown).

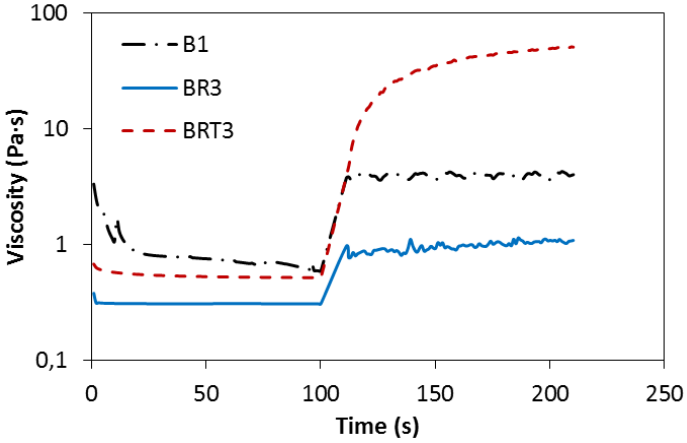

Figure 5.6 Viscosity as a function of time from flow peak hold tests for pure binder B1, binder and rosin mixture BR3, binder, rosin, and thixotropic agent mixture BRT3: the first 100 s with constant high shear rate of 10^4 s^{-1} (representing application process), the last 100 s with constant low shear rate of 10^{-2} s^{-1} (representing leveling process).

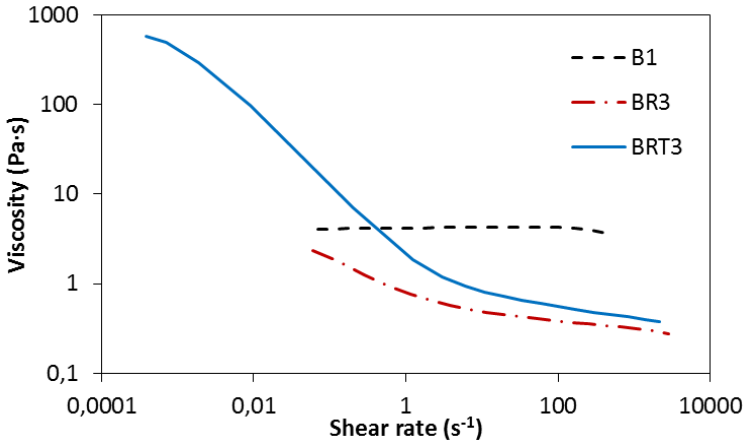

Figure 5.7 Viscosity as a function of shear rate from flow sweep tests for pure binder B1, binder and rosin mixture BR3, binder, rosin, and thixotropic agent mixture BRT3: the torque value was increased logarithmically from 1.77 to $2{\cdot}10^4$ μN·m.

Effects of thixotropic agents on full formulations

The effects of thixotropic agents on full formulations were studied based on comparison between full formulations and the ones without thixotropic agents. The results from flow peak hold and flow sweep tests are shown in Figures 5.8 and 5.9 as examples. Similar results were found for other formulations (plots not shown). After removing thixotropic agents (F1-w/oT), the overall viscosity decreased after switching from high shear rate to low shear rate in Figure 5.8; moreover, the viscosity was slightly increased at high shear rate, which can be seen from both figures. Higher viscosity at high shear rate could lower spray ability of coatings. It is worth to notice from both figures that, after switching from high to low shear rate, the viscosity could still build-up (structural recovery) without thixotropic agents though the overall viscosity was lower than the full formulations. It reveals that some other ingredients in the formulation may have thixotropic effects. The possible ingredients could be reaction products or additives, e.g., wetting agents.

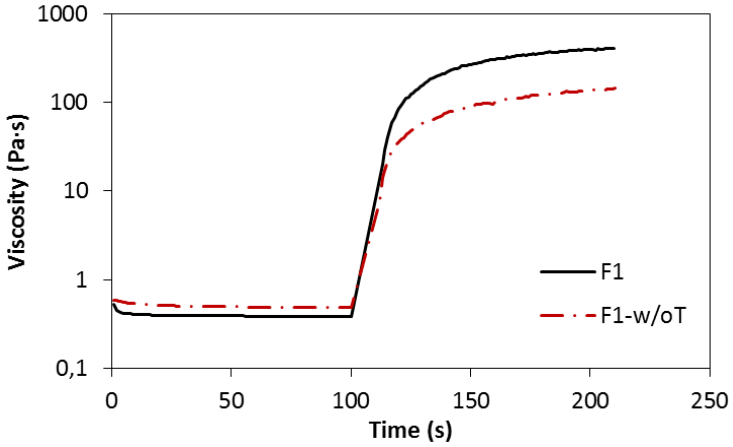

Figure 5.8 Viscosity as a function of time from flow peak hold tests for formulation 1 (F1) and formulation 1 without thixotropic agents (F1-w/oT): the first 100 s with constant high shear rate of 10^{3} s^{-1} (representing application process), the last 100 s with constant low shear rate of 10^{-2} s^{-1} (representing leveling process).

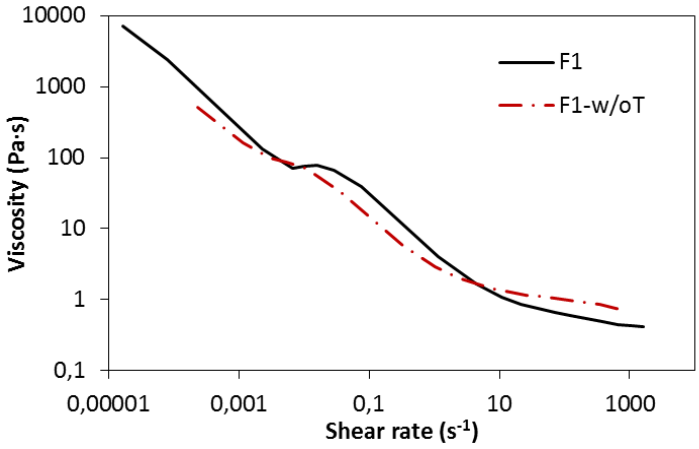

Figure 5.9 Viscosity as a function of shear rate from flow sweep tests for formulation 1 (Fl) and formulation 1 without thixotropic agents (Fl-w/oT): the torque value was increased logarithmically from 1.5 to 8460 μN·m.

Effects of pigments on full formulations

The effects of pigments can be seen based on comparison between full formulation and the mixture of binders, rosins and thixotropic agents because the difference between them is mainly the presence of pigments (small amount of wetting agent is also involved). The results from flow peak hold and flow sweep tests are shown in Figures 5.10 and 5.11.

On one hand, from both figures, the viscosities of F4 at high shear rates were nearly the same as BRT4, which indicated that the pigments did not increase the viscosity and harm the spray ability of the coating from viscosity point of view. This may be attributed to the thixotropic effects from thixotropic agents or other possible ingredients (like wetting agents or reaction products between pigments and rosin as deduced from the above section). On the other hand, after switching from high shear rate to low shear rate, the viscosity built up in a similar way for both samples; however, the final viscosity values of the mixture without pigments (BRT4) were much lower than those of the full formulation. Same observations were found for other formulations. Therefore, it can be concluded that the presence of pigments in a full formulation increases the overall viscosity at low shear rates, which inhibits leveling. However, this viscosity effects from pigments will disappear at high shear rates attributed to the thixotropic effects and therefore will not hinder the spray ability.

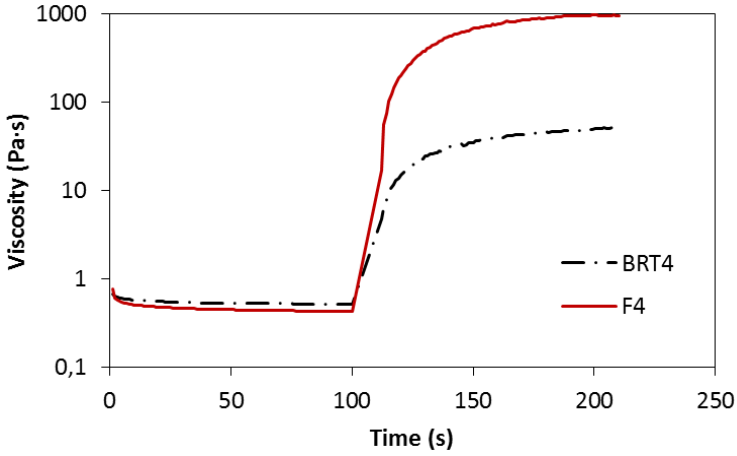

Figure 5.10 Viscosity as a function of time from flow peak hold tests for formulation 4 (F4) and mixture of binder, rosin, and thixotropic agents (BRT4): the first 100 s with constant high shear rate of 10^3 s^{-1} (representing application process), and the last 100 s with constant low shear rate of 10^{-2} s^{-1} (representing leveling process).

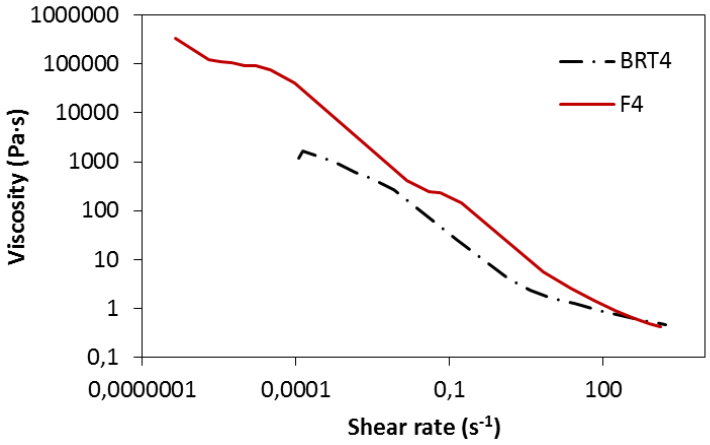

Figure 5.11 Viscosity as a function of shear rate from flow sweep tests for full formulation 4 (F4) and mixture of binder, rosin, and thixotropic agents (BRT4): the torque value was increased logarithmically from 1.77 to 9960 μN·m.

5.2.3 Conclusions

In this part, flow peak hold test and flow sweep test were demonstrated to be able to simulate the shear changing process from application to leveling. It was found that rosins had insignificant rheological effects on the binder system. Moreover, the thixotropic effects of thixotropic agents/thickeners were verified on decreasing slightly viscosities at high shear rates for better spray ability and increasing viscosities at low shear rates to prevent sagging. However, it was inferred that some other ingredients in the formulation may have thixotropic effects as well, such as reaction products between pigments and rosin, wetting agents which were further investigated regarding their effects on leveling and presented in the next part. Furthermore, pigments were found to increase viscosity at low shear rates yet not to increase viscosity at high shear rates, which indicated that they would not harm the spray ability from viscosity point of view while they would limit leveling. Overall, the hypothesis (4) that coating formulation ingredients affect leveling properties of AF coatings was found to be true.

5.3 Pre-screening of effective ingredients on leveling of AF coatings

In this part, different types of leveling additives, wetting agents, and solvents with different concentrations were investigated for their effects on leveling of AF coatings. The purpose was to pre-screen the most effective ingredients for further studies (presented in next chapter). Various leveling additives are commercially available and some of them are used in commercial coating formulations to promote leveling. However, it was unclear if they could have effects on leveling of AF coatings, which initiated the studies on them. Theoretically, wetting and dispersing agents are used in AF coatings to assist rosin in the covering of pigment surfaces, and thereby help avoiding agglomerates. Therefore, they may help in solvent and pigment distributions in AF coating system. In addition, less volatile solvents with lower evaporation rate may slow down the build-up of viscosity and leave more time for leveling.

5.3.1 Materials

A model AF coating was formulated based on commercial AF coatings and used in this study. The composition is shown in Table 5.5. The studied ingredients with different concentrations are summarized in Table 5.6. All leveling additives and wetting agents were acquired from BYK Additives & Instruments. The less volatile solvent was supplied by Hempel A/S. These ingredients were added to the model coating to reach the desired concentrations as specified in Table 5.6.

Table 5.5 Composition of the studied model AF coating.

Ingredients	Weight percentage (wt%)
Xylene/Dimethylbenzene	15
Methyl isobutyl ketone solvent	5
Zinc oxide	10
Bentonite	1
Talc	14
Cuprous oxide	25
Gum rosin	20
Acrylic binder	10

Table 5.6 The ingredients and their concentrations used for pre-screening.

Ingredients			Concentration wt%
Leveling additives	Acrylic-based	BYK 361N (high polarity) BYK 399 (medium polarity) BYK 392 (low polarity)	0.3, 0.5, 0.8
	PDMS-based	BYK 325 (high polarity) BYK 326 (B)(medium polarity) BYK 322 (low polarity)	0.1, 0.25, 0.5
Wetting agents	Deflocculating	BYK 110 (acidic) BYK 118 (zwitterionic) Disperbyk 106 (C) (acidic)	0.5, 1, 1.5
	Flocculation control	BYK 220S (thixotropic effects)	
Less volatile solvent		Naphtha (A)	2, 5, 7

As shown in Table 5.6, two types of leveling additives were studied. One is acrylic-based and the other is PDMS-based. For each type, various leveling additives with different levels of polarities were pre-screened to determine which polarity combines well with the model AF coating matrix. Similarly, different wetting agents with acidic or zwitterionic properties were scrutinized considering their unknown compatibilities with the model AF coating matrix. One wetting agent which might have thixotropic effects was also included in the studies. Those additives were suggested by BYK Additives & Instruments.

5.3.2 Experimental procedure

After sample preparations, applications using flat drawdown bar were conducted manually on glass panels giving around 300 µm of wet film thickness. The purpose of using glass panels was to assist in visual observation of leveling effects. The applied glass panels were placed horizontally along drying. Subsequently, roughness measurements of the dried coating films were performed using a mobile roughness measurement instrument (MarSurf PS10 from Mahr GmbH) as shown in Figure 5.12 with a maximum cut-off length of 2.5 mm. The arithmetic average of the absolute values of roughness profiles (*Ra*) was analyzed to indicate leveling performance. The maximum cut-off length of 2.5 mm means that waviness characteristics with wavelength longer than 2.5 mm are excluded from the Ra values. To include as much waviness characteristics as possible into the measurements, the maximum cut-off length was used with six sampling lengths. Therefore, the total evaluation length was 15 mm.

Figure 5.12 MarSurf PS10 mobile roughness measurement instrument.

5.3.3 Results and discussion

Results from roughness measurements showed that all the leveling additives increased *Ra* value of the model formulation and adding 1 wt% of wetting agents BYK 118 and 106 decreased slightly the Ra value of the model formulation. Accordingly, several hypotheses were proposed: 1) the concentrations used might be too low or too high; 2) a spiral applicator may show the effects on leveling more remarkably; 3) the Ra values of the model formulation may be already very low compared to commercial formulations.

Therefore, lower and higher concentrations were further studied for selected leveling additives 361N and 326. However, the results were similar as before and no direct correlation between the *Ra* value and the concentration was found as shown in Figure 5.13. In addition, the *Ra* value of model formulation was compared with commercial formulations and the results showed that the *Ra* value of model formulation was not as low as some commercial formulations (plots are not shown here).

Furthermore, a spiral applicator with a wavelength of 3.7 mm (more details about spiral applicators in next two chapters) was used to generate waviness on the coating surface and the results showed that only wetting agent 106 (C) reduced slightly the *Ra* value of the model formulation. In addition, it was found that having more than 7 wt% of naphtha solvent (A) decreased the *Ra* value of the model formulation. However, it was noticed that the maximum cut-off length of MarSurf was too short for measuring the surface waviness generated from the spiral applicator. Therefore, the waviness data was not obtainable using this roughness measurement instrument.

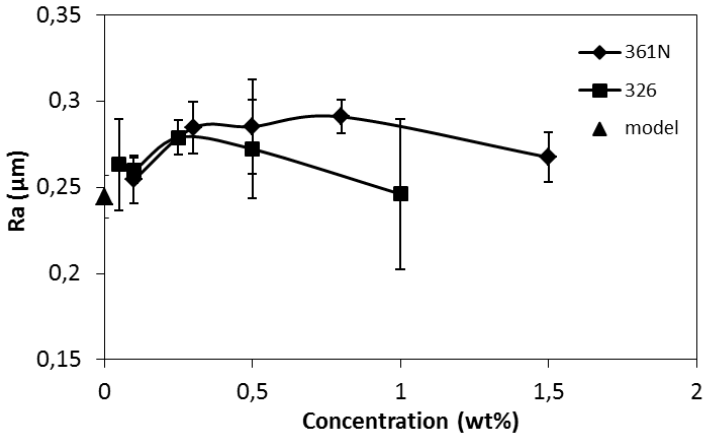

Figure 5.13 *Ra* values as a function of concentration of the added leveling agents 361N and 326 to the model formulation.

In addition, rheological studies were conducted for wetting agent C and naphtha solvent A using the same methodology as mentioned in section 5.1. The results of flow peak hold and flow sweep tests are shown in Figures 5.14 and 5.15. It can be seen from both figures that after switching from high to low shear rates, adding 1 wt% of wetting agent C slowed down the viscosity build-up process and decreased

the final viscosity of the model formulation. Moreover, having 7 wt% of naphtha solvent A decreased the overall viscosity of the model formulation. Therefore, they may promote leveling.

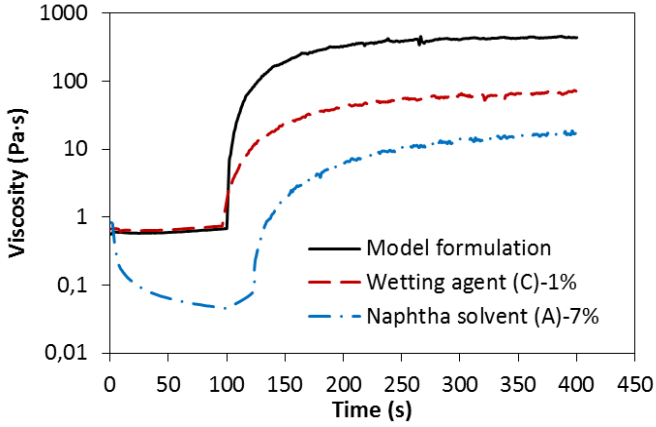

Figure 5.14 Viscosity as a function of time from flow peak hold test: the first 100 s with constant high shear rate (10^4 s^{-1}) and the last 300 s with constant low shear rate (10^{-2} s^{-1}) for model formulation, model formulation with 1 wt% of wetting agent (C), and model formulation with 7 wt% of naphtha solvent (A).

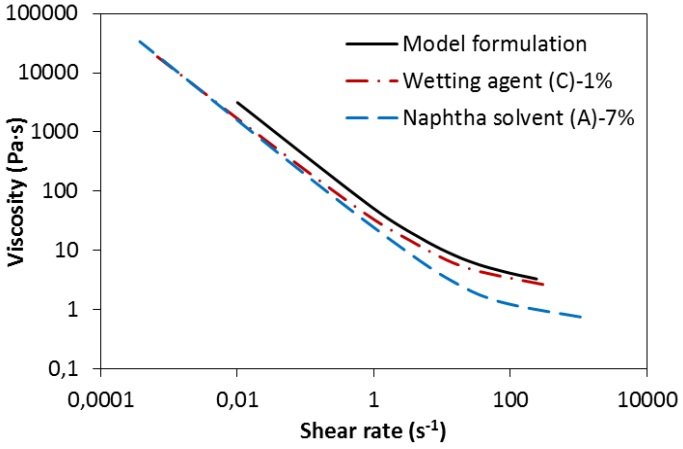

Figure 5.15 Viscosity as a function of shear rate from flow sweep test: from high torque (10^4 µN·m) to low torque (0.01 µN·m) for model formulation, model formulation with 1 wt% of wetting agent 106 (C), and model formulation with 7 wt% of naphtha solvent (A).

5.3.4 Conclusions

Overall, it was found that the rheological study was an essential step for coating leveling studies and it was important to analyze the rheological effects of different ingredients on leveling, which provided guidelines for the following leveling studies. In addition, the obtained rheological information was considered as valuable input to the formulation development work in coating industries. However, the obtained information was qualitative and inadequate in quantifying leveling performance. Moreover, coating samples were found to be very sensitive to the shear history and the expected differences in leveling effect (or rheological behavior) among different samples were small. Considering that, using rheological approach solely to study leveling was not sufficient.

Based on the results of the pre-screening study, leveling additive B, wetting agent C, and less volatile solvent A were selected to be studied more systematically for their effects on leveling of model AF coatings. Furthermore, the MarSurf PS10 could not include waviness characteristics with wavelength longer than 2.5 mm (the maximum cut-off length) generated from the spiral applicator. Hence, a novel approach on quantifying leveling performance including both roughness and waviness characteristics was developed and elaborated in the next chapter.

6 Leveling measurements of AF coatings using an optical 3D profilometer: effects of additives and solvent concentration and type

This chapter has been written in a manuscript format and a modified version will be submitted as "Leveling measurements of antifouling coatings using an optical profilometer: effects of additives and solvent concentration and type" to *Progress in Organic Coatings*. The authors to be included in the publication are *Xueting Wang, Claus Erik Weinell, Vicenç Tobar, Stefan Møller Olsen,* and *Søren Kiil*.

Abstract

Ship hulls require smooth FCC surfaces to decrease frictional drag and avoid sites of weakness for biofouling. Consequently, the leveling properties of AF coatings should be understood and optimized. In this chapter, a novel approach to quantitatively measure leveling performance of coating films was developed. Using this approach, dynamic surface textures during leveling process of selected model AF formulations were measured using a combination of an optical 3D profilometer and a retrofitted automatic film application system. It was found that the leveling rate was strongly coupled to the solvent evaporation rate and the associated development in coating viscosity. For low viscous coatings, three leveling stages were observed. High viscous coatings, on the other hand, only went through one leveling stage.

Experimental data showed that an underlying tie-coat (relative to a flat acrylic panel) had negative effects on the smoothness of the top coat. In addition, using an anti-sagging agent enabled control of sagging, but resulted in negative effects on leveling. Nevertheless, it was still possible to obtain good leveling performance with anti-sagging agent in a formulation.

The effects of minor amounts of three types of additives and two types of solvents on leveling of the model formulations (from spraying application) were found to be less significant than those seen from

spiral-drawdown application. It is therefore important to take into account the application method when studying leveling.

6.1 Introduction

On ship hulls, various layers of protective coatings are applied to fulfil different requirements. The outermost layer is normally a FCC of which the primary role is to limit biofouling and the associated drag resistance.[88,98] However, following application, the coating surface is not entirely smooth. An irregular surface not only affects the esthetics but also constitutes sites of weakness, i.e., potential starting points for corrosion, cracking, blistering and biofouling.[5,6] In addition, a non-smooth FCC surface will increase the frictional resistance itself. Therefore, it is desirable to obtain smooth FCC surfaces, though the major benefits will be seen only when the ship is still free of biofouling.

6.1.1 Leveling of coatings

For most coatings, a smooth surface can be achieved by proper leveling and the first studies of this can be dated back to the 1920s. However, advances in understanding the mechanisms and the influencing factors have been slow.[82] Waring[75] was probably the first, in 1931, to conduct an analytical study of leveling of a pigment-vehicle mixture. Later, in 1961, leveling phenomenon (brush mark studies) was described by Smith, Orchard, and Rhind-Tutt. They stated that leveling is mainly driven by surface tension and retarded by viscous drag.[54] In 1963, Orchard[56] studied leveling theoretically; the so-called Orchard equation is representative of the leveling process, where the amplitude of a sinusoidally rippled liquid surface decreases exponentially with time. The rate of leveling was found to be a function of the average film thickness, the surface tension, dynamic viscosity and the ripple wavelength. Orchard found that the gravitational effect can be neglected when the wavelength is less than about three mm. Due to various simplifying assumptions, the equation is only applicable to non-volatile liquids and Newtonian flow, far from non-Newtonian coatings rheology. Experimental work of Overdiep[60] showed that the Orchard equation failed to give a qualitative description of leveling of solvent-based alkyd coatings. Overdiep found that a surface-tension-gradient resulting in a reversal process was another driving force for leveling. The reversal process means that the initial peaks would become valleys and the initial valleys would become peaks. The mechanism is, as explained by Wilson,[63] that the solvent concentration near peaks is higher than that near valleys during solvent evaporation, which results in a lower surface tension near the peaks. This gradient drives flow from peaks to valleys, which enhances the leveling process. Due to the imbalance in solvent concentration, this process will continue and the

reversal phenomenon is the result. Based on the work from Overdiep, Wilson continued with development work on models for coating films.[62–64] However, these investigations were highly ideal because they neglected the dependence of coating viscosity on shear, the effects of thixotropy, and the presence of solvent evaporation.[82] Later, from 1995 to 2011, leveling studies were focused in different directions: numerical simulation of the surface-tension-gradient effects on leveling of a two-component fluid,[99] the thixotropic effect on leveling,[55,57] and leveling of thermoset waterborne coatings.[100,101]

Approaches for studying and quantifying leveling have been pursued.[60,81,102] However, most of the previous methods were specifically designed for certain type of coating systems or could not be applied directly to coating films containing solvents. Recently, novel approaches for leveling studies were reported for powder and automotive coating systems, which are different compared to FCCs. Bosma *et al.*[66] developed a method for estimation of leveling behavior of powder coatings in a quantitative manner and the evolution of surface texture in automotive coatings was studied in details by Peters *et al.*[58] A very recent work presented by Seeler *et al.*[59] investigated coating film leveling through simulations and experiments; however, most samples presented were simplified systems: Newtonian model liquids with and without solvent evaporation.

In the present work, a new approach for measuring leveling performance of coatings was developed. It involves a combination of an automatic spiral-drawdown application and a 3D measurement system based on an optical profilometer. Using this macroscopic approach, a well-defined sinusoidal surface pattern could be formed on the coating surface. The dynamic surface texture information was collected non-destructively in short intervals during leveling and solvent evaporation.

6.1.2 Strategy of investigation

Two main types of FCCs, with different antifouling mechanisms, are commercially available. One is the FR coatings, which present a smooth surface with low surface energy and high elasticity that makes it difficult for marine species to adhere during sailing. The other is the traditional biocide-based AF coatings, which are normally highly pigmented coatings containing biocides that are released into seawater to limit biofouling. For AF coatings, the solids content (about 80 wt% or 58 vol%) is very high and the final coating surfaces are rougher than the ones of FR coatings. Consequently, to investigate significant effects, the target of this leveling study was model AF formulations based on commercial AF coatings. Unlike FR coatings, AF coatings cure by physical drying only.

The aim of the work has been to study the effects of coating ingredients on leveling of AF coatings and investigate the underlying leveling mechanisms. The ingredients considered were a silicone additive

(silicone oil), a silicone surfactant (leveling additive), a wetting and dispersing agent, and a solvent. The motivations for choosing these ingredients were based on the results from the pre-screening process presented in the last chapter, previously published investigations and advice given by experts in the coating industry. Schwartz and co-workers[71] found that the presence of surfactant slowed down the leveling rate of Newtonian liquids due to the resulting surface-tension-gradient forces. For the solvent case, less volatile solvents should slow down the evaporation rate and consequently prolong the drying time, which may leave longer time for leveling before the coating loses its flow ability due to viscosity build-up. For most AF coatings, wetting and dispersing agents are used to assist rosin in the wetting and covering of pigment surfaces, thereby expelling air and water, and enhance pigment dispersion. Accordingly, these additives may have an influence on leveling and many types are commercially available for coatings. In practice, leveling and sagging are conflicting; good conditions for leveling may lead to sagging problems. As a result, optimal conditions are pursued to get the best leveling without causing sagging. Thus, the effects of anti-sagging agents are also included in the present investigation.

6.2 Equipment and methodology

6.2.1 Equipment

A wide-area 3D measurement system (profilometer) with a VR-3100 sensor head from KEYENCE was used in this work to obtain dynamic surface texture information through scanning of solvent-containing coating surfaces. The coating film application was performed using a system as shown in Figure 6.1 (left) based on retrofitting a commercial film applicator (Coatmaster from Erichsen). The aluminum part above the glass provided horizontal movement with adjustable speed and moving direction. A spiral rod applicator is placed in front of the moving part as shown in Figure 6.1.

To start the measurements immediately after application, without handling the sample, film application was performed directly on top of the specimen stage of the VR-3100 head (see Figure 6.1 right) which is located on the right side of the film application system. Notice that it is important to obtain instantaneous surface information right after application because leveling starts immediately. All the coating samples were applied on acrylic panels. A template was placed on top of the stage to fix the position of the panels so that the same position of each panel was measured every time.

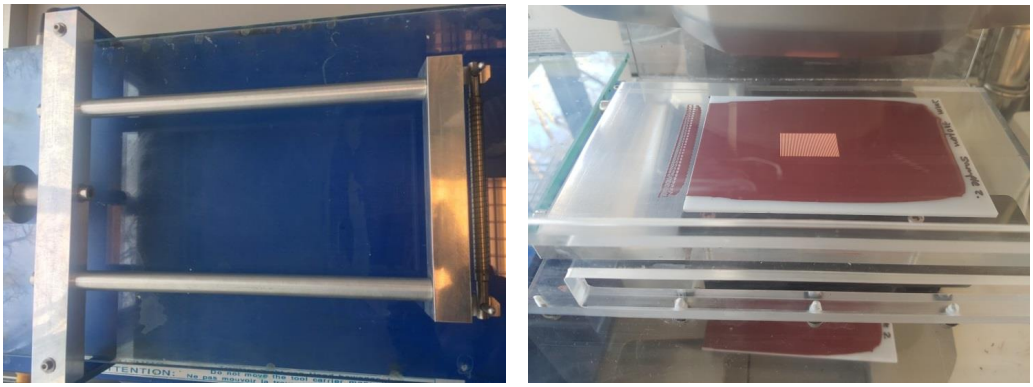

Figure 6.1 The retrofitted automatic film application system (seen from the top) (left) and the specimen stage of the VR-3100 head (right).

6.2.2 Roughness and waviness profile

The profilometer provides surface information with various surface texture parameters. The roughness of a ship hull surface is a complex function of superposed undulations and cannot be described by a single parameter.[103] In fact, it was reported that more than 59 roughness parameters can be used to describe a surface geometry.[104] However, it is not realistic to use all of them for scientific comparisons and research. Generally speaking, a ship hull surface profile consists of two major components: roughness and waviness, which have different scales of wavelength (see Figure 6.2). During measurements using the profilometer, the surface profile can be filtered by introducing appropriate cut-off wavelengths. Firstly, a primary profile can be obtained by applying a low-pass cut-off length λ_s to remove the wavelength components shorter than λ_s. The removed components are regarded as not relevant to a targeted roughness profile. Following, if a high-pass filtering of the profile with a cut-off wavelength λ_c is used, then the characteristics with longer wavelength (waviness) will be filtered out and basically the roughness profile is obtained. If the profile is low-pass filtered with a cut-off wavelength λ_c and high-pass filtered with a cut-off wavelength λ_f, the wavelength characteristics shorter than λ_c and longer than λ_f are removed and the waviness profile is obtained as illustrated in Figure 6.2.[105] On ship hull surfaces, the wavelengths of the surface profiles are not uniform and have a distribution typically from 0.1 to 30 mm. Surface irregularities with wavelengths between 1 and 10 mm are known as orange peel.[59]

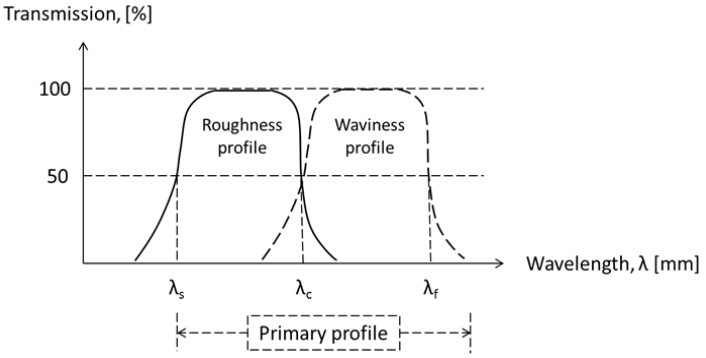

Figure 6.2 Differentiation of roughness and waviness characteristics by using filtering cut-off wavelengths based on ISO standards.[105]

6.2.3 Materials

Based on commercial AF coatings, various model formulations were formulated. The raw materials were supplied by Hempel A/S. Coatings were produced using high-speed dispersion and basic mixing of ingredients was done using a shaker. During coating sample preparation, the fineness of grind was targeted to a maximum of 40 µm. Subsequently, the viscosities of model formulations were measured at 25°C and a shear rate of 117.4 s^{-1} using a DHR-2 Rheometer from TA Instruments. The shear rate was chosen for comparison with the viscosity values measured using a KU-1 Viscometer from Brookfield at 200 RPM. Normally, the viscosity of commercial AF coatings is about 0.95-2.2 Pa·s at 117.4 s^{-1}.

Due to the fact that the viscosity of model formulation 1 (M1) turned out to be extremely high (>8 Pa·s) after preparation, model formulation 2 (M2) was formulated after minor modifications of M1 to reach a lower viscosity of about 2.2 Pa·s. Furthermore, to determine the effects of viscosity on leveling, the M1 coating was diluted with xylene (the main solvent) to reach a relative moderate viscosity of about 4.3 Pa·s (not shown in Table 6.1, see Table 6.2 "M1-diluted"). To control sagging and investigate the influence of anti-sagging agent, another model formulation M3 was formulated by adding an anti-sagging agent. The compositions of M1, M2 and M3 are shown in Table 6.1.

To investigate the effects of different solvents and additives on leveling of model formulations, coating samples were prepared as listed in Table 6.2.

Table 6.1 Compositions of model formulations M1, M2, and M3 (in weight percentage).

M1	M2	M3
Xylene/Dimethylbenzene (20%)	Xylene/Dimethylbenzene (22.5%)	Xylene/Dimethylbenzene (21%)
Methyl isobutyl ketone solvent (4%)	Methyl isobutyl ketone solvent (4%)	Methyl isobutyl ketone solvent (4%)
Zinc oxide (10%)	Zinc oxide (10%)	Zinc oxide (10%)
Bentonite (2%)	Bentonite (1.5%)	Bentonite (2%)
		Polyethylene wax (2%)
Talc (12%)	Talc (11%)	Talc (11%)
Cuprous oxide (24%)	Cuprous oxide (24%)	Cuprous oxide (24%)
Gum rosin (18%)	Gum rosin (18%)	Gum rosin (18%)
Acrylic binder (10%)	Acrylic binder (9%)	Acrylic binder (8%)

Table 6.2 Coating samples with preparation method and notation. A=naphtha solvent (less volatile than xylene), B=solution of a polyether-modified polymethylalkylsiloxane (silicone surfactant/leveling additive), C=salt of a polymer with phosphoric acidic groups (wetting and dispersing agent), and D=PDMS (additive normally used in FR coatings)[106]

Sample notation	Preparation
M1	Follow formulation M1
M2	Follow formulation M2
M3	Follow formulation M3
M1-diluted	Diluting M1 with xylene
M1-A-5%	Replacing 5% of xylene with A for M1
M1-A-7%	Replacing 7% of xylene with A for M1
M1-A-10%	Replacing 10% of xylene with A for M1
M2-A-10%	Replacing 10% of xylene with A for M2
M3-A-10%	Replacing 10% of xylene with A for M3
M2-B-2%	Adding 2% of B to M2
M2-C-2%	Adding 2% of C to M2
M2-D-2%	Adding 2% of D to M2
M3-C-2%	Adding 2% of C to M3

Different amounts of xylene (5, 7, 10 wt%) were replaced by naphtha (a less volatile solvent), here termed A, for three model formulations. It was suggested to replace maximum 10 wt% of xylene with solvent A by experts from coating industry. In addition, 2 wt% of additives were added to M2 and M3 respectively. Additives B and C were acquired from BYK Additives & Instruments. Adding 2 wt% of an additive changes the concentration of the other ingredients in the formulation by maximum 0.5 wt%, which was considered sufficiently low to neglect the scaling of the other compound concentrations accordingly.

6.2.4 Methodology

To conduct the film application, two types of applicators were designed and manufactured as shown in Figure 6.3. The flat applicator (left) resulted in a flat geometry on top of the coating film and the spiral applicator (right) provided a well-defined sinusoidal surface geometry similar to brush marks and surface patterns after spraying. Both applicators gave around 300 µm of wet film thickness. The wavelength of the sinusoidal geometry was defined by the gap between two spiral coils, which is approximately 3.7 mm. The two applicators were made of stainless steel-316.

Figure 6.3 The two types of applicators used in the investigations: flat applicator (left) and spiral applicator (right).

It was found that the position where coating samples were placed on the panels and the sample volume had an influence on the evenness of the coating film thickness. To obtain an even coating film, the sample volume was set to 9 ml (added by pipette). Moreover, the sample was placed at the same position on the panel and with the same loading pattern every time (using a mold as shown in Figure 6.4).

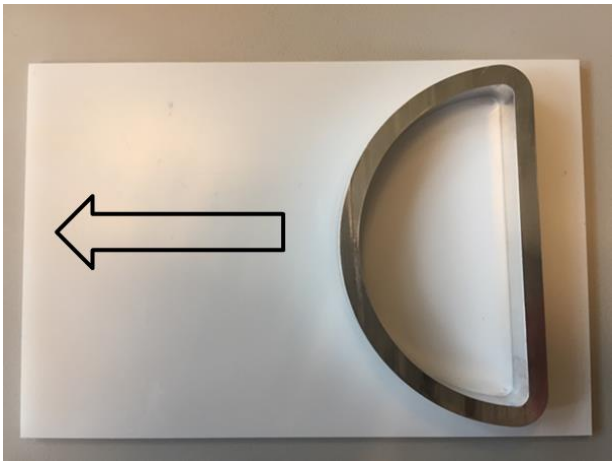

Figure 6.4 Mold used for loading liquid coating samples. The arrow indicates the direction of coating film application.

In the evaluation of surface leveling properties, various surface texture parameters were considered: the average height for roughness profile (*Ra*) and waviness profile (*Wa*) of multiple defined lines in the scanned sampling area, the average maximum peak to valley distance for roughness profile (*Rz*) and waviness profile (*Wz*) of multiple defined lines in the scanned sampling area, and the average height at each measurement point in the scanned sampling area (*Sa*). The parameter calculating methodologies employed by the software comply with ISO standards.[107,108]

When applying different cut-off lengths, λ_c (0.25 mm, 0.8 mm, and 2.5 mm), to the same surface measurement, the values of *Ra* were affected, while the effects on *Wa* were practically insignificant as shown in Figure 6.5. Since λ_c defined the upper limit for the roughness (*Ra*), an increase of λ_c from 0.25 mm to 2.5 mm included higher roughness characteristics. However, for waviness (*Wa*), the increase of λ_c as the lower limit, excluded lower waviness characteristics from the waviness profiles. Consequently, 2.5 mm was chosen for the cut-off length λ_c considering that waviness parameters (*Wa* and *Wz*) were the most relevant ones for leveling studies. As a result, cut-off values and filters were selected as follows: 100 µm for λ_s, 2.5 mm for λ_c, and 18 mm for λ_f to obtain *Ra*, *Rz*, *Wa* and *Wz* values; and 100 µm low-pass filter and 25 mm high-pass filter to obtain *Sa* values.

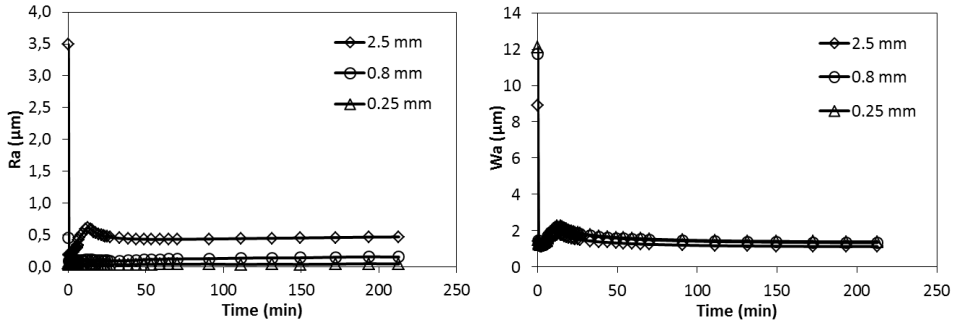

Figure 6.5 Roughness, *Ra* (left), and waviness, *Wa* (right), over time when using different cut-off lengths, λ_c (2.5, 0.8, and 0.25 mm), to the same coating surface measurement.

Evaporation rate experiments

Evaporation rate experiments were performed for selected samples to obtain solvent evaporation profiles. The coating films were applied under the same conditions as those used in the profilometer. Immediately after coating application and onwards, the coated panels were weighed using a precision balance (ENTRIS623I-1S from Sartorius with an accuracy of 0.001 g).

Spraying application

To evaluate the effects of ingredients on leveling in more realistic conditions, application using airless spraying equipment was performed by the same person for selected coatings on flat panels (three replicates). During spraying, most panels were placed vertically, but some were set in a horizontal position for comparison. In practical use, a layer of tie-coat is normally applied to secure good adhesion of the subsequent top coat. However, it was found that the layer of tie-coat also had surface texture itself. Therefore, a few samples were sprayed without tie-coat to investigate the effects on the top coat of the underlying tie-coat. A panel with tie-coat only was also prepared.

Furthermore, surface measurements were conducted using the profilometer after the sprayed samples had dried at room temperature for five days. Each replicate was measured eight times at eight different positions on the panel.

6.2.5 Experimental uncertainty analysis

Considering the entire laboratory procedure, experimental uncertainties are due to the following sources: sample preparation, equipment operation and analysis, and laboratory conditions. The sample uncertainty can be attributed to the inhomogeneity of the coating sample from the same batch, which was kept low by manually stirring the liquid sample prior to experimentation. Operational uncertainties originated from the sample loading position and the sample volume, which could be similar, but not identical in all cases. To minimize the influence of laboratory conditions (e.g., ventilation drafts), experiments were conducted inside a glass cabinet with a stable air circulation at steady ambient temperature.

The uncertainty from the profilometer analysis was estimated by measuring the same surface area 24 times of a dried coating film after spiral application. Standard deviations were within 3% for roughness (*Ra* and *Rz*) and waviness measurements (*Wa* and *Wz*) and within 0.4% for surface roughness (*Sa*).

To estimate the overall experimental uncertainties, which were found to be mainly due to sample inhomogeneity and the loading process, the procedure was repeated three times for the surface measurement and four times for the evaporation rate experiment for coating M2. The results are shown in Figure 6.6. It can be seen that the experimental uncertainties are fairly low for both surface and solvent evaporation rate measurements.

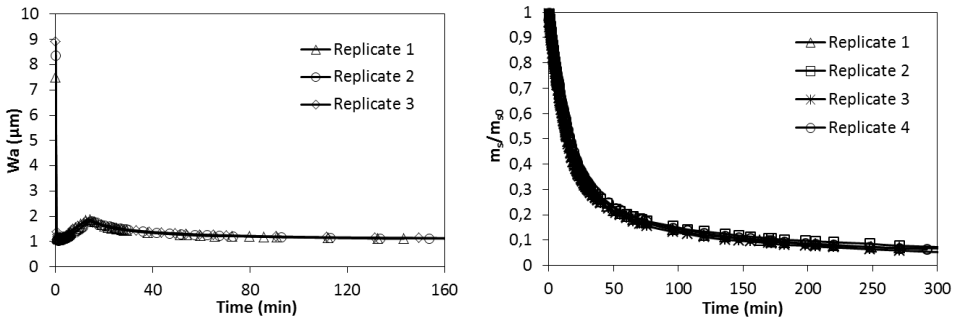

Figure 6.6 Transient *Wa* values for three replicates of surface measurements (left) and the ratio of residual solvent concentration to the initial solvent concentration (m_s/m_{s0}), based on four replicates, over time (right). Coating M2 was used.

6.3 Results and discussion

In this section, the effects of experimental conditions on leveling are presented together with evaporation rate measurements. Furthermore, the effects of coating ingredients on the leveling of AF coatings are demonstrated and quantified. Finally, results from spraying applications are presented.

6.3.1 Effects of applicator type and application conditions

Experiments using the two types of applicators, shown in Figure 6.3, were performed under the same conditions for the same coating sample. The results are shown in Figure 6.7. It can be seen that in the spiral applicator case, *Wa* changes are significantly higher than those of the flat applicator. Meanwhile, the scale of *Wa* values are much larger than those of the flat applicator. Due to that, the spiral applicator was used in the subsequent experiments to provoke surface waviness and show the leveling process.

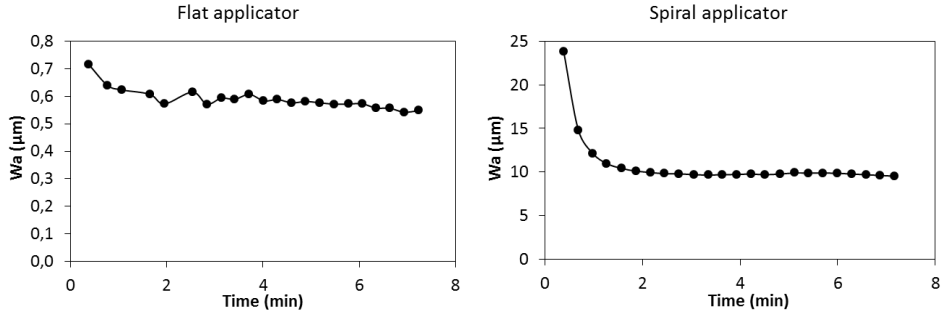

Figure 6.7 Comparison of the waviness parameter, *Wa*, over time using two applicators: flat (left) and spiral (right) for a commercial coating. Notice the big difference in scale on the y-axis.

Coating application speed and vertical force during application can also influence the results. Therefore, experiments using different application speeds (20, 40, 60, and 80 mm/s) with the same vertical force (270 g) were conducted for coating M2. The results (not shown) confirmed that the application speed affected the surface texture development; the surface texture parameter (*Wa*) increased with application speed. Similar results were found for commercial AF coatings.

Furthermore, the effects of different vertical forces (0, 270, 370, and 540 g) were studied for coating M1-diluted and M2 under the same application speed (80 mm/s). The results (not shown) showed that the

effects of the vertical force on leveling were insignificant considering the experimental uncertainty. Consequently, the maximum application speed (80 mm/s) with constant vertical force (270 g) was used for the subsequent experiments.

6.3.2 Evaporation rate experiments

Results of evaporation rate experiments for coatings M1 and M2 are shown in Figure 6.8, together with changes in the surface texture parameter (*Wa*).

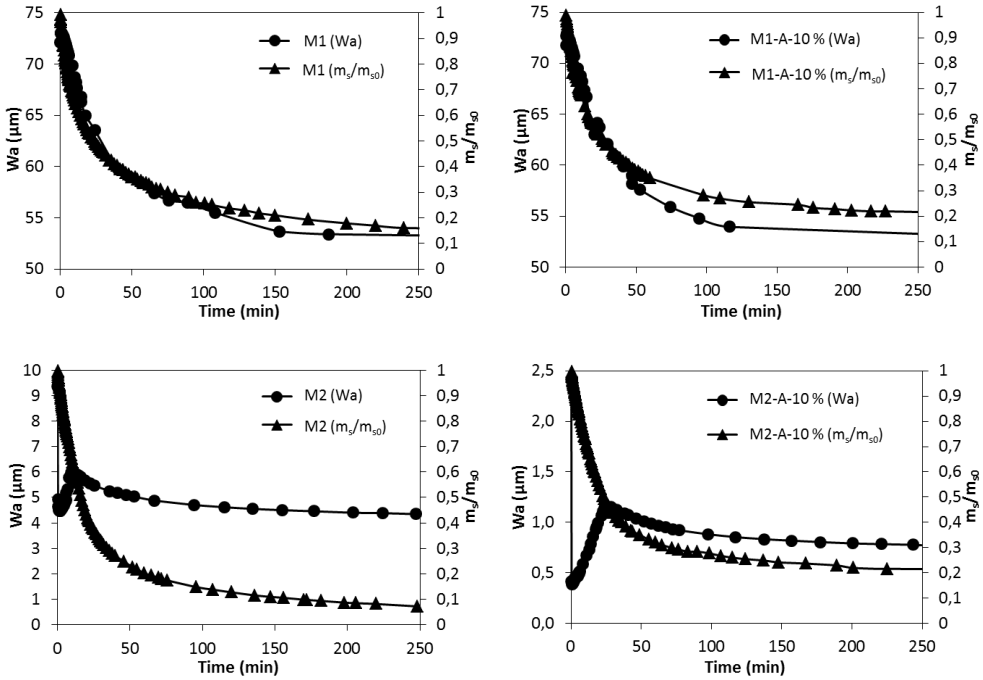

Figure 6.8 Surface texture parameter (*Wa*) and the ratio of residual solvent concentration to the initial solvent concentration (m_s/m_{s0}) as a function of time. The inserts show: coating M1 (upper left), coating M1 after replacing 10% of xylene with less volatile solvent (naphtha) A (upper right), coating M2 (bottom left) and coating M2 after replacing 10% of xylene with less volatile solvent (naphtha) A (bottom right). Notice the large difference in Wa scale between M1 and M2.

It can be seen that the solvent evaporation curves initially exhibit a constant evaporation rate period (for both M1 and M2), where the external solvent mass transport resistance dominates. Later the evaporation rate declines and is now dominated (and eventually controlled) by solvent diffusion through the coating film.[61]

For the M1 coatings (the two upper curves), the changes in *Wa* values over time are coupled to the evaporation curves and the associated development in coating viscosity. The replacement of 10% of xylene with less volatile solvent (naphtha) A has a small effect on the *Wa* values.

Compared to the M1 coatings, on the other hand, *Wa* values of the M2 coatings (the two lower curves) seem to develop in a very different way. First of all, in the first part of the constant evaporation rate period, an initial large drop of *Wa* occurs (the first *Wa* points are overlapping with the first data points on the evaporation curve). Then *Wa* increases, before it abruptly starts to decrease. Second, the changes in *Wa* values are rather small (of the order of one μm), except the very first data points, compared to those of M1 (about 25 μm change). In addition, based on a comparison between left and right hand figures, the replacement of 10% of xylene with naphtha A, prolongs the initially constant evaporation rate period from about 20 mins to 30 mins and has a correspondingly larger effect on the leveling compared to M1. Furthermore, after the constant evaporation rate period, the evaporation rate declined much faster for M2-A-10% than M2 and a larger amount of solvent A (about 20%) was trapped in the coating film (the m_s/m_{s0} value did not change much after 250 mins).

The initial drop that occurs at the very beginning of the evaporation (within one min) is most likely attributed to the low viscosity of M2 coatings which gives the coating more flow ability to level out immediately after application. The images and profile pictures obtained (not shown), verified that, after application, a liquid glossy 'fast-leveling layer' appears on the top surface due to the high solvent content, which leads to a very low surface roughness and waviness.

Furthermore, the initial drop is mainly attributed to a decrease of waviness rather than roughness. After about one min, the solid content is increasing gradually to a certain level, where the liquid 'fast-leveling layer' gradually disappears due to fast solvent evaporation. During this process, the peaks and valleys become clearer due to the loss of solvent (see Table 6.3), and therefore *Wa* value starts to increase gradually. Meanwhile, the pigments inside the coating film are gradually exposed on top of the surface and the surface roughness (not shown) starts to increase. The exposed pigments can be seen in Figure 6.9.

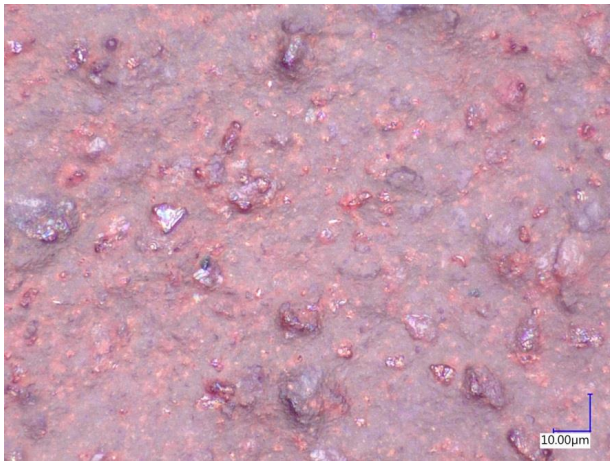

Figure 6.9 Digital microscope (KEYENCE (VHX-6000)) image of a dried M2 coating surface.

During this process, solvent evaporation is limited mainly by external mass transfer, which corresponds to the constant evaporation rate period. The increase stops after around 10 mins for M2 and 30 mins for M2-A-10% from where on the following process is very similar to those of M1 coatings and evaporation continues mainly through intra film solvent diffusion.

Summarizing, there are three leveling stages for low viscous coatings from this application approach: the initial stage with dramatic drop of surface texture parameters (fast leveling), the middle stage with gradual increase of surface texture parameters, and the final stage with gradual decrease of surface texture parameters (slow leveling). Solvent evaporation is dominated by external mass transport with a high evaporation rate in the first two stages and by internal solvent diffusion in the final stage.

Another evidence for the three leveling stages noticed in the waviness profiles (see Table 6.3) is that the waviness of the sinusoidal surface ripples decreases significantly from the very first measurement (8 s) to the second (29 s). Moreover, a reversal process is observed: some peaks become valleys and vice versa. This observation confirms the theory[60,63] that leveling is driven by both surface tension and the surface-tension-gradient from peaks to valleys. After the reversal process, the waviness height of peaks and valleys enhances for a period (108-743 s) due to the solvent evaporation and subsequently starts to decrease (after 743 s).

Table 6.3 Waviness profiles at different times after application with same axis scales for M2 coating.

Time (s)	Waviness profile
8	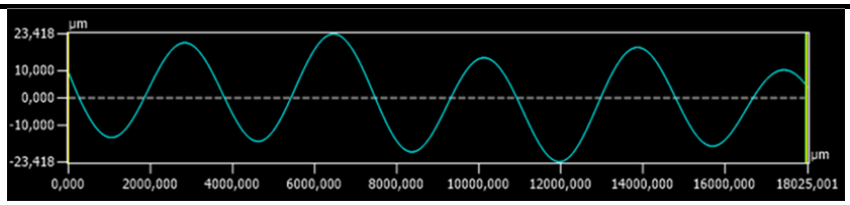
29	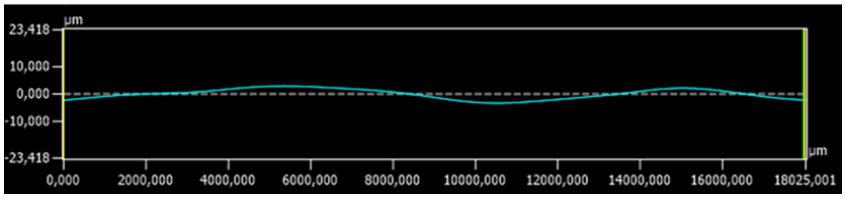
108	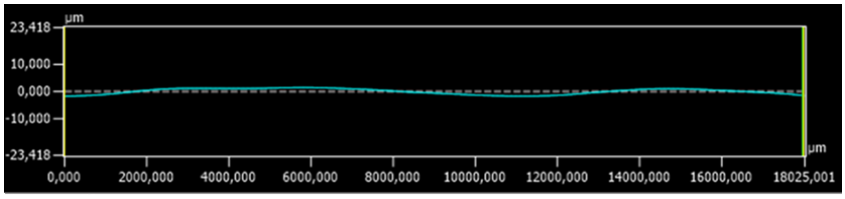
217	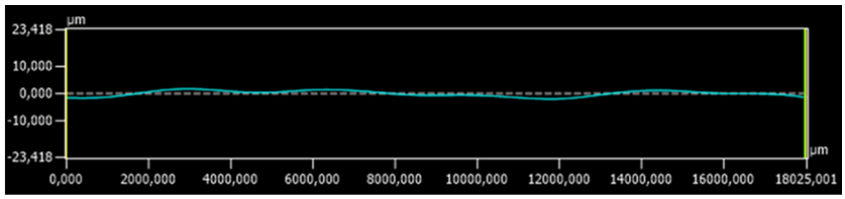
743	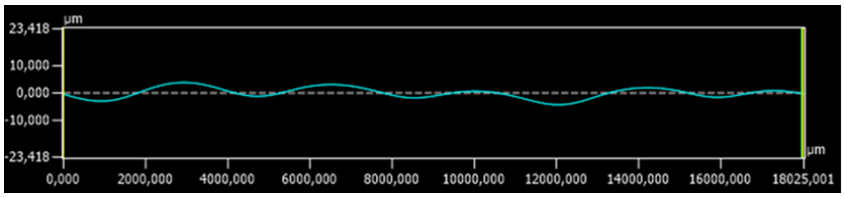
12766	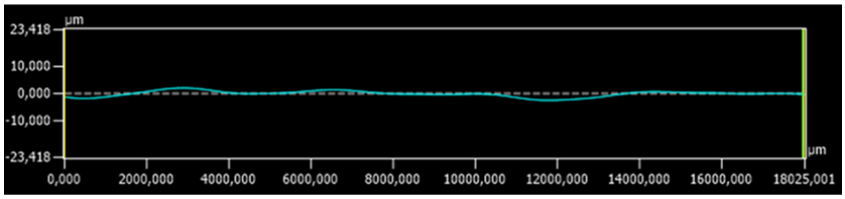

6.3.3 Effects of coating ingredients on leveling of coatings M1 and M2

The effects of replacing xylene with less volatile solvent (naphtha) A with different concentrations on leveling of coating M1 are shown in Figure 6.10. It can be seen that the effects are insignificant considering the experimental uncertainty. The effects of adding 2% of polyether-modified polymethylalkylsiloxane solution (silicone surfactant/leveling additive) B, salt of a polymer with acidic groups (wetting and dispersing agent) C, and PDMS (silicone additive) D on leveling of coating M1 were also found to be insignificant (plots not shown).

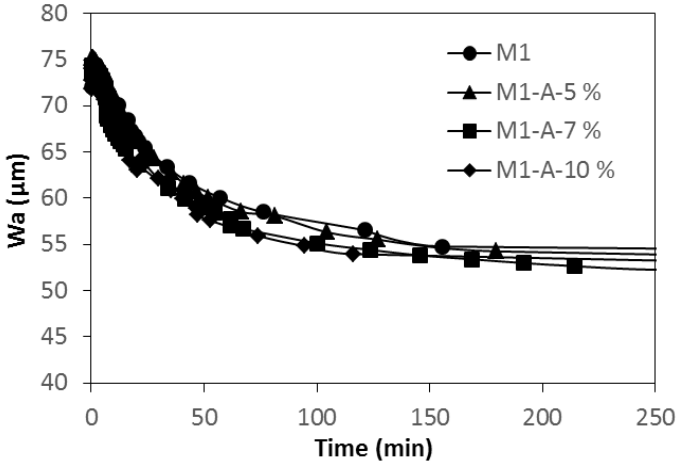

Figure 6.10 Surface texture parameter (*Wa*) over time when replacing different percentages (0, 5, 7, and 10%) of xylene solvent with a less volatile solvent (naphtha) A for coating M1.

The insignificant effects might be attributed to the high viscosity of the coating M1 which results in a low flow ability. After application, the top coating surface in contact with air rapidly formed a 'skin'. However, due to solvent remaining inside the coating film, leveling could still take place, and the rate of solvent evaporation was limited by internal solvent diffusion rather than external mass transport.

Due to the high viscosity of coating M1, a similar formulation M2 with a lower viscosity (within the viscosity range of commercial AF coatings) was formulated. Figure 6.11 shows the effects of different additives and the less volatile solvent on leveling of coating M2.

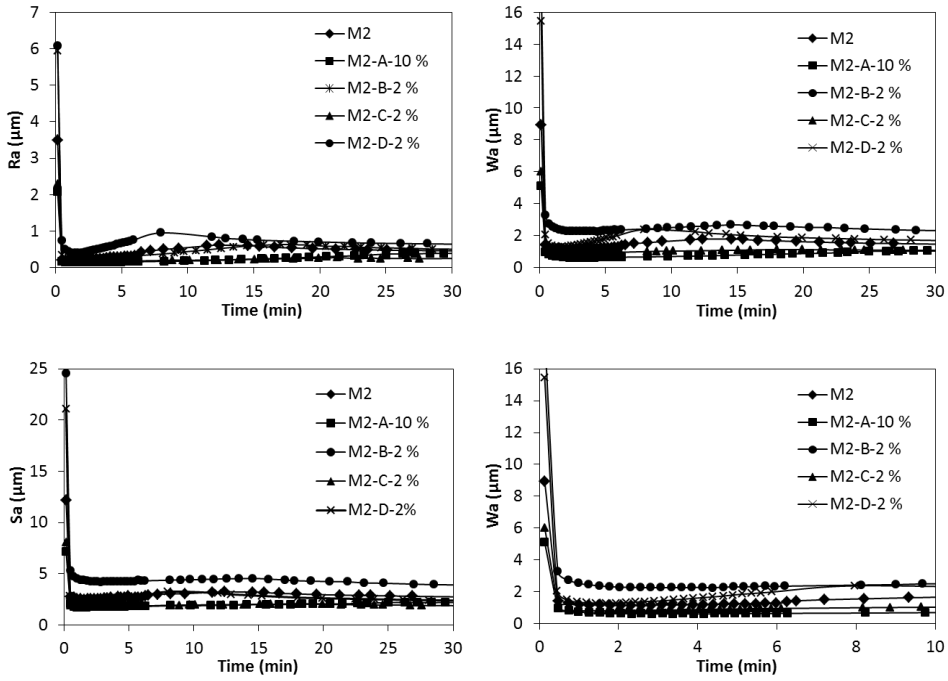

Figure 6.11 Surface texture parameters (*Ra*, *Wa* and *Sa*) over time after adding 2% of polyether-modified polymethylalkylsiloxane solution (silicone surfactant/leveling additive) B, salt of a polymer with acidic groups (wetting and dispersing agent) C, PDMS (silicone additive) D, and after replacing 10% of xylene with less volatile solvent (naphtha) A for coating M2. The lower right hand plot shows *Wa* changes within the first 10 mins.

It is evident from the plots that the addition of 2% of silicone surfactant B increases slightly the waviness, *Wa*, and the entire surface roughness, *Sa*, which indicates that silicone surfactant B has negative effects on leveling performance of coating M2. This result is in agreement with the findings from Schwartz and co-workers.[71] After adding 2% of PDMS (silicone additive) D, the roughness, Ra, and waviness, *Wa*, values are increased though the entire surface roughness is not much affected. Therefore, PDMS does not have positive effects on leveling of coating M2. All the plots show that adding 2% of wetting and dispersing agent C and replacing 10% of xylene with a less volatile solvent (naphtha) A decrease slightly all the surface texture parameters. However, the reductions are not great. These effects are further investigated in a later section using spraying application.

6.3.4 Effects of initial coating viscosity on leveling and evaporation

The major difference between M1 and M2 coatings is the viscosity which leads to the different leveling behaviors after application. Therefore, to further investigate the effects of viscosity on leveling, a comparison of model formulations with three viscosities (8, 4.3, 2.2 Pa·s) is shown in Figure 6.12 (other surface texture parameters show similar results, which are not shown).

The effects of viscosity on leveling behavior and surface texture of the final dry coatings are significant. First, it can be seen that different viscosities give different initial values of *Wa* at about 15 second. Second, there is an initial drop after application for coating M1-diluted, which is similar to coating M2. However, after the initial drop, the increasing value of *Wa* did not occur in a similar way to coating M2. The possible reason may be due to the higher viscosity of coating M1-diluted compared to coating M2. The higher viscosity probably limits the initial drop to a much lower extent (due to the low flow ability) so that the increasing process of *Wa* (arising from the enhanced peaks and valleys) was not remarkable. Notice that the second data point of M1-diluted dropped to about 55 μm which is far higher than that of M2 (about 5 μm).

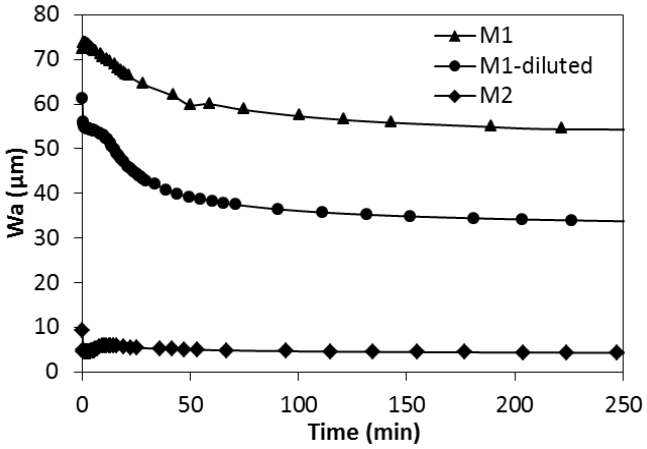

Figure 6.12 Surface texture parameter (*Wa*) as a function of time for model formulations with different viscosities measured at a shear rate of 117.4 s^{-1}: M1 (8 Pa·s), M1-diluted (4.3 Pa·s), and M2 (2.2 Pa·s).

6.3.5 Spraying application and sagging control

To further evaluate the ingredient effects on leveling of M2 coating, samples M2, M2-C-2%, and M2-A-10% were sprayed vertically and horizontally on flat panels for surface measurements. However, sagging appeared on the vertically sprayed panels, especially for the sample M2-C-2%. Furthermore, to evaluate the effects of the underlying tie-coat layer, a pure tie-coat layer sprayed on a flat panel was also measured. The average values from all measurements are summarized in Table 6.4.

Table 6.4 Comparison of surface measurements from different application methods. Each value is the average of three replicates. Only the highest standard deviation is indicated for each parameter.

Application method	**Sample**	***Ra* (µm) ±0.12**	***Rz* (µm) ±0.78**	***Wa* (µm) ±0.44**	***Wz* (µm) ±1.86**	***Sa* (µm) ±0.35**
Drawdown (no sagging)	M2	0.47	2.10	1.13	6.41	2.26
	M2-A-10%	0.34	1.68	0.70	3.64	1.61
	M2-C-2%	0.44	2.28	0.88	5.35	1.58
Spraying horizontally (no sagging)	M2	0.96	5.52	1.89	9.26	3.38
	M2-A-10%	0.96	5.08	1.84	9.62	3.57
	M2-C-2%	0.90	4.67	1.61	8.32	2.94
Spraying vertically (sagging)	M2	1.16	5.83	3.36	16.40	5.55
	M2-C-2%	1.27	5.84	3.58	17.64	5.59
	Tie-coat	2.77	13.28	4.53	24.21	7.12

Comparing the results from drawdown and horizontally spraying application without sagging, it can be seen that the values of all the parameters from spraying application are higher than those from drawdown application for the same sample. The effects of adding 2% of C and replacing 10% of xylene with A on leveling are insignificant when employing spraying application. In addition, the values of those parameters for pure tie-coat are much higher than those with one layer of top coat after vertical spraying, which means that the top coat can cover some of the tie-coat surface texture.

Due to sagging, the parameter values from vertical spraying are higher than those from horizontal spraying, in particular for waviness. Therefore, during spraying application on ship hulls, a better leveling effect can easily be compromised by unacceptable sagging values.

Effects of tie-coat and anti-sagging agent E

Coating M3 with anti-sagging agent E was vertically sprayed on flat panels with and without tie-coat (the same tie-coat as used for coating M2). No sagging was observed. The results of surface measurements are shown in Figure 6.13.

It can be seen that all surface parameters are increased after spraying with underlying tie-coat. It confirms again the negative effect of the tie-coat on the surface texture of the final top coat. Compared to the results of coating M2 sprayed vertically with sagging (see Table 6.4), surface texture parameters of coating M3 are still increased after adding anti-sagging agent. It indicates that although anti-sagging agents can stop sagging, they limit leveling as well.

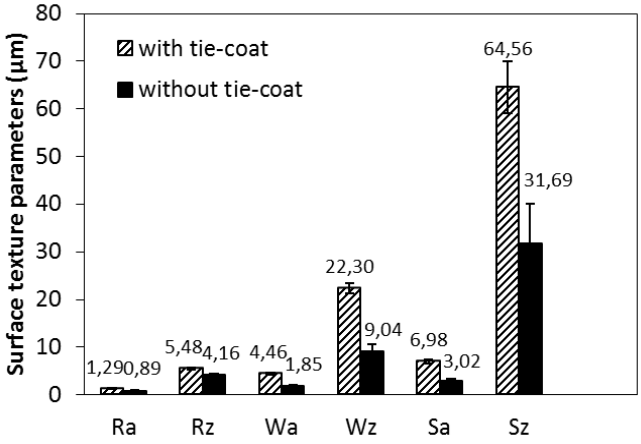

Figure 6.13 Surface texture parameters of dried model formulation (M3) with anti-sagging agent E after vertical spraying on flat panels with and without tie-coat. Each data point is the average of all measurements and the error bars shown represent the standard deviations of all measurements.

Effects of coating ingredients on leveling of coating M3

The effects of wetting and dispersing agent C and less volatile solvent (naphtha) A on leveling of coating M3 were further investigated. Samples M3, M3-A-10%, and M3-C-2% were sprayed vertically on flat panels with tie-coat. No sagging was visually observed when the wet film thickness was controlled below 300 µm for M3, 350 µm for M3-A-10%, and 275 µm for M3-C-2%. Furthermore, the three samples were also measured after spiral-drawdown application using the profilometer. The surface measurement

results of the three samples are summarized and compared with M2 samples in Figure 6.14 after spiral-drawdown applications and in Figure 6.15 after vertical spraying applications.

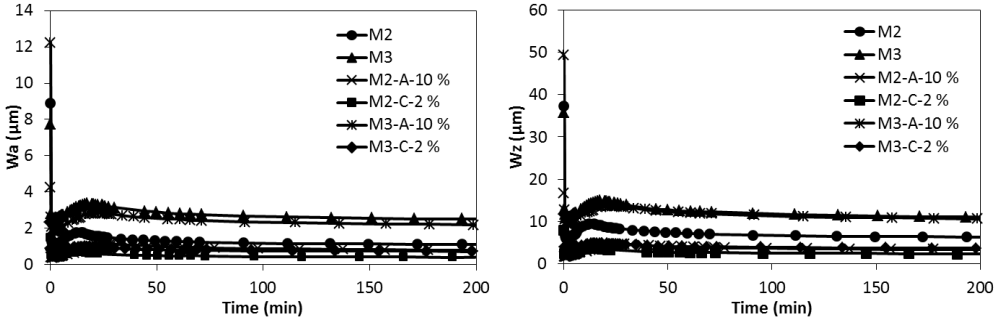

Figure 6.14 Waviness parameters, *Wa* and *Wz*, over time for coating M2 (without anti-sagging agent E), M3 (with anti-sagging agent E), M2-A-10% (without anti-sagging agent E and replacing 10% of xylene with less volatile solvent, naphtha, A), M2-C-2% (without anti-sagging agent E and with dispersing agent C), M3-A-10% (with anti-sagging agent E and replacing 10% of xylene with less volatile solvent, naphtha, A), and M3-C-2% (with anti-sagging agent E and dispersing agent C).

Figure 6.14 shows that after using anti-sagging agent E, surface waviness of coating M3 increases compared to coating M2, which means that leveling becomes worse when adding anti-sagging agent. This is in agreement with the aforementioned results from the spraying application. For coating M3, replacing 10% of xylene with less volatile solvent (naphtha) A does not show significant effects in decreasing surface waviness. Nevertheless, adding 2% of dispersing agent C decreases the waviness of M3 largely to a similar effect level as M2-A-10%. It means that it is possible to obtain good leveling performance with anti-sagging agent involved in the formulation.

The surface measurement results of the final dried coating after spraying are different as shown in Figure 6.15. Adding 2% of wetting agent C and replacing 10% of xylene with naphtha solvent A increase surface waviness of coating M3, which indicates that surface leveling of coating M3 becomes worse. The possible reason may be due to the uncertainty from spraying application (e.g., human operation uncertainties). Another reason might be that the spray ability of those samples was not tuned from the formulation point of view. Therefore, the effects of ingredients on leveling of model formulations, using the spiral-drawdown application, could not be reproduced with spraying application.

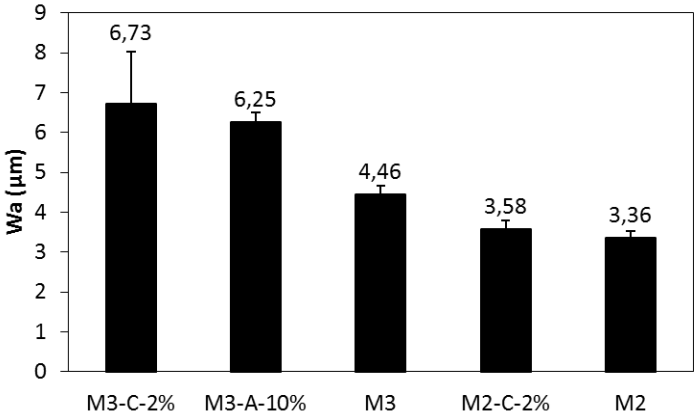

Figure 6.15 *Wa* values of dried samples M3-C-2% (with anti-sagging agent E and wetting agent C), M3-A-10% (with anti-sagging agent E and replacing 10% of xylene with naphtha solvent A), M3 (with anti-sagging agent E), M2-C-2% (without anti-sagging agent E and with wetting agent C), M2 (without anti-sagging agent E) after spraying vertically with tie-coat. Each data point is the average of all measurements and the error bars shown represent standard deviations based on all measurements.

6.4 Conclusions

An approach for quantitatively measuring leveling performance of coatings was developed using a combination of an optical 3D profilometer and a retrofitted automatic film application system. Using this approach on model formulations for AF coatings, the effects of coating ingredients on leveling performance and the underlying leveling mechanisms were investigated. A special made spiral applicator was found to generate well-defined sinusoidal surface textures with waviness patterns.

It was found that leveling rate was strongly coupled to the solvent evaporation rate and the associated development in coating viscosity. Thus, the hypothesis (5) was found to be true. The leveling behavior for coatings with a low viscosity developed quite differently compared to coatings with a high viscosity. Three leveling stages, coupled to the evaporation process, were discovered for less viscous coatings, while high viscous coatings only went through the final stage.

Due to a less controlled process, the effects of additives and solvents on leveling of model formulations observed from the spiral-drawdown application were not found when using spraying application.

Moreover, when coatings are sprayed on ship hulls, a better leveling effect can be easily compromised by sagging problem.

6.5 Additional results

After developing the aforementioned approach, the leveling processes of commercial AF and FR coatings were compared using the optical profilometer. Hempaguard X7 (FR) and Globic 9000 (AF) were used, the same coatings as used in the drag comparison in chapter 4. Both coatings were supplied by Hempel A/S. The film application for both coatings was performed using the automatic application system with the spiral applicator giving about 300 µm of wet film thickness. The changes of waviness, *Wa*, are shown in Figure 6.16.

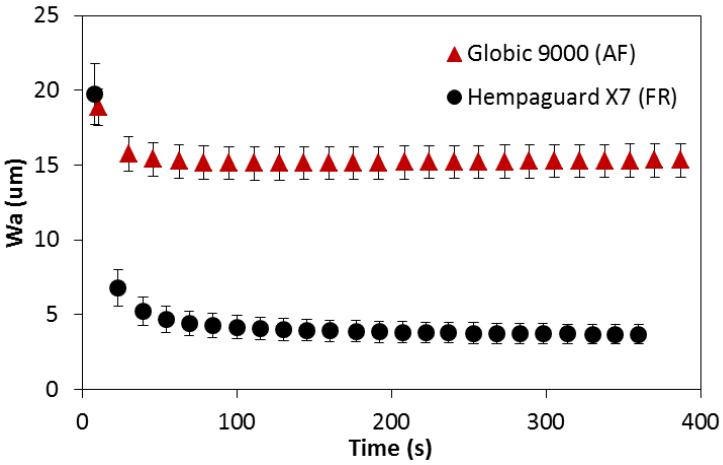

Figure 6.16 Waviness parameter, *Wa*, over time for commercial AF (Globic 9000) and FR (Hempaguard X7) coatings. The spiral applicator giving around 300 µm of wet film thickness was used.

Figure 6.16 shows that Hempaguard X7 reached much lower waviness than Globic 9000 (about 10 µm), which confirmed that FR coating had better leveling performance than AF coating. In addition, previous results from chapter 4 showed that FR coating led to less skin friction than AF coating (about 5.6%). Therefore, the overall hypothesis behind the project that improving leveling properties of AF coatings leads to lower surface waviness and thereby less drag resistance was verified to be true. Accordingly, the ideal target (FR coatings) for waviness reduction of AF coatings would be approximately 10 µm.

7 Leveling kinetics of coatings with solvent evaporation and non-Newtonian rheology

This chapter has been written in a manuscript format and a modified version will be submitted as "Leveling kinetics of coatings with solvent evaporation and non-Newtonian rheology" to *Progress in Organic Coatings*. The authors to be included in the publication are *Xueting Wang, Yixin Huang, Claus Erik Weinell, Stefan Møller Olsen,* and *Søren Kiil*.

Abstract

In this chapter, two AF coatings (a model and a full commercial system) were considered in a leveling kinetics study. Using an optical 3D profilometer, an advanced rheometer, and evaporation rate measurements, the transient effects of wet film thickness, application wavelength, and coating viscosity on leveling could be investigated.

The model coating was able to level faster and had better final leveling performance than the commercial coating. This was attributed to the different viscosity profiles of the two coatings, the main difference being that the commercial coating contained additives (thixotropic and wetting agents) that affect the coating rheology.

A semi-empirical model, based on the so-called Orchard equation for ideal conditions, but modified here to take into account solvent evaporation and non-Newtonian rheology, was developed for the leveling kinetics. Due to the differences in rheological behavior for the two coatings considered, adjustable model parameters needed to be fitted for each coating case. Overall, viscosity build-up was found to be the dominating parameter for leveling.

7.1 Introduction

The appearance and performance of coatings depend on the ability of the coating to level. One example is orange peel after spraying application, where a rough coating texture (similar to the surface of an

orange) can result from unbalanced coating formulation or spray conditions.[109] This affects the esthetic appearance of coatings and constitutes sites of potential weakness, which may harm the coating performance.[81,82] Another example is FCCs on ship hulls where the coating surface must be smooth to lower skin friction and the associated fuel consumption. A non-smooth surface also leads to more biofouling.[98]

7.1.1 Leveling studies of coatings

The importance of leveling for surface protection was early recognized and leveling of coatings has been studied since the 1920s. However, progressing the understanding of the mechanisms and the influencing factors of leveling has been slow.[82] In 1961, the leveling phenomenon was investigated by Smith, Orchard, and Rhind-Tutt through brush mark studies.[54] Two years later, a systematic study of leveling was published by Orchard,[56] wherein he proposed a rate equation which later became known as the so-called Orchard equation:

$$ln\left(\frac{a_0}{a_t}\right) = \frac{16\pi^4\sigma h^3 t}{3\lambda^4\eta} \tag{7.1}$$

where, a_t and a_0 represent amplitudes of surface 'waves' at time t and time zero, respectively. σ is the coating surface tension, h represents the average film thickness, λ is the wavelength, and η is the coating viscosity. He proposed that surface tension is the dominant driving force for leveling when the wavelength is less than one cm.[56] Orchard, as a basis for his equation, assumed a sinusoidally structured coating surface on a smooth substrate as illustrated in Figure 7.1.

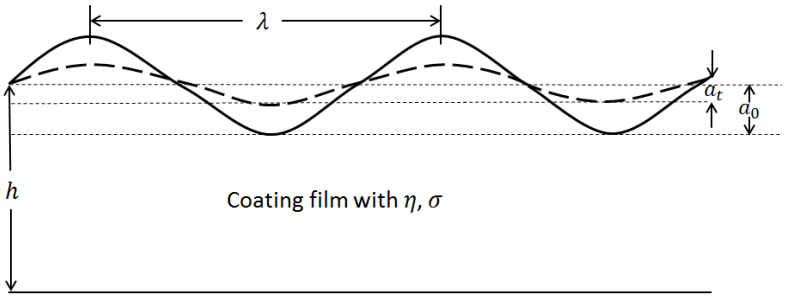

Figure 7.1 Schematic illustration of a sinusoidally structured coating film. The solid line (wavy curve) represents the initial coating surface with amplitude a_0 and the dashed line (wavy curve) represents the coating surface with amplitude a_t after leveling time t. h is the average film thickness, λ is the wavelength, η is the coating viscosity, and σ is the surface tension of the coating film, respectively.

The Orchard equation was derived assuming that the average film thickness, the application wavelength, and the coating viscosity do not change over time. This, of course, is unrealistic for coatings containing solvents that evaporate during and after application. The surface tension was also assumed to be constant, which is in good agreement with the work of Smith and co-workers,[54] Overdiep[60] and Fabian,[59] who found that surface tension in practice typically only changes a few percent over the course of leveling. One thing to notice, is that the Orchard equation (because of the assumption of no evaporation and Newtonian liquid) predicts that with time, an entirely smooth surface is formed (a_t goes to zero, when t goes to infinity), which is not useful for practical coating applications, where this performance is not achieved.

Coating viscosity is probably the most important parameter for leveling. In practice, it will vary from the initial liquid coating viscosity and gradually increase and essentially become infinite as the coating changes from a viscoelastic liquid to a viscoelastic solid. This happens due to solvent evaporation and chemical or physical curing of the coating. Coating viscosity is also a function of shear which changes from high shear during application to much lower shear during leveling. The thixotropic (time-dependent shear-thinning) effect complicates the viscosity behaviors during leveling even more. In addition, due to solvent evaporation, the average film thickness decreases over time. It is perhaps not surprising, that Overdiep[60] could demonstrate that the Orchard equation failed, even qualitatively, to describe leveling of solvent-based alkyd coatings.

Wilson, based on the Overdiep model, continued the development work on models for coating films.[62–64] Various numerical models were developed based on the so-called lubrication theory, a time-dependent solution of the Navier-Stokes equations.[99,110–113] In those models, two assumptions were needed: 1) the amplitude is small relative to the average film thickness, and 2) the wavelength is long relative to the average film thickness. Various effects were included in the models, such as gravitational pull, surface-tension-gradient effects (also known as Marangoni effects) arising from non-uniformities in the local concentration of solvent,[63] and non-Newtonian effects. However, the models only included one or a couple of those effects.[59] Overall, it has been a challenge to cover all phenomena in one model.

In previous investigations,[60,81,102] measurements of leveling were not quantitative and most of the approaches were designed for certain specialized types of coatings such as alkyd coating, spin coating, or powder coating. However, Bosma *et al.*[66] developed a method for estimation of leveling behavior of powder coatings in a quantitative manner. In the same year, the evolution of surface texture in automotive coatings was investigated systematically by Peters *et al.*,[58] where Newtonian flow without solvent evaporation, Newtonian flow with solvent evaporation, and viscoelastic coatings with non-Newtonian behavior were studied separately, using model liquids and commercial coatings. They found that the evolution of surface texture was strongly correlated to temperature and solvent content.

7.1.2 Strategy of investigation

In the present investigation, the new approach developed in the earlier work (presented in chapter 6), was used to study leveling. The technique involves a combination of an automatic spiral-drawdown application and a 3D measurement system based on an optical profilometer. With this macroscopic approach, a well-defined sinusoidal surface structure can be generated on the coating surface, thereby allowing the effects of important physical parameters (average film thickness, application wavelength, and coating viscosity) on leveling to be systematically studied. Furthermore, by combining the macroscopic approach with separate measurements in an advanced rheometer, dynamic data for waviness, average film thickness, wavelength, and viscosity could be collected non-destructively during leveling process. As a consequence, it was possible to quantify the leveling kinetics of coatings with solvent evaporation and non-Newtonian rheology.

As a case study for the investigations, a FCC was selected. More specifically, a conventional biocide and solvent-based AF coating type was used. FCCs are applied as top layers on ship hulls to prevent biofouling growth and thereby to limit drag resistance.[1] A rough FCC surface can increase the frictional resistance and constitute sites of weakness, i.e., potential starting points for corrosion, cracking, blistering and biofouling.[5,6] The reason for choosing an AF coating is that it presents a rather rough coating surface due to the high pigment volume concentration (> about 40%) and it cures by physical drying only (no crosslinking).

7.2 Materials and methodology

7.2.1 Equipment

Surface measurements of coatings, after film application on acrylic panels with a retrofitting commercial film applicator (Coatmaster from Erichsen), were conducted using an optical 3D profilometer from KEYENCE. Viscosity measurements were performed using a DHR-2 rheometer from TA Instruments. Detailed descriptions for both equipment and uncertainty analysis can be found in the previous work (see chapter 5 and 6). Equipment uncertainty for waviness measurements using the profilometer was about 3%.

Spiral rod applicators with different dimensions (see Figure 7.2) were tailor-made and used in the experiments. The spiral applicators provided well-defined sinusoidal surface geometries and ensured various initial wet film thicknesses and wavelengths. For the sinusoidal geometry, the wavelength was defined by the gap between two spiral wires. The initial wet film thickness was controlled by the depth

of the grooves between two wires which was determined by the size of the wires, the larger the wire, the larger the grooves. All applicators were made of stainless steel-316.

Figure 7.2 Spiral applicators with different dimensions of application wavelength and targeted initial wet film thickness.

7.2.2 Materials

A commercial AF coating (Globic 9000 78950) and two model AF coatings were used in the investigations. The two model AF coatings were prepared based on a simplified reference formulation which was formulated based on commercial AF coatings. The composition of the simplified reference formulation is shown in Table 7.1. The two model coatings had higher solvent contents than the reference formulation; sample S1 26.9 wt% and sample S2 27.6 wt%.

The raw materials were all supplied by Hempel A/S. Coatings were produced using high-speed dispersion. During coating sample preparation, the fineness of grind was targeted to 40 µm.

To investigate the effects of viscosity on leveling, coating samples with different solvent contents (31, 29, 28, 27, 25, and 24 wt%) were prepared based on sample S1 to give different initial viscosities.

Table 7.1 Composition of a simplified reference AF coating formulation.

Ingredients	Concentration (wt%)
Xylene/Dimethylbenzene	20
Methyl isobutyl ketone solvent	4
Zinc oxide	10
Bentonite	2
Talc	12
Cuprous oxide	24
Gum rosin	18
Acrylic binder	10

7.2.3 Methodology

Surface measurements (waviness and wavelength measurements)

The detailed operational procedure for surface measurements using the film application system and profilometer, as well as how to differentiate roughness and waviness based on choosing proper cut-off lengths can be found in the previous chapter. Here will only be given a concise description.

The waviness parameter, Wa (the average height for waviness profile of multiple defined lines in the scanned sampling area), was used to evaluate the leveling performance. The calculating methodology used for Wa complies with ISO standards.[107,108] To obtain the waviness profile, cut-off length values of 2.5 mm and 0.8 mm (λ_c) were applied for coating surfaces generated from spiral applicators with wavelengths of 3.7, 1 or 2 mm, respectively. Meanwhile, the wavelength changes during leveling process could also be obtained from the transient surface measurements.

Average film thickness measurements

The average film thickness decrease, due to solvent evaporation, was directly measured using the profilometer. The same application procedure as for the surface measurements was used. Then the coated panel was placed at a location where the edge of the coating film could be scanned by the profilometer as shown in Figure 7.3 (left). Subsequently, the average film thickness was measured from the surface profile (Figure 7.3, right). Thus, transient average film thickness values during solvent

evaporation and the leveling process were obtainable from the same location at different times after film application.

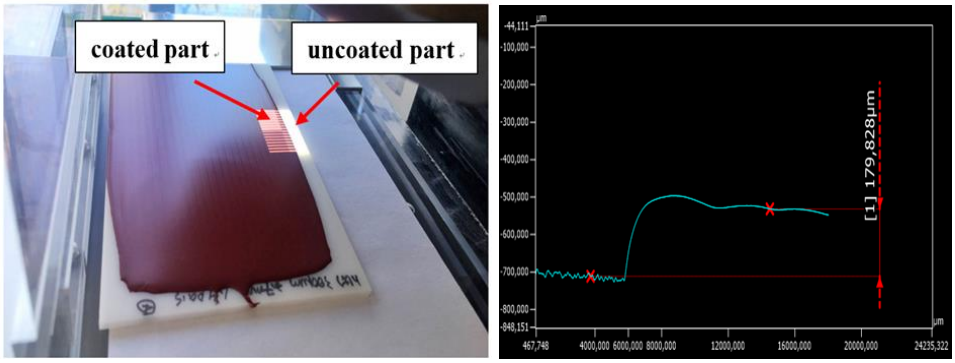

Figure 7.3 The average film thickness measurement after application (left) and an example of a measurement series obtained from the surface profile (right) at a given point in time. In the figure to the right, the average film thickness was estimated to about 180 µm, as indicated in the figure.

Evaporation rate experiments

To obtain solvent evaporation profiles, separate evaporation rate experiments were performed. The coating films were applied under the same conditions as those used in the surface measurements to simulate the solvent evaporation process during surface measurements. Immediately after coating application and onwards, the coated panels were weighed using a precision balance (ENTRIS623I-1S from Sartorius with an accuracy of 0.001 g). For each sample, the same procedure was repeated three times.

7.2.3.1 Experimental procedure for studying effects of individual physical parameters on leveling

The following experimental procedures were performed to study the effects on leveling of coating sample S1 of different individual physical parameters, including the initial wet film thickness, the application wavelength, and the coating viscosity.

To investigate the effects of the initial wet film thickness, film applications with different spiral applicators (300, 400, and 500 µm) with the same initial wavelength (3.7 mm) were conducted.

Immediately after each application, the surface measurement was initiated. Three repetitions were done for the initial wet film thickness of 300 µm.

To investigate the effects of the application wavelength, film applications with different applicators (1, 2, and 3.7 mm) with the same initial wet film thickness (300 µm) were performed. The same experimental procedure was repeated three times for each wavelength.

The effects of viscosity on leveling were studied using coating samples with different solvent contents (31, 29, 28, 27, 25, and 24 wt%). The viscosity of each sample was measured using a DHR-2 rheometer under the same constant shear rate of 117.4 s^{-1} (similar to the shear rate generated from a KU-1 Viscometer from Brookfield as used in industry). The film application for each sample was performed using the spiral applicator with a wavelength of 3.7 mm giving an initial wet film thickness of 300 µm. Following application, the surface measurement was performed for each sample. For two coating samples, the film application and surface measurement procedure were repeated three times.

Separate evaporation rate experiments were conducted for coating samples with solvent contents of 29, 27, and 24 wt% to further understand the effects of viscosity on leveling. For each sample, two repetitions were performed.

7.2.3.2 Collection of experimental data series for model development

Using the spiral applicator with a wavelength of 3.7 mm, all coating samples were applied on acrylic panels aiming at an initial wet film thickness of 300 µm. After application, changes in waviness (Wa), wavelength, and average film thickness were obtained in the same ways as in the aforementioned "surface measurements" and "average film thickness measurements" sections. Both surface measurements (for obtaining waviness and wavelength values) and average film thickness measurements were repeated five times for sample S2 and three times for the commercial AF coating.

Viscosity measurements

The solvent contents of applied and curing coatings, corresponding to different experimental times during a leveling experiment, were obtained from the solvent evaporation rate experiments (using approximately the same film thickness, application method, and laboratory air conditions for leveling and evaporation). Subsequently, these solvent content-time data sets (see Table 7.2 for an example) enabled the formulation of a series of separate coating samples with the exact same solvent contents as

those observed in the time series, which could then be used for viscosity measurements at a constant shear rate corresponding to leveling. In other words, it was (approximately) possible to follow the viscosity development of a given coating during simultaneous leveling and solvent evaporation. However, one limitation for the coatings considered was that the prepared samples could only cover the coating conditions within the initial 8.5 minutes after application because of too high viscosity values at later times (where the coating went from a viscoelastic liquid to a viscoelastic solid).

Table 7.2 Samples prepared for viscosity measurements and their corresponding solvent contents at different times during leveling of sample S2 after application.

Sample No.	Time after application (s)	Solvent content (wt%)
1	0	27.55
2	50	27.02
3	95	26.46
4	130	26.00
5	225	24.94
6	330	23.97
7	429	21.98
8	510	21.00

Initially, sample 1 with the highest solvent content (27.55 wt%) was prepared. Then sample 1 was divided into eight containers and seven of them were subjected to intensive solvent evaporation at room temperature by manually stirring the coatings on the balance until the desired solvent content was reached (the weight was monitored during this process).

Subsequently, the viscosities of the coating samples were measured using the DHR-2 rheometer with two steps of flow peak hold tests: the first step with high shear rate (10^3 s^{-1}) representing the application process; followed immediately by the second step with low shear rate (10^{-2} s^{-1}), representing the leveling process. Each sample was measured three times. Based on the transient viscosity curves obtained during the low shear rate period, the viscosity value at the targeted time was adopted for each sample to represent the corresponding transient viscosity during the leveling process, in accordance with the surface (waviness) measurements.

It should be mentioned that uncertainties exist in the approach of obtaining transient viscosity values during leveling. The obtained viscosity values may not exactly represent the real viscosities during leveling due to the unknown corresponding shear rates at different times after application. During the leveling procedure, the coating might experience lower shear rates than the value used in the viscosity measurements (10^{-2} s^{-1}). Moreover, rheometer results showed that the shear stress was increasing during the measurement because viscosity was increasing when the shear rate was controlled to be constant. However, the shear stress should be decreasing during leveling after the sudden removal of application where high shear stress was imposed to the coating.[59] Thus, there are limitations in obtaining correct viscosity values during leveling.

In summary, experimental series of coupled values of waviness (Wa), application wavelength (λ), average film thickness (h), and coating viscosity (η) were collected at different times (t) during leveling. These data series were subsequently used in the development of the semi-empirical leveling equation.

7.2.3.3 Development of leveling model

The complexity of the leveling process, when solvent evaporation takes place and film thickness and coating viscosity change over time, is high. In this case, to capture the leveling process in one single equation requires a semi-empirical approach. Due to the lack of scientifically-based alternatives, a semi-empirical model based on the Orchard equation was used as shown below.

$$ln(\frac{a_t}{a_0}) = -\frac{16\pi^4\sigma h^3}{3\lambda^4\eta}t \implies ln(\frac{Wa_t}{Wa_0}) = d\frac{h(t)^a}{\lambda(t)^b\eta(t)^c}t \tag{7.2}$$

Notice, that the amplitude, a_t and a_0, have been replaced by the waviness, Wa_t and Wa_0 (the deductive method is presented in Appendix C). Besides, as explained in the introduction section, surface tension σ does not undergo significant changes during solvent evaporation and has, together with the other constants, been lumped into the constant d. a, b, and c are new exponents for average film thickness, wavelength and viscosity.

Using minimization of the sum of least squares (eq. 7.3), the exponent of each individual physical parameter could be estimated.

$$S_{min} = \sum_{i=1}^{n}\left[ln(Wa_t/Wa_0)_{exp} - ln(Wa_t/Wa_0)_{model}\right]^2 \tag{7.3}$$

The 'fmincon' solver of MATLAB was used for actual implementation. The values of a, b, and c were constrained to positive values and the value of d was constrained to be negative because the natural

logarithm term of the model (as written in eq. 7.2) was always negative. The MATLAB codes[114] are summarized in Appendix D.

7.3 Results and discussion

The effects of initial wet film thickness, application wavelength, and coating viscosity on leveling of coatings with solvent evaporation were investigated and will be presented in the coming paragraphs. Subsequently, the semi-empirical model is used to describe the leveling process.

7.3.1 Effects on leveling of initial wet film thickness

The effects of different initial wet film thicknesses on leveling of sample SI are shown in Figure 7.4.

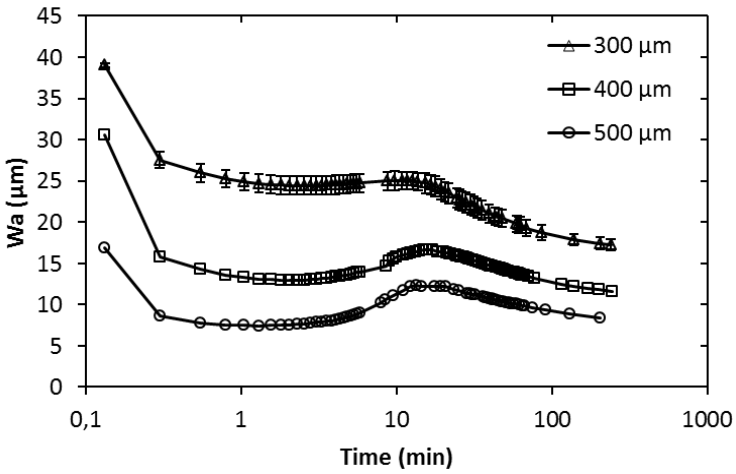

Figure 7.4 Transient waviness (*Wa*) values over time after drawdown application for different initial wet film thicknesses (300, 400, and 500 µm). The error bars shown for 300 µm case represent the standard deviations from three repetitions. Notice that the x-axis is in logarithmic scale to emphasize the curve development immediately after application.

It can be seen that the very first *Wa* value measured decrease when the initial wet film thickness is increased, which suggests that a higher film thickness results in a more adequate flow around the spiral

applicator and provides better leveling performance. However, compared to their initial *Wa* values, the final *Wa* values dropped respectively 56, 62, and 50% for initial wet film thickness of 300, 400, and 500 µm. Thus, no clear trend was found for the effects of initial wet film thickness on the leveling rate based on the obtained data. Nevertheless, we think it is possible that the initial *Wa* value at time zero, which was not measurable with the present equipment (one measurement takes 15 s), could be proportional to the depth of the grooves on the spiral applicator, which thereby defines the initial wet film thickness. In other words, the initial *Wa* value at time zero could be higher when the initial wet film thickness is higher. Consequently, the initial leveling rate (the slopes between the first data point and the value at time zero) may increase with the initial wet film thickness. However, this could not be confirmed.

7.3.2 Effects on leveling of application wavelength

The effects on leveling of different initial wavelengths of the sinusoidal surface, generated with the spiral applicator, are presented in Figure 7.5. It can be seen that waviness, *Wa*, increases with wavelength, which means a larger wavelength leads to a worse leveling result. For the 1 mm case, the captured initial waviness is already so low due to the initial fast leveling rate, that further leveling does not seem possible.

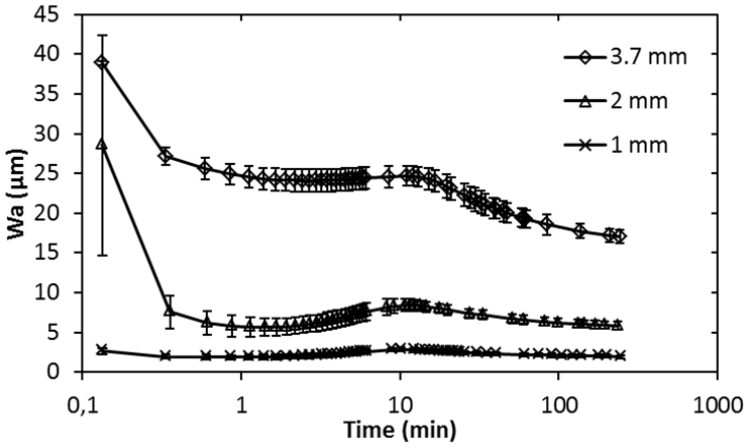

Figure 7.5 Transient waviness (*Wa*) values over time after drawdown application with different initial wavelengths of the sinusoidal surface (1, 2, and 3.7 mm). Each data point is the average value of three repetitions and the error bars shown represent the standard deviation. Notice that the x-axis is in logarithmic scale to emphasize the curve development immediately after application.

7.3.3 Effects on leveling of coating viscosity

The viscosities measured of the samples with different solvent contents were 1.06, 1.68, 2.27, 4.09, 6.52, and 8.56 Pa·s under a shear rate of 117.4 s^{-1}. Normally, the viscosity we see of commercial AF coatings is about 0.95-2.2 Pa·s at this shear rate.

The effects of those initial coating viscosities on leveling are shown in Figure 7.6. It can be seen that the waviness, *Wa*, increases with viscosity. Notice, that the spectrum of the *Wa* value is very broad. Moreover, all samples behave in a similar way except the one with the highest viscosity (8.56 Pa·s). The initial decrease of *Wa* (fast leveling period) was not observed for the sample with a viscosity of 8.56 Pa·s.

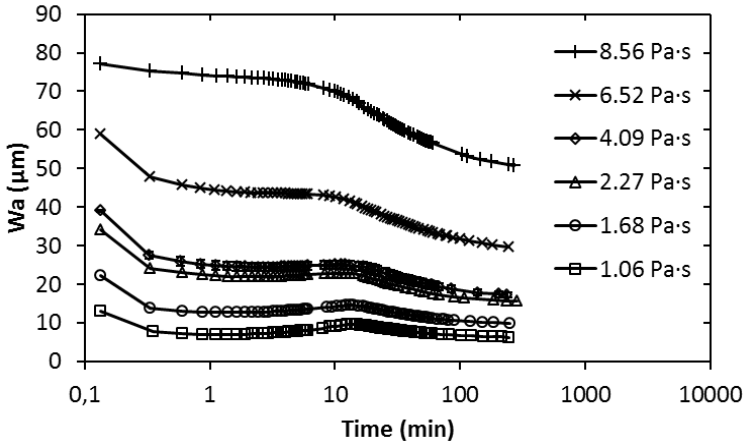

Figure 7.6 Transient waviness (*Wa*) values over time after drawdown application for coating sample S1 with different initial viscosities (1.06, 1.68, 2.27, 4.09, 6.52, and 8.56 Pa·s). The error bars shown for 4.09 Pa·s case represent the standard deviations from three repetitions. They are too small to be seen. Notice that the x-axis is in logarithmic scale to emphasize the curve development immediately after application.

The effects of viscosity on leveling can be further demonstrated with the aid of solvent evaporation rate experiments. Results, for selected samples with initial viscosities of 1.68, 4.09, and 8.56 Pa·s, are shown in Figure 7.7. It can be seen that the sample with the lowest initial viscosity has the longest constant evaporation rate period (10 minutes versus 7 and 5 minutes for 4.09 and 8.56 Pa·s), corresponding to the longest time before 'skin' forms on the surface of the coating at which point the viscosity increases

rapidly and the leveling rate goes down. Hence, it confirms that the leveling is retarded by the increased viscosity resulting from solvent evaporation. However, lower viscosity leads to sagging and therefore a compromise in viscosity should be found.

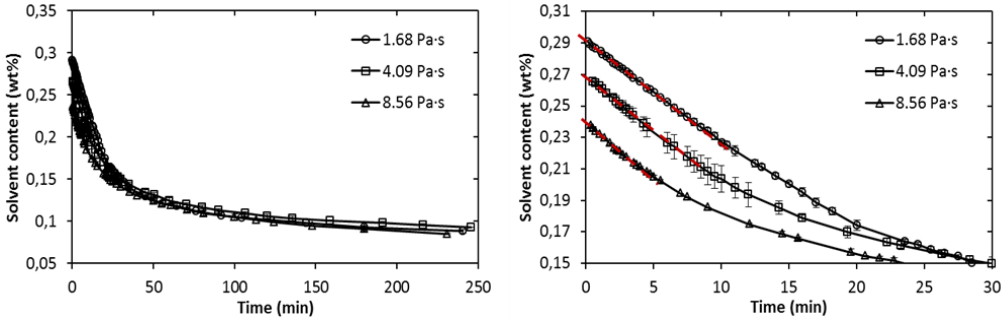

Figure 7.7 Solvent content over time during evaporation rate experiments for coating sample S1 with three different initial viscosities (solvent contents): 1.68 Pa·s (29.09 wt%), 4.09 Pa·s (26.92 wt%), and 8.56 Pa·s (24 wt%). The plot on the right hand side shows more details within the initial 30 mins. The red dashed lines indicate the initial constant evaporation rate period. Each data point is the average value of two repetitions and the error bars shown represent the standard deviations (most of them are too small to be seen).

7.3.4 Simultaneous tracking of solvent content, film thickness, viscosity, wavelength and waviness

The full experimental series of coating parameters within the first seven minutes after application are summarized in Figure 7.8 for the model coating (sample S2) (left) and the commercial AF coating (right).

It can be seen that during the leveling process, the wavelength value did not change much and only small fluctuations around the expected value (3.7 mm) were observed for the model coating. Moreover, it was found that the average film thickness decreased (about 10-12%) linearly with time (about 3.7 µm per minute) within this time span (the film thickness reached a plateau after a couple of hours as shown in Figure 7.9). The solvent content curve exhibits a similar trend, which is reasonable because the reduction of average film thickness is directly related to the solvent evaporation.

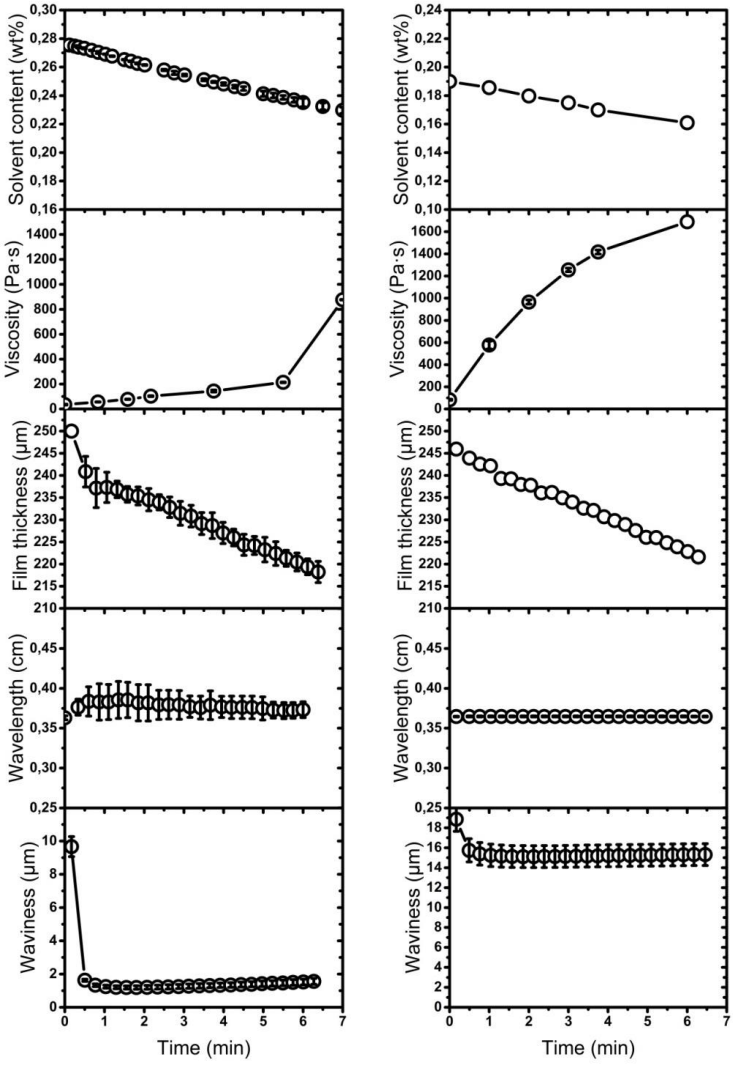

Figure 7.8 The transient process of solvent evaporation and leveling for the model AF coating S2 (left) and the commercial AF coating (right). The coating parameters followed were (from top to bottom): solvent content, coating viscosity, average film thickness, application wavelength, and waviness. Each data point is an average value except for solvent content and film thickness in the right hand plot. The error bars shown represent the standard deviations of repetitions.

Compared to the results of the coating sample S2 (see Figure 7.8), the waviness values of the commercial coating were much higher and the final leveling result was poorer than for sample S2. Furthermore, the viscosity build-up of the commercial coating was very different. This, most likely, is because the overall solvent contents of the commercial coating (from 16 to 19 wt%) were lower than those of sample S2 (23-27.5 wt%). For sample S2, the viscosity value was 1465 Pa·s when the solvent content was 22 wt%, which means that the viscosity would be even higher when the solvent content was lower than 19 wt%. However, for the commercial coating, the viscosity was 83 Pa·s when the solvent content was 19 wt%. The reason why the commercial coating could have such low viscosity at the same solvent content as the model sample S2 was most likely that the additives inside the commercial coating (thixotropic and wetting agents) imposed rheology effects to the coating. This was probably also responsible for the difference in viscosity build-up. Consequently, the poor leveling performance could be attributed to the viscosity development.

Overall, the coating viscosity was found to be the dominant parameter affecting the leveling process, because viscosity showed the largest changes (increased about 2379% for S2 and 1940% for the commercial coating) among all parameters during the leveling process.

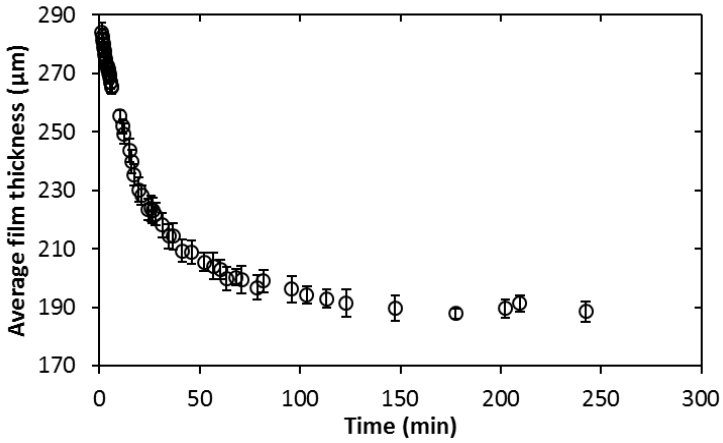

Figure 7.9 Average film thickness over time for sample S1 after application using the spiral drawdown applicator giving 300 µm initial average film thickness with 3.7 mm wavelength.

7.3.5 Development of semi-empirical model for leveling

7.3.5.1 Relationship between final leveling performance and initial coating parameters

The relationships between final leveling performance and the initial coating parameters (film thickness and wavelength) were correlated based on the experimental results shown in Figure 7.4 and 7.5. To correlate the final waviness values with the different initial film thicknesses, the following relationship was proposed

$$\frac{Wa_t}{Wa_0} = Eh^{\beta} \tag{7.4}$$

where E is a constant. The exponent β for the film thickness dependency can be estimated from the slope of a plot of $\ln(Wa_t/Wa_0)$ against $\ln(h)$. For correlating the final waviness values with the different initial wavelengths, a similar relationship was used:

$$\frac{Wa_t}{Wa_0} = E'\lambda^{\gamma} \tag{7.5}$$

where E' is a constant and the exponent γ for the wavelength can be estimated from the slope of a plot of $\ln(Wa_t/Wa_0)$ against $\ln(\lambda)$. The empirical models obtained are shown in eq. (7.6) and (7.7):

$$\frac{Wa_t}{Wa_0} = (975787\ \mu m^{2.77\pm0.024})h^{-2.77\pm0.024} \tag{7.6}$$

$$\frac{Wa_t}{Wa_0} = (0.015\ mm^{-1.68\pm0.030})\lambda^{1.68\pm0.030} \tag{7.7}$$

The correlation coefficients for eq. (7.6) and (7.7) were 0.9999 and 0.9997, respectively. Equation (7.6) and (7.7) are valid when the film thickness h is within 300-500 µm and the wavelength is within 1-3.7 mm for coating sample S1, respectively. The two equations can be used for estimating and comparing the waviness decay or final leveling performance of a similar coating with different initial film thicknesses and wavelengths, respectively.

7.3.5.2 Transient model fitting

According to the experimental data provided in Figure 7.8, the application wavelength is practically constant during leveling process. In addition, the film thickness change is also very little (about 10-12%). On the other hand, viscosity changes 2379% (1940% for the commercial coating). Therefore, the

viscosity was assumed to be the only important parameter during solvent evaporation and leveling and the semi-empirical model of eq. (7.2) was adjusted to the following model.

$$ln(\frac{Wa_t}{Wa_0}) = d\frac{h(t)^a}{\lambda(t)^b\eta(t)^c}t \Longrightarrow ln(\frac{Wa_t}{Wa_0}) = \frac{f}{\eta(t)^e}t \tag{7.8}$$

where the film thickness term, $h(t)^a$, and the wavelength term, $\lambda(t)^b$, were lumped into a new constant *f*. Consequently, the semi-empirical model of eq. (7.8) was fitted to the transient experimental data of waviness and viscosity for the two coatings. The results are shown in Figure 7.10. The values obtained for *e* and *f* are provided in Table 7.3 with the associated errors.

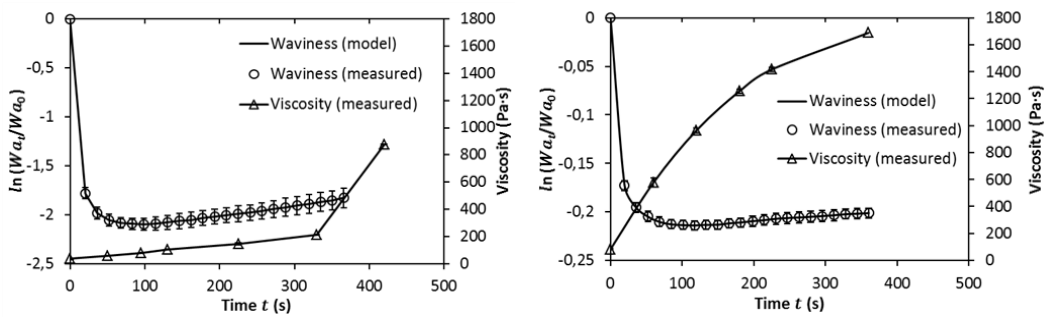

Figure 7.10 Comparison of waviness values obtained from experiments and calculated from the model (Equation 7.8, right hand side) as a function of time for model AF coating S2 (left) and the commercial AF coating (right). The viscosity profiles are also included. For both experiments and simulations, each data point is an average of five (model coating) and three repetitions (commercial coating) and the error bars represent the standard deviations.

Table 7.3 Estimated values and errors for the constants in Equation (7.8).

Constant	Model coating S2		Commercial AF coating	
	Estimated value	**Estimated error**	**Estimated value**	**Estimated error**
e	1.64	±0.017	1.40	±0.018
f	-34.68 $kg^{1.64}\cdot m^{-1.64}\cdot s^{-2.64}$	±2.888 $kg^{1.64}\cdot m^{-1.64}\cdot s^{-2.64}$	-23.25 $kg^{1.40}\cdot m^{-1.40}\cdot s^{-2.40}$	±2.877 $kg^{1.40}\cdot m^{-1.40}\cdot s^{-2.40}$

Figure 7.10 shows that the simulation of waviness is in very good agreement with measured values for both coatings. It can be seen from Table 7.3 that the values for *e* and *f* are somewhat different for the two coatings, which is probably attributed to the different waviness profiles (leveling performance) resulting from the different viscosity developments. In practice, viscosity behavior could be easily altered by additives present in the formulation. Therefore, it is not possible to match experimental values with model simulations without a separate fitting of the adjustable model parameters for a given coating. However, the model remains universal (at least for the coatings studied).

7.4 Conclusions

Using an optical 3D profilometer in combination with an advanced rheometer and gravimetric evaporation rate experiments, transient data for leveling of coatings with simultaneous solvent evaporation and viscosity development could be obtained. Results showed that higher film thickness, shorter application wavelength, and lower coating viscosity led to better final leveling performance. By far, the most important parameter to consider for transient effects during leveling process is the coating viscosity.

The relationships between the final leveling performance and the coating parameters (initial average film thickness and wavelength) were correlated and both parameters were found to be of significant importance. Furthermore, a semi-empirical model could be fitted with very good agreement to the transient experimental data for both coatings. The two fitting parameters for the viscosity dependencies in the model were similar, but not identical for the two coatings. This was attributed to different rheology additives (thixotropic and wetting agents) present in the formulations. Therefore, the hypothesis (6) was found to be false.

Overall, the direct experimental approach can be a valuable tool in the optimization of leveling of coatings.

8 Concluding remarks

This thesis presents the results of three years of research focusing on drag resistance of ship hulls and leveling related studies of AF coatings. The influences of spray-applied FCC surfaces and the effects of simulated welding seams on drag resistance were systematically investigated using a pilot-scale rotary setup. Rheological studies of formulation ingredients and the effects of additives on leveling of AF coatings were covered. The kinetics of the leveling process of freshly applied AF coatings was thoroughly analyzed using a specially-designed setup which combined an automated coating application system with an optical 3D profilometer to record the evolution of surface texture of wet coatings after film application.

This chapter summarizes the main conclusions from this thesis work. Challenges in the field and suggestions for future work are presented at the end of the chapter.

8.1 Conclusions

To determine the differences in economy and provide guidelines for ship operators in choosing the right FCC technology, the drag resistances of newly applied AF and FR coatings were compared using a pilot-scale setup with rotating cylinders. The rotary setup was found to be sufficiently sensitive to detect the differences in drag resistance (measured as torque acting on the rotor cylinder shaft) between AF and FR coating surfaces. The results revealed that FR coatings caused less skin friction than AF coatings. Accordingly, the benefit in fuel saving from using FR coating is only valid in the initial sailing period when the ship hull is still free of biofouling. During seawater immersion of coating, water absorption amounts for both AF and FR coatings were found to be considerable. Nevertheless, the influences of water absorption on drag resistance were proved to be insignificant for FR coating and water absorption lowered the skin friction of AF coating. Those findings are significant for both coating suppliers and shipping companies as the FCCs are exposed to seawater for most of their life spans.

The effects of welding seams on drag resistance were thoroughly investigated based on experiments using a specially-designed flexible rotor and the findings were further confirmed using CFD simulations.

The welding seam height and density were demonstrated to have significant effects on drag resistance, especially at high sailing speeds. On account of that, the welding seam height is suggested to be controlled below 5 mm when ships are constructed in shipyards to lower drag resistance and achieve considerable economic benefits. For the existing ships, the welding seams can be ground accordingly. Moreover, the effects on drag resistance of welding seams were confirmed to be comparable to those of FCC surfaces and experimental results indicated that FCC surfaces resulted in higher drag resistance than welding seams when welding seam height was below 5 mm at full-scale conditions. Furthermore, friction drag that mainly resulted from the ship hull surface was proved to be dominant in the total drag resistance based on CFD simulation results. Therefore, the ship hull surface conditions and thereby the FCC surface conditions were concluded to be vital and should be optimized to minimize the total resistance and fuel consumption for a marine vessel. Thus, environmental benefits will also be achieved.

Following the above conclusions from drag force studies, leveling properties of coating films were studied in order to explore methods to improve leveling performance of AF coatings and thereby optimize coating surface conditions. In the first step, substantial information was obtained from rheological studies of coating ingredients regarding their rheological effects on leveling. First of all, the shear changing process from application to the subsequent leveling was successfully simulated from flow peak hold and flow sweep tests using the rheometer. Rosins were found to have insignificant rheological effects on binder systems. Thixotropic agents were proved to have thixotropic effects which are preferred for sagging control. Furthermore, it was inferred that, besides thixotropic agents, some other ingredients in the formulation may have thixotropic effects as well. They could be reaction products between pigments and rosins or additives, for instance, wetting agents. Besides, the presence of pigments was found to increase the viscosity significantly at low shear rate, which inhibits leveling. However, this viscosity effect of pigments disappeared at high shear rate probably attributed to the thixotropic effects, which indicated that the presence of pigments in formulations would not harm the spray ability from viscosity point of view. Overall, it was verified that coating formulation ingredients affect leveling properties of AF coatings. In addition, the acquired rheological information was valuable input to coating formulation development work in coating industries. However, the obtained information from rheological studies was quite qualitative and inadequate in quantifying leveling performance. Besides, it was found that coatings were very sensitive to the shear history and the expected differences in leveling effect (or rheological behavior) among different coating samples were small. Therefore, it was concluded that using rheological approach solely was not sufficient to study leveling.

On the other hand, a stylus-based roughness measurement instrument was found to be insufficient to cover long wavelength characteristics (waviness characteristics) on the coating surface generated from a

spiral applicator. Besides, it can only be used on dry surfaces. Consequently, a novel approach for quantitatively measuring leveling performance including both roughness and waviness characteristics was developed using a combination of an optical 3D profilometer and a retrofitted automatic film application system. Moreover, it was found that the effects of the investigated additives (leveling additives and wetting agents) and solvents on leveling of model AF coatings observed from this approach could not be well reproduced from the spraying application. The high uncertainty from manual spraying application causing variations in surface texture may be responsible for that. Furthermore, it was found that a better leveling effect could be easily compromised by sagging problem or inappropriate spraying application. Therefore, optimizing spraying application may be more crucial than improving formulation for better leveling performance. Meanwhile, the underlying leveling mechanisms were investigated in this part. It was found that leveling rate of AF coatings was strongly coupled to the solvent evaporation rate and the associated development in coating viscosity, which verified the hypothesis (5). In addition, different leveling behaviors were found between coatings with low and high viscosities, respectively.

The effects of physical parameters including initial wet film thickness, wavelength and viscosity on leveling performance were studied separately. Experimental results showed that higher initial wet film thickness, shorter wavelength, and lower viscosity led to better final leveling performance. Furthermore, it was confirmed that the most important parameter to consider for transient effects during leveling process was the coating viscosity. Furthermore, the relationship between the final leveling performance and the coating parameters (initial wet film thickness and wavelength) were correlated and both parameters were found to be of significant importance. In addition, transient data for leveling of coatings with simultaneous solvent evaporation and viscosity development were obtained using the optical 3D profilometer in combination with an advanced rheometer and gravimetric evaporation rate experiments. Based on those data, a semi-empirical model was fitted with very good agreement to the transient experimental data for two coatings (one model and one full commercial AF coating). The two fitting parameters for the viscosity dependencies in the model were found similar, yet not identical for the two coatings. This was attributed to different rheological additives (thixotropic and wetting agents) present in the formulations. Therefore, the hypothesis (6) was proved to be false because leveling kinetics of AF coatings could not be quantified using a universal model due to the fact that the rheological behavior varies with formulation. Nevertheless, the presented direct experimental approach was proved to be a valuable tool in the optimization of leveling of coatings.

In summary, the FCC surface conditions and welding seams have proved to have significant effects on the long-term drag performance of marine vessels, especially the FCC surfaces influencing the friction drag which was confirmed to play the dominant role in the total drag resistance. In addition, it can be

concluded that the developed approach for quantifying leveling is vital to the overall leveling studies. Moreover, the rheological method has proved to be very useful and necessary for leveling studies and formulation optimization. Furthermore, solvent evaporation process and viscosity build-up process were found to be the core parts of leveling studies.

8.2 Suggestions for future work

Due to the time limitation of the PhD work, the reasons for the drag difference between AF and FR coatings were not further investigated. Nevertheless, we suspect that besides the surface roughness and waviness, the material elasticity may be another important reason. Therefore, it will be very interesting to study the effects of material elasticity on drag resistance.

During the study of welding seams, it was a challenge to simulate the rotary setup with welding seams on the designed flexible rotor geometry using CFD approach in order to compare directly with the experimental results. The challenge was due to the complexity of the geometry and tiny size of the welding seams with structured mesh adopted. Therefore, it may be relevant to improve the simulation in the future. It would also be interesting to study welding seams using another drag measurement setup, for instance, towing tank, so that the results could be compared to those from the rotary setup.

Based on the rheological study of coating ingredients, it was found that some other ingredients may have thixotropic effects besides thixotropic agents. It would be very interesting and worthy to pursue what ingredients and how they impart thixotropic effects on coatings. For coating suppliers, it would provide valuable information to formulation optimization work. Based on this thesis work, rheological study is strongly recommended to be performed to understand the rheological behaviors of coatings in general, especially for formulation development purpose in coating industries.

Although the effects of studied ingredients on leveling were found to be insignificant, it is still important to investigate the effects of pigment size, distribution, and more solvent types on leveling (and/or wetting) in the future work.

For future leveling studies, it is suggested that sagging issue should always be considered at the same time. Besides, to improve leveling and thereby coating surface smoothness, the future focus should be on spraying application. It will be necessary to study the effects of various spraying application conditions on leveling. Thus, potential practical methods to improve leveling may be found. The author believes that it will bring both academic and industrial values to the overall leveling study. In addition,

further studies on tie-coat may be necessary due to its negative effects on leveling, for instance, how to improve surface smoothness of tie-coat.

The developed semi-empirical model in this work was based on the Orchard equation. In the future, other models that include the dependencies of other parameters (film thickness and wavelength) might be developed. Furthermore, this thesis showed that it was a challenge to develop a universal model for quantifying leveling kinetics of AF coatings with solvent evaporation due to the different rheological behaviors. Nevertheless, it might be possible to develop a universal model for coatings possessing similar rheological behaviors (mainly viscosity build-up process) regardless of the coating technologies, such as FCCs, anticorrosive coatings, and automotive coatings. It means that the viscosity behaviors of large amounts of different coatings should be scrutinized and categorized before model development.

Overall, the pilot-scale rotary setup has shown to be very useful for drag resistance studies, and it should be used for future drag/friction related investigations. For instance, the specially-designed rotor may be potentially used for systematical drag investigations of the effects of barnacles and other large scale hull irregularities. The novel approach using the optical 3D profilometer combined with the automated application system can be directly used for fast-screening and development of new coating formulations. Leveling studies are relevant not only for FCCs, but also for all types of coatings which require either aesthetic appearance (such as decorative coatings and automotive coatings) or friction reduction effect (for example, flow efficiency coatings for gas pipes). Therefore, the additional outcome of this research work has been the introduction of a new tool for the coating formulators.

References

(1) Yebra, D. M.; Kiil, S.; Dam-Johansen, K. Antifouling Technology - Past, Present and Future Steps towards Efficient and Environmentally Friendly Antifouling Coatings. *Prog. Org. Coatings* **2004**, *50* (2), 75–104.

(2) Lindholdt, A.; Dam-Johansen, K.; Yebra, D. M.; Olsen, S. M.; Kiil, S. Estimation of Long-Term Drag Performance of Fouling Control Coatings Using an Ocean-Placed Raft with Multiple Dynamic Rotors. *J. Coatings Technol. Res.* **2015**, *12* (6), 975–995.

(3) Lindholdt, A. Fuel Efficiency and Fouling Control Coatings in Maritime Transport. Ph.D. Dessertation. Technical University of Denmark, 2015.

(4) Schultz, M. P.; Bendick, J. A.; Holm, E. R.; Hertel, W. M. Economic Impact of Biofouling on a Naval Surface Ship. *Biofouling* **2011**, *27* (1), 87–98.

(5) Patton, C. T. *Paint Flow and Pigment Dispersion*, second.; John Wiley & Sons, Ed.; Wiley-Interscience: New York, 1979.

(6) Lejars, M.; Margaillan, A.; Bressy, C. Fouling Release Coatings: A Nontoxic Alternative to Biocidal Antifouling Coatings. *Chem. Rev.* **2012**, *112* (8), 4347–4390.

(7) Swain, G. W. Biofouling Control: A Critical Component of Drag Reduction. In *Proceedings of the International Symposium on Sea Water Drag Reduction,* Newport, RI, USA, 22-23 July 1998; The Naval Undersea Warfare Center: Newport, RI, USA, 1998; pp 155–161.

(8) Lindholdt, A.; Dam-Johansen, K.; Olsen, S. M.; Yebra, D. M.; Kiil, S. Effects of Biofouling Development on Drag Forces of Hull Coatings for Ocean-Going Ships: A Review. *J. Coatings Technol. Res.* **2015**, *12* (3), 415–444.

(9) Kiil, S.; Dam-Johansen, K.; Weinell, C. E.; Pedersen, M. S.; Codolar, S. A. Dynamic Simulations of a Self-Polishing Antifouling Paint Exposed to Seawater. *J. Coatings Technol.* **2002**, *74* (929), 45–54.

(10) Kiil, S.; Dam-Johansen, K.; Weinell, C. E.; Pedersen, M. S.; Codolar, S. A. Estimation of Polishing and Leaching Behaviour of Antifouling Paints Using Mathematical Modelling: A Literature Review. *Biofouling* **2003**, *19* (Suppl.1), 37–43.

(11) Noguer, A. C. Experimental Investigation of the Behaviour and Fate of Block Copolymers in Fouling-Release Coatings. Ph.D. Dessertation. Technical University of Denmark, 2016.

(12) Thorlaksen, P. C. W.; Blom, A.; Bork, U. Fouling Control Coating Compositions. US9534121B2, January 3, 2017.

(13) Hunsucker, K. Z.; Vora, G. J.; Hunsucker, J. T.; Gardner, H.; Leary, D. H.; Kim, S.; Lin, B.; Swain, G. Biofilm Community Structure and the Associated Drag Penalties of a Groomed Fouling Release Ship Hull Coating. *Biofouling* **2018**, *34* (2), 162-172.

(14) Townsin, R. L.; Anderson, C. D. Fouling Control Using Low Surface Energy, Foul Release Technology. In *Advances in Marine Antifouling Coatings and Technologies*; Hellio, C., Yebra, D., Eds.; Woodhead Publishing Limited and CRC Press LLC: Boca Raton, FL, 2009; pp 693–708.

(15) Khor, Y. S.; Xiao, Q. CFD Simulations of the Effects of Fouling and Antifouling. *Ocean Eng.* **2011**, *38* (10), 1065–1079.

(16) Mirabedini, S. M.; Pazoki, S.; Esfandeh, M.; Mohseni, M.; Akbari, Z. Comparison of Drag Characteristics of Self-Polishing Co-Polymers and Silicone Foul Release Coatings: A Study of Wettability and Surface Roughness. *Prog. Org. Coatings* **2006**, *57* (4), 421–429.

(17) Kiil, S.; Weinell, C. E.; Pedersen, M. S.; Dam-Johansen, K. Analysis of Self-Polishing Antifouling Paints Using Rotary Experiments and Mathematical Modeling. *Ind. Eng. Chem. Res.* **2001**, *40* (18), 3906–3920.

(18) Yebra, D. M.; Kiil, S.; Dam-Johansen, K.; Weinell, C. Reaction Rate Estimation of Controlled-Release Antifouling Paint Binders: Rosin-Based Systems. *Prog. Org. Coatings* **2005**, *53* (4), 256–275.

(19) Man Diesel & Turbo. Basic Principles of Ship Propulsion. https://marine.man.eu/docs/librariesprovider6/propeller-aftship/basic-principles-of-propulsion.pdf?sfvrsn=0 (accessed May 12, 2017).

(20) Schultz, M. P.; Swain, G. W. The Influence of Biofilms on Skin Friction Drag. *Biofouling* **2000**, *15* (1–3), 129–139.

(21) Townsin, R. L.; Byrne, D.; Svensen, T. E.; Milne, A. Estimating the Technical and Economic Penalties of Hull and Propeller Roughness. *SNAME Trans.* **1981**, *89*, 295–318.

(22) Todd, J. H. Resistance and Propulsion. In *Principles of naval architecture*; Comstock, J., Ed.; The society of naval architects and marine engineers: New York, 1980; pp 288–462.

(23) Candries, M.; Atlar, M.; Mesbahi, E.; Pazouki, K. The Measurement of the Drag Characteristics of Tin-Free Self-Polishing Co-Polymers and Fouling Release Coatings Using a Rotor Apparatus. *Biofouling* **2003**, *19* (Suppl.1), 27–36.

(24) Weinell, C. E.; Olsen, K. N.; Christoffersen, M. W.; Kiil, S. Experimental Study of Drag Resistance Using a Laboratory Scale Rotary Set-Up. *Biofouling* **2003**, *19* (Suppl.1), 45–51.

(25) Grasshoff, K.; Kremling, K.; Ehrhardt, M. *Methods of Seawater Analysis*, Third.; Grasshoff, K., Kremling, K., Ehrhardt, M., Eds.; Wiley-VCH Verlag GmbH: Weinheim, 2007.

(26) Holm, E.; Schultz, M.; Haslbeck, E.; Talbott, W.; Field, A. Evaluation of Hydrodynamic Drag on Experimental Fouling-Release Surfaces, Using Rotating Disks. *Biofouling* **2004**, *20* (4–5), 219–226.

(27) Schultz, M. P.; Myers, A. Comparison of Three Roughness Function Determination Methods. *Exp. Fluids* **2003**, *35* (4), 372–379.

(28) Barton, A. F.; Sargison, J. E.; Brandner, P.; Walker, G. J. A Force Balance to Measure the Total Drag of Biofilms on Test Plates. *16th Australas. Fluid Mech. Conf.* **2007**, 819–824.

(29) Swain, G. W.; Kovach, B.; Touzot, A.; Casse, F.; Kavanagh, C. J. Measuring the Performance of Today's

Antifouling Coatings. *J. Sh. Prod.* **2007**, *23* (3), 164–170.

(30) Leer-Andersen, M.; Larsson, L. An Experimental/Numerical Approach for Evaluating Skin Friction on Full-Scale Ships with Surface Roughness. *J. Mar. Sci. Technol.* **2003**, *8*, 26–36.

(31) Candries, M.; Atlar, M. Experimental Investigation of the Turbulent Boundary Layer of Surfaces Coated With Marine Antifoulings. *J. Fluids Eng.* **2005**, *127* (2), 219–232.

(32) Zargiel, K. A.; Swain, G. W. Static vs Dynamic Settlement and Adhesion of Diatoms to Ship Hull Coatings. *Biofouling* **2014**, *30* (1), 115–129

(33) Lackenby, H. The Thirty-Fourth Thomas Lowe Gray Lecture: Resistance of Ships, with Special Reference to Skin Friction and Hull Surface Condition. In *Proceedings of the Institution of Mechanical Engineers*; June 1962; Vol. 176, pp 981–1014.

(34) Munk, T.; Kane, D.; Yebra, D. M. The Effects of Corrosion and Fouling on the Performance of Ocean-Going Vessels: A Naval Architectural Perspective. In *Advances in Marine Antifouling Coatings and Technologies*; Hellio, C., Yebra, D. M., Eds.; Woodhead Publishing Limited and CRC Press LLC: Boca Raton, FL, 2009; pp 148–176.

(35) Howell, D.; Behrends, B. A Review of Surface Roughness in Antifouling Coatings Illustrating the Importance of Cutoff Length. *Biofouling* **2006**, *22* (6), 401–410.

(36) Usta, O.; Korkut, E. A Study for the Effect of Surface Roughness on Resistance Characteristics of Flat Plates. In *Marine Coatings*; London, UK, 2013.

(37) Townsin, R. L.; Byrne, D. Speed, Power and Roughness: The Economics of Outer Bottom Maintenance. In *The Royal Institution of Naval Architects*; London, UK; pp 459–483.

(38) The Specialist Committee on Powering Performance Prediction. In *24th International towing tank conference (ITTC)*; Edinburgh, Scotland, UK.

(39) Candries, B. M.; Anderson, C. D.; Atlar, M. Foul Release Systems and Drag: Observations on How the Coatings Work. *J. Prot. Coatings Linings* **2001**, *18* (4), 38–43.

(40) White, A. H. A Technical and Economic Evaluation of Two Different Coating Systems on High Speed Catamarans. Ph.D. Dessertation, University of Newcastle-upon-Tyne, 1999.

(41) Candries, M. Drag, Boundary-Layer and Roughness Characteristics of Marine Surfaces Coated with Antifoulings. Ph.D. Dessertation, University of Newcastle-Upon-Tyne, 2001.

(42) Tezdogan, T.; Demirel, Y. K.; Kellett, P.; Khorasanchi, M.; Incecik, A.; Turan, O. Full-Scale Unsteady RANS CFD Simulations of Ship Behaviour and Performance in Head Seas Due to Slow Steaming. *Ocean Eng.* **2015**, *97*, 186–206.

(43) Ozdemir, Y. H.; Barlas, B.; Yilmaz, T.; Bayraktar, S. Numerical and Experimental Study of Turbulent Free Surface Flow for a Fast Ship Model. *Shipbuild. Theory Pract. Nav. Archit. Mar. Eng. Ocean Eng.* **2014**, *65* (1), 39–54.

(44) Demirel, Y. K.; Khorasanchi, M.; Turan, O.; Incecik, A.; Schultz, M. P. A CFD Model for the Frictional Resistance Prediction of Antifouling Coatings. *Ocean Eng.* **2014**, *89*, 21–31.

(45) Ciortan, C.; Bertram, V. RANSE Simulations for the Effect of Welds on Ship Resistance. In *Numerical Towing tank Symposium*; Marstrand, Sweden, September 2014.

(46) Demirel, Y. K.; Khorasanchi, M.; Turan, O.; Incecik, A. CFD Approach to Resistance Prediction as a Function of Roughness. In *Transport Research Arena*; Paris, 2014.

(47) Clauser, F. H. The Turbulent Boundary Layer. *Adv. Appl. Mech.* **1956**, *4*, 1–51.

(48) Schultz, M. P.; Flack, K. A. Turbulent Boundary Layers Over Surfaces Smoothed by Sanding. *J. Fluids Eng.* **2003**, *125* (5), 863–870.

(49) Schlichting, H.; Gersten, K. *Boundary-Layer Theory*, Ninth.; Springer-Verlag Berlin Heidelberg: Berlin, 2017.

(50) Shabbir, A.; Turner, M. G. A Wall Function for Calculating the Skin Friction with Surface Roughness. In *ASME Turbo Expo*; Vienna, 2004; pp 1661–1671.

(51) Granville, P. Three Indirect Methods for the Drag Characterization of Arbitrarily Rough Surfaces on Flat Plates. *J. Sh. Res.* **1987**, *31* (1), 70–77.

(52) Grigson, C. Drag Losses of New Ships Caused by Hull Finish. *J. Sh. Res.* **1992**, *36* (2), 182–196.

(53) Perlin, M.; Dowling, D. R.; Ceccio, S. L. Freeman Scholar Review: Passive and Active Skin-Friction Drag Reduction in Turbulent Boundary Layers. *J. Fluids Eng.* **2016**, *138* (9).

(54) Smith, N. D. P.; Orchard, S. E.; Rhind-Tutt, A. J. The Physics of Brushmarks. *Surf. coatings Int.* **1961**, *44* (9), 618–633.

(55) Cohu, O.; Magnin, A. The Levelling of Thixotropic Coatings. *Prog. Org. Coatings* **1996**, *28* (2), 89–96.

(56) Orchard, S. E. On Surface Leveling in Viscous Liquids and Gels. *Appl. Sci. Res. Sect. A* **1963**, *11* (4–6), 451–464.

(57) Livescu, S.; Roy, R. V.; Schwartz, L. W. Leveling of Thixotropic Liquids. *J. Nonnewton. Fluid Mech.* **2011**, *166* (7–8), 395–403.

(58) Peters, C. A.; Nichols, M. E.; Ellwood, K. R. J. The Evolution of Surface Texture in Automotive Coatings. *J. Coatings Technol. Res.* **2011**, *8* (4), 469–480.

(59) Seeler, F.; Hager, C.; Tiedje, O.; Schneider, M. Simulations and Experimental Investigation of Paint Film Leveling. *J. Coatings Technol. Res.* **2017**, *14* (4), 767–781.

(60) Overdiep, W. S. The Leveling of Paints. *Prog. Org. Coatings* **1986**, *14*, 159–175.

(61) Kiil, S. Quantification of Simultaneous Solvent Evaporation and Chemical Curing in Thermoset Coatings. *J. Coatings Technol. Res.* **2010**, *7* (5), 569–586.

(62) Wilson, S. K. The Levelling of Paint Films. *IMA J. Appl. Math.* **1993**, *50* (2), 149–166.

(63) Wilson, S. K. The Derivation and Analysis of a Model of the Drying Process of a Paint Film. *Surf. Coatings Int. Part B Coatings Trans.* **1997**, *80* (4), 162–167.

(64) Howison, S. D.; Moriarty, J. A.; Ockendon, J. R.; Terrill, E. L.; Wilson, S. K. A Mathematical Model for Drying Paint Layers. *J. Eng. Math.* **1997**, *32* (4), 377–394.

(65) Wulf, M.; Uhlmann, P.; Michel, S.; Grundke, K. Surface Tension Studies of Levelling Additives in Powder Coatings. *Prog. Org. Coatings* **2000**, *38* (2), 59–66.

(66) Bosma, M.; Brinkhuis, R.; Rensen, E.; Watson, R. A New Method for the Quantitative Determination and Prediction of Sag and Levelling in Powder Coatings. *Prog. Org. Coatings* **2011**, *72* (1–2), 26–33.

(67) Biermann, V. M. *Rheol. Acta.* **1968**, *7* (2), 138–163.

(68) Tsai, B.; Carvalho, M. S.; Kumar, S. Leveling of Thin Films of Colloidal Suspensions. *J. Colloid Interface Sci.* **2010**, *343* (1), 306–313.

(69) Shin, J. Y.; Bousfield, D. W. The Leveling of Surface Irregularities in Pigment Coatings on Porous Substrates. *Appita* **2009**, *62* (4), 279–284.

(70) Schwartz, L. W.; Weidner, D. E. Modeling of Coating Flows on Curved Surfaces. *J. Eng. Math.* **1995**, *29* (1), 91–103.

(71) Schwartz, L. W.; Weidner, D. E.; Eley, R. R. An Analysis of the Effect of Surfactant on the Leveling Behavior of a Thin Liquid Coating Layer. *Langmuir* **1995**, *11* (10), 3690–3693.

(72) Ramkrishnan, A.; Kumar, S. Electrohydrodynamic Effects in the Leveling of Coatings. *Chem. Eng. Sci.* **2013**, *101*, 785–799.

(73) Froehlich, M. Two Coating Problems: Thin Film Rupture and Spin Coating. Ph.D. Dessertation., Duke University, 2009.

(74) Gong, X.; Ted Davis, H.; Scriven, L. E. Role of van Der Waals Force in Latex Film Formation. *J. Coatings Technol. Res.* **2008**, *5* (3), 271–283.

(75) Waring, R. K. An Analytical Study of Leveling. *J. Rheol. (N. Y. N. Y).* **1931**, *2* (3), 307–314.

(76) Childs, P. R. N. Vorticity and Rotation. In *Rotating Flow*; Elsevier, 2011.

(77) Camina, M.; Howell, D. M. *J. Oil Colour Chem. Ass.* **1972**, *55*, 929.

(78) Quach, A.; Hansen, C. M. Evaluation of Leveling Characteristics of Some Latex Paints. *J. Paint Technol.* **1974**, *46* (592), 40–46.

(79) Sarker, H. Effect of Cutting Variables, Bore Diameter and Tool Wear on Surface Finish in Fine Boring of Cl Bushes. *Indian J. Technol.* **1974**, *12* (10), 436–439.

(80) Mezger, T. G. *The Rheology Handbook*, Third revi.; Vincentz Network: Hanover, 2011.

(81) Dodge, S. J. Quantitative Measures of Leveling. *J. Paint Technol.* **1972**, *44* (564), 72–78.

(82) Quach, A. Polymer Coatings. Physics and Mechanics of Leveling. *Ind.Eng.Chem.Prod.Res.Develop.* **1973**, *12* (2), 110–116.

(83) Townsin, R. L. The Ship Hull Fouling Penalty. *Biofouling* **2003**, *19* (Suppl.1), 9–15.

(84) Buskens, P.; Wouters, M.; Rentrop, C.; Vroon, Z. A Brief Review of Environmentally Benign Antifouling and Foul-Release Coatings for Marine Applications. *J. Coatings Technol. Res.* **2013**, *10* (1), 29–36.

(85) Granville, P. S. Drag-Characterization Method for Arbitrarily Rough Surfaces by Means of Rotating Disks. *J. Fluids Eng.* **1982**, *104* (3), 373–377.

(86) Monty, J. P.; Dogan, E.; Hanson, R.; Scardino, A. J.; Ganapathisubramani, B.; Hutchins, N. An Assessment of the Ship Drag Penalty Arising from Light Calcareous Tubeworm Fouling. *Biofouling* **2016**, *32* (4), 451–464.

(87) Granville, P. S. *Similarity-Law Characterization Methods for Arbitrary Hydrodynamic Roughnesses*; Final Report Naval Ship Research and Development Center: Bethesda, MD, May 1978.

(88) Schultz, M. P. Effects of Coating Roughness and Biofouling on Ship Resistance and Powering. *Biofouling* **2007**, *23* (5), 331–341.

(89) Callow, M. Ship Fouling: Problems and Solutions. *Chem. Ind.* **1990**, (5), 123–127.

(90) Oikonomou, E. K.; Iatridi, Z.; Moschakou, M.; Damigos, P.; Bokias, G.; Kallitsis, J. K. Development of Cu^{2+}- and/or Phosphonium-Based Polymeric Biocidal Materials and Their Potential Application in Antifouling Paints. *Prog. Org. Coatings* **2012**, *75* (3), 190–199.

(91) Yonehara, Y.; Yamashita, H.; Kawamura, C.; Itoh, K. A New Antifouling Paint Based on a Zinc Acrylate Copolymer. *Prog. Org. Coatings* **2001**, *42* (3–4), 150–158.

(92) Schultz, M. P. The Relationship Between Frictional Resistance and Roughness for Surfaces Smoothed by Sanding. *J. Fluids Eng.* **2002**, *124* (2), 492–499.

(93) Lyman, J.; Fleming, R. H. Composition of Seawater. *J. Mar. Res.* **1940**, *3*, 134–146.

(94) Li, L.; Gao, Z.; Moan, T. Analysis of Lifting Operation of a Monopile Considering Vessel Shielding Effects in Short-Crested Waves. *Int. J. Offshore Polar Eng.* **2016**, *26* (4), 408–416.

(95) Arpaci, V. S.; Larsen, P. S. *Convection Heat Transfer*; Prentice Hall: NJ, USA, 1984.

(96) Andereck, C. D.; Liu, S. S.; Swinney, H. L. Flow Regimes in a Circular Couette System with Independently Rotating Cylinders. *J. Fluid Mech.* **1986**, *164*, 155–183.

(97) International Organization for Standardization. *Plastics — Resins in the Liquid State or as Emulsions or Dispersions — Determination of Apparent Viscosity Using a Single Cylinder Type Rotational Viscometer Method. (ISO 2555)*; 2018.

(98) Wang, X.; Olsen, S. M.; Andres Martinez, E.; Olsen, K. N.; Kiil, S. Drag Resistance of Ship Hulls: Effects of Surface Roughness of Newly Applied Fouling Control Coatings, Coating Water Absorption, and Welding Seams. *J. Coatings Technol. Res.* **2018**, *15* (4), 657–669.

(99) Eres, M. H.; Weidner, D. E.; Schwartz, L. W. Three-Dimensional Direct Numerical Simulation of Surface-Tension-Gradient Effects on the Leveling of an Evaporating Multicomponent Fluid. *Langmuir* **1999**, *15* (5), 1859–1871.

(100) Kojima, S.; Moriga, T.; Takenouchi, K. The Leveling of Thermosetting Waterborne Coatings. Part III: Leveling under Controlled Conditions. *Polym. Eng. Sci.* **1995**, *35* (24), 1949–1954.

(101) Kojima, S.; Moriga, T.; Takenouchi, K. The Leveling of Thermosetting Waterborne Coatings. Part IV: Effects of Film Thickness. *Polym. Eng. Sci.* **1995**, *35* (24), 1955–1961.

(102) Mahmoodi, S.; Guoqing, H.; Khajavi, M. N. Two-Dimensional Spin Coating with a Vertical Centrifugal Force and the Effect of Artificial Gravity on Surface Leveling. *J. Coatings Technol. Res.* **2016**, *13* (6), 1123–1137.

(103) King, M. J. The Measurement of Ship Hull Roughness. *Wear* **1982**, *83* (2), 385–397.

(104) Gadelmawla, E. S.; Koura, M. M.; Maksoud, T. M. A.; Elewa, I. M.; Soliman, H. H. Roughness Parameters. *J. Mater. Process. Technol.* **2002**, *123* (1), 133–145.

(105) Boryczko, A. Distribution of Roughness and Waviness Components of Turned Surface Profiles. *Metrol. Meas. Syst.* **2010**, *17* (4), 611–620.

(106) Martinelli, E.; Sarvothaman, M. K.; Galli, G.; Pettitt, M. E.; Callow, M. E.; Callow, J. A.; Conlan, S. L.; Clare, A. S.; Sugiharto, A. B.; Davies, C.; *et al.* Poly(Dimethyl Siloxane) (PDMS) Network Blends of Amphiphilic Acrylic Copolymers with Poly(Ethylene Glycol)-Fluoroalkyl Side Chains for Fouling-Release Coatings. II. Laboratory Assays and Field Immersion Trials. *Biofouling* **2012**, *28* (6), 571–582.

(107) International Organization for Standardization. *Geometrical Product Specifications (GPS)-Surface Texture: Areal-Part 2: Terms, Definitions and Surface Texture Parameters. (ISO 25178-2)*; 2012.

(108) International Organization for Standardization. *Geometrical Product Specifications (GPS)-Surface Texture: Profile Method-Terms, Definitions and Surface Texture Parameters. (ISO 4287)*; 1998.

(109) Overdiep, W. S. The Effect of a Reduced Solvent Content of Solvent- Borne Solution Paints on Film Formation. *Prog. Org. Coatings* **1986**, *14*, 1–21.

(110) Eres, M. H.; Schwartz, L. W.; Roy, R. V. Fingering Phenomena for Driven Coating Films. *Phys. Fluids* **2000**, *12* (6), 1278–1295.

(111) Durst, F.; Raszillier, H.; Schwartz, L. W. Theoretical and Numerical Modeling of Coating Flow on Simple and Complex Substrates Including Rheology, Drying and Marangoni Effects. *Adv. Coat. Dry. Thin Film.* **2002**, 105–128.

(112) Roy, R. V.; Roberts, A. J.; Simpson, M. E. A Lubrication Model of Coating Flows over a Curved Substrate in Space. *J. Fluid Mech.* **2002**, *454*, 235–261.

(113) Schwartz, L. W.; Eley, R. R. A Mathematical Model for Three-Dimensional Coating Flow with Thixotropy. In *16th International Coating Science and Technology Symposium*; Atlanta, September 2012.

(114) Sin, G.; Gernaey, K. V. Data Handling and Parameter Estimation. In *Experimental Methods In Wastewater Treatment*; Loosdrecht, M. C. M. van, Nielsen, P. H., Lopez-Vazquez, C. M., Brdjanovic, D., Eds.; IWA Publishing: London, 2016.

Appendix A: Approach to determine drag resistance

The shaft power (*SP*) can be calculated based on the following equation:

$$SP = \frac{P_E}{PC} \tag{A.1}$$

where *PC* is the propulsive coefficient representing the overall efficiency of the propeller and shafting.[88] The value of this parameter usually ranges from 0.5 to 1.[19] The towing power, P_E, which is essential to move a ship through water, can be calculated from:

$$P_E = F_T U = \frac{1}{2}\rho C_T U^3 S \tag{A.2}$$

where F_T is the total drag resistance, U is the speed of the ship, ρ is the density of seawater, C_T is the total resistance coefficient, and S is the wetted hull area.

The total resistance coefficient consists of a residuary resistance coefficient, C_R, an air resistance coefficient, C_A, and a skin friction coefficient, C_F, expressed as:

$$C_T = C_R + C_F + C_A \tag{A.3}$$

The residual drag force due to wave and wake-making is given by:

$$F_R = \frac{1}{2}\rho C_R U^2 S \tag{A.4}$$

The skin friction force, which is due to the tangential shear stress on the ship hull caused by seawater flowing over it, is given by:

$$F_F = \frac{1}{2}\rho C_F U^2 S \tag{A.5}$$

The air resistance force is given by:

$$F_A = \frac{1}{2}\rho C_A U^2 S_{air} \tag{A.6}$$

where S_{air} is the cross-sectional area of the ship above water.[19]

Appendix B: Conversion of torque values into friction coefficient

As mentioned in the literature chapter, the measured torque, M_t consists of four parts: the drag from the cylinder periphery surface, M_c, from the top and bottom surfaces of the cylinder, M_d, from the outer shaft surface area, M_s, and the friction from the bearings, M_b. Therefore, the torque picked up by the sensor can be expressed by the following equation:

$$M_t = M_c + M_d + M_s + M_b \tag{B.1}$$

Since only the drag from the cylinder periphery is relevant to the study, the other three parts should be eliminated by applying a correction M_{cor}, which is shown as follows

$$M_{cor} = M_d + M_s + M_b \tag{B.2}$$

This correction can be obtained by measuring the torque of smooth cylinders as a function of heights. The relationship between torque and cylinder height is assumed to be linear and the interception with the y-axis (zero cylinder height) after extrapolation of the line will be the value of M_{cor}. Notice that, M_{cor} is a function of tangential velocity. The linear relationship between torque and cylinder height was found by Weinell *et al.*[24]. As a result, the M_c will be finally calculated by subtracting M_{cor} from the measured torque value as following

$$M_c = M_t - M_{cor} \tag{B.3}$$

The obtained torque value M_c can be converted into the skin friction coefficient C_F based on an assumption that the torque can be related to the wall shear stress, τ_w, given by

$$M_c = \tau_w S r \tag{B.4}$$

where S is the wetted surface area excluding the end surfaces and r is the radius of cylinder. The wetted surface area can be calculated by

$$S = 2\pi r l \tag{B.5}$$

where l is the cylinder height. According to Schlichting's book[49], the wall shear stress can be described as follows

$$\tau_w = \frac{1}{2} C_F \rho U^2 \tag{B.6}$$

where ρ is the fluid density, and U is the rotational speed of the cylinder. Based on the above equations, the conversion equation is obtained as follows

$$C_F = \frac{M_c}{\rho U^2 r^2 \pi l} \tag{B.7}$$

Appendix C: The deductive method for replacing amplitude with waviness in Equation (7.2)

In this deductive method, a sinusoidal surface profile was used to simplify the case. The evolving of the sinusoidal profile during leveling process is illustrated in Figure C.1.

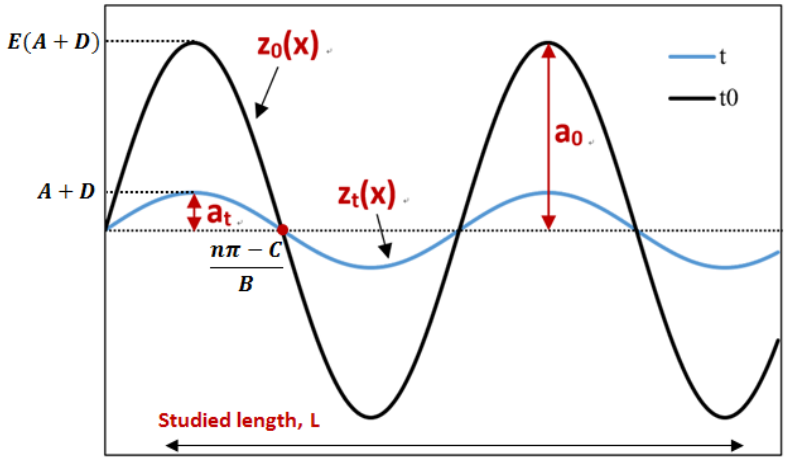

Figure C.1 Schematic illustration of the evolution of sinusoidal surface profile during leveling process. $Z_0(X)$ curve represents the surface profile at time t_0 with amplitude of a_0, and $Z_t(X)$ curve represents the surface profile at time t with amplitude of a_t. The amplitudes of two profiles are also expressed by constants A, B, C, D, and E. n is a natural number.

As shown in Figure C.1, the surface profiles $Z_0(X)$ and $Z_t(X)$ can be expressed by

$$z_t(x) = Asin(Bx + C) + D \tag{C.1}$$

$$z_0(x) = E[Asin(Bx + C) + D] \tag{C.2}$$

where the meanings of constants A, B, C, D, and E are illustrated in Figure C.1. Based on the above equations, the amplitudes can be expressed as follows

$$a_t = A + D \tag{C.3}$$

$$a_0 = E(A + D) \tag{C.4}$$

Based on the calculation methodology of the profilometer, waviness parameter, Wa, is defined as

$$W_a = \frac{1}{l}\int_0^l |Z(x)|dx \tag{C.5}$$

where, l is the evaluation length, $Z(x)$ is the function describing the surface profile which determine the height at position x along the evaluation length. Combining Equation C.5 with C.1 and C.2, the following equations are derived

$$Wa_t = \frac{1}{L}\int_0^L z_t(x)dx = \frac{1}{L}\int_0^L [Asin(Bx + C) + D]dx \tag{C.6}$$

$$Wa_0 = \frac{1}{L}\int_0^L z_0(x)dx = \frac{E}{L}\int_0^L [Asin(Bx + C) + D]dx \tag{C.7}$$

Thus, the ratio of waviness is proved to be same as the ratio of amplitude as follows

$$\frac{a_t}{a_0} = \frac{Wa_t}{Wa_0} = \frac{1}{E} \tag{C.8}$$

Appendix D: MATLAB codes for model development

Main function

```
clear       % Clear workspace
close all   % Close open figure windows
clc         % Clear command window

% Initial guessing values for the parameters
a=3;        % Exponent of viscosity e
b=-100;     % Constant f
c=1;        % Exponent of average film thickness
d=-3;       % Exponent of wavelength

% Defining parameters
Par=[a,b,c,d];

% Loading experimental data
ydata=xlsread('y.xlsx',1);
tdata=xlsread('dt.xlsx',1);
hdata=xlsread('h(t).xlsx',1);
etadata=xlsread('viscosity(t).xlsx',1);
sigmadata=xlsread('surface_tension.xlsx',1);
lambdadata=xlsread('wavelength.xlsx',1);

% Function
ymodel=xueting(sigmadata,hdata,lambdadata,etadata,tdata,Par);

% Plot
plot(tdata,ymodel,'k-',tdata,ydata,'k-O')

% Defining parameter and data matrix
DataIndex=[1,2,3,4,5];
ParameterIndex=[1,2];

Parameters_Initial=Par(ParameterIndex);

% Set options for the minimization algorithm. Display iterations, tolerances for
% acceptance of minimum and maximum function evaluations
options = optimset('display','iter','tolfun',1.0e-06, 'tolx',1.0e-5, 'maxfunevals',
10^10,'MaxIter',150000);

% Chosen algorithm fmincon: Finds local minimum. Very dependent on starting guess %
and optimization surface contour.
lb=[0,-10000];
ub=[500,0];

fp=1;lp=length(lambdadata);

% Minimizing objective function by a constrained solver
```

```
[ParameterMinimum,SquaredSumError] =
fmincon(@(Parameters_Initial)Functionfminsearch(Parameters_Initial,ParameterIndex,D
ataIndex,ydata(fp:lp,:),...

tdata(fp:lp,:),hdata(fp:lp,:),etadata(fp:lp,:),sigmadata(fp:lp,:),lambdadata(fp:lp,
:),Par),Parameters_Initial,[],[],[],[],lb,ub,[],options);

% To verify the minimum point obtained from fmincon, it is possible to run a new
% search from the found minimum. This is done using lsqnonlin.
options = optimset('display', 'iter', 'tolfun', 1.0e-06, 'tolx', 1.0e-5,
'maxfunevals', 10000);    % Set options for the minimization algorithm.
[ParameterMinimum,SquaredSumError,Residual] =
lsqnonlin(@(ParameterMinimum)Functionlsqnonlin(ParameterMinimum,ParameterIndex,Data
Index,ydata(fp:lp,:),...

tdata(fp:lp,:),hdata(fp:lp,:),etadata(fp:lp,:),sigmadata(fp:lp,:),lambdadata(fp:lp,
:),Par),ParameterMinimum,lb,ub,options);

% Display the results (see "Sin2016" Table 5.4)
theta_0   = Parameters_Initial';   % Set names for table
theta_min = ParameterMinimum';
Results   = table(theta_0,theta_min,'RowNames',{'a','b'})

% Estimate the uncertainty
% Estimate the uncertainty of the parameter estimators and the model prediction
% uncertainty. In this step, the covariance matrix of the parameter estimators is
% computed. From the covariance matrix, the standard deviation, 95 % confidence
% interval as well as the correlation matrix are obtained.

% Calculate the covariance of parameter estimators. Get the Jacobian matrix using
% built-in "lsqnonlin"-function but with no iteration (setting maxfunevals = 0)

options = optimset('display', 'iter','tolfun',1.0e-06, 'tolx',1.0e-5,
'maxfunevals', 0); % No iteration # Want this set to iter?
% Calculated as above (step 3), now only to estimate Jacobian and residuals
[~,~,residual,~,~,~,Jacobi] =
lsqnonlin(@(ParameterMinimum)Functionlsqnonlin(ParameterMinimum,ParameterIndex,Data
Index,ydata(fp:lp,:),...

tdata(fp:lp,:),hdata(fp:lp,:),etadata(fp:lp,:),sigmadata(fp:lp,:),lambdadata(fp:lp,
:),Par),ParameterMinimum,[],[],options);

% The Jacobian is reported in a column vector format, which is reformated below to
a matrix format
Jacobian = []; Jacobian(:,:) = Jacobi;

% Degrees of freedom calculation
n = length(residual);
p = length(ParameterMinimum);
DegreesFreedom = n - p;

% Statistics
SquaredSumError = residual'*residual;
Variance = SquaredSumError/DegreesFreedom; % Variance of errors.
```

```
CovarianceParameters    = Variance*inv(Jacobian'*Jacobian); % Covariance of
parameter estimators
StandardDeviation       = sqrt(diag(CovarianceParameters))'; % Standard deviation
of parameter estimators
CorrelationParameters   = CovarianceParameters ./
[StandardDeviation'*StandardDeviation]; % Correlation matrix for the parameters

alpha   = 0.025;  % Significance level
tcr     = tinv((1-alpha),DegreesFreedom); % Critical t-dist value at alpha

ConfidenceIntervalP95    = [ParameterMinimum-StandardDeviation*tcr;
ParameterMinimum+StandardDeviation*tcr]; %+-95% confidence intervals

% Display results (see "Sin2016" Table 5.5)
sigma      = StandardDeviation';
P95_Lower  = ConfidenceIntervalP95(1,:)';
P95_Upper  = ConfidenceIntervalP95(2,:)';
Statistics = table(theta_min,sigma,P95_Lower,P95_Upper,'RowNames',{'a',    'b'})

disp('     Correlation Matrix')
disp({'a',    'b'})
disp(CorrelationParameters)

% Calculate confidence intervals on the model output
% Perform a simulation with the model using estimated parameters;
Par(ParameterIndex) = ParameterMinimum ; % Substitute relevant parameters and use
estimated parameters

ymodel=xueting(sigmadata,hdata,lambdadata,etadata,tdata,Par)

plot(tdata(fp:lp,1),ymodel(fp:lp,1),'b-',tdata(fp:lp,2),ymodel(fp:lp,2),'r-
',tdata(fp:lp,3),ymodel(fp:lp,3),'k-',...
    tdata(fp:lp,4),ymodel(fp:lp,4),'m-',tdata(fp:lp,5),ymodel(fp:lp,5),'g-',...
    tdata(fp:lp,1),ydata(fp:lp,1),'b--O',tdata(fp:lp,2),ydata(fp:lp,2),'r--
O',tdata(fp:lp,3),ydata(fp:lp,3),'k--O',...
    tdata(fp:lp,4),ydata(fp:lp,4),'m--O',tdata(fp:lp,5),ydata(fp:lp,5),'g--O')
```

Fitting model

```
function y=xueting(sigma,h,lambda,eta,time,Par)

% sigma=
% h=
% lambda=
a=Par(1);
b=Par(2);
c=Par(3);
d=Par(4);

y=b.*time.*1./eta.^a;
```

Maximum likelihood estimate function (Constrained minimization)

```
function Residual =
Functionfminsearch(ParametersInitial,ParameterIndex,DataIndex,ydata,tdata,hdata,eta
data,sigmadata,lambdadata,Par)

% Update parameter vector
Par(ParameterIndex) = ParametersInitial;

% Solution of the model
ymodel=xueting(sigmadata,hdata,lambdadata,etadata,tdata,Par);

% formulate the objective function
Error=ymodel(:,DataIndex)-ydata(:,DataIndex) ;      % Error between model and data
Residual=Error(:)'*Error(:);                        % Residuals in vector form
```

LSQnonlin for verification

```
function Residuals =
Functionlsqnonlin(ParameterMinimum,ParameterIndex,DataIndex,ydata,tdata,hdata,etada
ta,sigmadata,lambdadata,Par)

% Update parameter vector
Par(ParameterIndex) = ParameterMinimum;

% Solution of the model
ymodel=xueting(sigmadata,hdata,lambdadata,etadata,tdata,Par);

% formulate the objective function
Error=ymodel(:,DataIndex)-ydata(:,DataIndex) ;       % Error between model and data
Residuals=Error(:);                                  % Residuals in vector form
```

Department of Chemical and Biochemical Engineering - CoaST
Technical University of Denmark
Søltofts Plads, Building 229
2800 Kgs. Lyngby
Denmark
Phone: +45 45 25 28 00
Web: www.kt.dtu.dk